Neuronal activity-dependent development of layer 4 pyramidal cells in the primary visual cortex

Inauguraldissertation
zur
Erlangung der Würde eines Doktors der Philosophie
vorgelegt der
Philosophisch-Naturwissenschaftlichen Fakultät
der Universität Basel

von

Elieke Maria Christina Willems, MSc

2022

Genehmigt von der Philosophisch-Naturwissenschaftlichen Fakultät

auf Antrag von:

Prof. Dr. Peter Scheiffele

Prof. Dr. Fiona Doetsch

Prof. Dr. Theofanis Karayannis

Basel, 18. Oktober 2022

_____

The Dean of Faculty

Prof. Dr. Marcel Mayor

Abstract

Intricate neuronal circuits are at the base of several vital functions and complex behaviours. The proper functioning of these networks relies foremost on the correct development of these circuits, which emerge from an interplay of innate genetic programs and activity-dependent plasticity mechanisms. The extent to which neuronal activity plays a role, in particular the contributions of activity that is spontaneously generated by immature neuronal circuitry, is not precisely known. Furthermore, while the dendritic morphology is an important morphological feature that determines how a neuron is integrated in the circuitry, much remains to be understood on how the dendritic tree is formed and reshaped during development. The current thesis provides insight into these questions, by providing a detailed description of the development of both thalamocortical (TC) axon ingrowth in layer 4 (L4) of the primary visual cortex (V1) and the development of basal dendritic morphology of L4 pyramidal V1 neurons. Furthermore, we explored the influence of spontaneous activity on the basal dendritic development of L4 pyramidal neurons of V1. Central for studying these developmental processes was the development of a pioneering surgical protocol to virally introduce the expression of fluorescent proteins and molecular silencers in the dorsal Lateral Geniculate Nucleus (dLGN) at postnatal day 0 (P0). The proposed surgical protocol for viral injections is therefore the first stereotactic protocol that accomplishes transgene expression in a spatially restricted target region in the neonate brain without the use of the Cre/loxP expression system.

Using this novel stereotactic injection protocol, we introduced the expression of a fluorescent protein in neurons from the dLGN and studied TC axon ingrowth in L4 of V1. TC axon ingrowth was not yet complete at birth; instead, the number of axons/axonal arborizations increased until P10 after which axonal coverage remained stable. Furthermore, the number of axonal varicosities that colocalized with the presynaptic marker vlgut2 appeared to increase in parallel with axonal ingrowth, suggesting that the number of presynaptic structures increases during early postnatal development.

Several trends emerged when evaluating the dendritic morphological development of sparsely labelled L4 neurons. First, the dendritic length increased throughout the first two weeks of postnatal development. Second, the dendritic complexity appeared to increase between P4 and P10, as the number of secondary and tertiary dendrites, along with the number of branch points increased. Interestingly, these dendritic parameters showed a tendency to decrease between P10 and P15, suggesting that part of the dendritic complexity previously gained is subsequently lost. This raises the hypothesis that the loss in dendritic complexity is caused by the pruning of aberrant secondary and tertiary branches. We then markedly reduced TC activity through the expression of the molecular silencer Kir2.1 in the dLGN and studied the effect on basal dendritic morphology at P13. Silencing TC activity seemed to be associated with an increased dendritic length. Furthermore, the basal dendritic structure appeared to be more complex, indicated by an increase in the number of tertiary dendrites, branch points and Sholl radius. The number of primary dendrites, which also remained constant during development, was not affected by silencing TC activity. This raises the hypothesis that the number of primary dendrites is established early in development independent from neuronal activity from the dLGN. Though the results presented are preliminary, the trend emerges that silencing thalamocortical activity leads to an increased level of dendritic complexity. Considering the role attributed to activity-dependent genetic programs in dendritic pruning, we hypothesize that the apparent increase in dendritic complexity is caused by the failure of pruning aberrant connections, in absence of spontaneous thalamocortical input. Future studies will have to be carried out to test this hypothesis.

Table of contents

1. Introduction

1.1 General introduction

Charles Darwin was ahead of his time when stating in 1871 that the brain is the most important of all organs (Jacyna, 2009). The human brain is one of the most complicated organs evolved (Schoenemann, 2006). Intricate circuits interconnecting its building blocks, the neurons, underly fundamental functions such as breathing, and sleep and hunger regulation, but also support complex behaviours that are essential for our ability to interact with our environment, such as sensory perception, learning and memory, speech, and our ability to interpret social cues. The proper functioning of the networks underlying these abilities relies foremost on the correct formation of these circuits during development. Several common neurological disorders, such as autism and epilepsy, have been linked to abnormal neuronal circuit development (Faust et al., 2021; Neniskyte and Gross, 2017; Penn and Shatz, 1999). Therefore, insight into the mechanisms underlying normal brain development is essential for understanding what happens when this process goes awry.

In the developing brain, refined neuronal networks underlying perception and complex behaviour emerge from an interplay of innate genetic programs and activity-dependent plasticity mechanisms. Early molecular programs determine cell fate and guide the growing axons to their appropriate targets through gradients of molecular guidance cues (Flanagan, 2006; Goodman and Shatz, 1993; McLaughlin and O'Leary, 2005). The intersection of such genetic programs and their regulation by neuronal activity leads to further refinement of these crude circuits (reviews: Kutsarova, Munz, & Ruthazer 2017; Cadwell *et al.* 2019). The extent to which neuronal activity plays a role, in particular, the contribution of activity that is spontaneously generated by the immature neuronal network and the mechanism of how it instructs wiring, is however not precisely known.

In the pre- and early postnatal brain, spontaneous activity can be observed in multiple sensory systems, including the somatosensory, auditory and visual system (Bansal et al., 2000; Khazipov et al., 2004; Tritsch et al., 2007). In these systems, spontaneous activity is generated in the periphery and transmitted to the primary sensory cortices through thalamic nuclei (Leighton and Lohmann, 2016). These spontaneous activity patterns appear to be evolutionarily conserved, as they have been observed during development in flies, rodents and humans (Ackman and Crair, 2014; Akin et al., 2019; Colonnese et al., 2010); a finding that strongly suggest that spontaneous activity is important for correct neuronal development.

Due to its characteristics, the mouse visual system lends itself very well to study spontaneous activity. First of all, mice are born with closed eyelids which open at the end of the second postnatal week. In addition, retinal ganglion cells are not yet responsive to light the first ten days after birth (Tiriac et al., 2018). Therefore, it is possible to study the influence of spontaneous activity before eye opening largely independent of stimulus-induced activity. Furthermore, many important visual response features, such as direction selectivity and orientation selectivity already exist at eye opening (Rochefort et al., 2011; Thompson et al., 2017a). The developmental processes that take place within the first two weeks of postnatal development are thus crucial to prepare the visual system for the onset of vision. Notably, the concurrence of spontaneous activity within this same time period points to an instructive role for spontaneous activity in the development of the mouse visual system.

Multiple types of spontaneous activity exist throughout the visual system, such as cortically generated spontaneous activity, thalamic waves and different types of retinal waves, which appear in distinct stages of development. Of these different types of spontaneous activity, one of the most studied in the mouse visual system are retinal waves. These retinal waves are so-called due to their characteristic spatial-temporal

pattern, making it appear as if activity spreads as a wave throughout the retina. Through its axonal projections, the wave of depolarization spreads from the retina, to the superior colliculus (SC) and via the dorsal Lateral Geniculate Nucleus (dLGN), to the primary visual cortex (V1), where the wave travels across V1 maintaining the same retinotopic direction (Ackman et al., 2012a).

In the spatial-temporal characteristics of the retinal wave pattern, information on the spatial relation between neurons is encoded, thereby shaping and matching the retinotopic maps between structures of the visual system (Ackman and Crair, 2014; Cang *et al*., 2005; Huberman *et al.*, 2008). Important in establishing this influence has been the use of genetically altered mouse models, binocular enucleation, and drugs, which all disrupt the spatial-temporal pattern and/or frequency of the retinal waves (Arroyo and Feller, 2016; Leighton and Lohmann, 2016; Lokmane et al., 2013; Stellwagen and Shatz, 2002). In addition to the defect in retinotopic map refinement in the dLGN, SC and V1, manipulating retinal waves also results in distorted retinal axon sorting, leading to a defect in eye segregation in both the dLGN and SC (Ackman and Crair, 2014). Yet, most studies on the influence of retinal wave activity on V1 development have been focused on how spontaneous activity affects the wiring upstream of V1; both retinotopic map deformation and distorted eye segregation in V1 are caused by a defect in retinogeniculate and thalamocortical wiring. Currently little is known about the influence of retinal wave activity on the formation and function of local cortical circuits in V1, which depend on the morphology and electrophysiological properties of individual V1 neurons.

One important morphological feature of a neuron that determines how it is integrated in neuronal circuitry is the dendritic structure. The length of a neuron's dendrites and the extent of dendritic branching are a few of the dendritic parameters that determine from what physical area and thus from how many pre-synaptic neurons a post-synaptic neuron is able to receive information. Furthermore, dendrites play an important role in filtering signals from multiple pre-synaptic neurons by integrating these signals into a single response, a process which is called dendritic integration (Branco and Häusser, 2011; Magee, 2000). Albeit its importance, the study on dendritic tree formation during early development and the influence of spontaneous activity generated in the periphery on this process, has received little attention over the years and only a few studies exist to date (Richards et al., 2020).

Most of these studies have focused on the influence of spontaneous activity on the neurons that are strongest innervated by thalamocortical axons, and therefore are directly exposed to input from the periphery, namely layer 4 (L4) neurons. A study in the primary visual cortex (V1) of ferrets, in which cortical development evolves on a slower timescale, reported that dendritic complexity of pyramidal L4 neurons increased most between postnatal day 14 (P14) and P26 (Callaway and Borrell, 2011). The authors further found that both stellate cells and pyramidal cells of L4 of V1 possess an apical dendrite in early development and that stellate cells lose this apical dendrite at P22 to acquire their typical stellate dendritic configuration. More interestingly, eliminating retinal waves by binocular enucleation prevented the loss of the apical dendrite in stellate cells (Callaway and Borrell, 2011). A later study in mice, reported that stellate cells from the barrel cortex also initially possess an apical dendrite, which they lose at P6 (Nakazawa et al., 2018). Furthermore, Nakazawa and colleagues (2018) demonstrated that the dendritic morphological changes in L4 neurons, which lead to the formation of the characteristic barrels in the somatosensory cortex, depend on the activity they receive from the thalamocortical axons. Whether morphological changes were mostly influenced by spontaneous activity or stimulus-induced activity in these studies could however not be determined since both activity patterns coexist in the somatosensory system in this time frame.

The above-described studies demonstrate that dendritic morphology can change rapidly and markedly during early postnatal development. Furthermore, functional thalamocortical input may play a major role in L4 neuronal development. Nevertheless, no data is available on dendritic changes in L4 of the mouse primary visual cortex (V1) specifically and how they are influenced by spontaneous thalamocortical input. Therefore, the central focus of my PhD thesis is to understand how spontaneous activity from the periphery influences

the dendritic development of L4 neurons in V1. In addition, to facilitate the study of this question, insight into the development of axonal ingrowth is needed. Previous studies exploring thalamocortical axon ingrowth were conducted in a variety of species looking at innervation patterns of the cortex in general. Though these studies provide a coarse impression of axonal ingrowth, a comprehensive overview of the dynamics of thalamocortical ingrowth in a specific region, such as L4 of V1, is still lacking. Therefore, the first aim of my PhD research was to provide a detailed description of thalamocortical axon ingrowth in L4 of V1 during the first two weeks of postnatal development.

The following introduction chapter will introduce the key concepts relevant for my research question. I will take the same route as light information travels to the cortex and provide a short description of the adult retina, dorsal Lateral Geniculate Nucleus and primary visual cortex of the mouse. Then, I zoom in on the early developmental processes that are responsible for the stereotypic formation of the brain, with a focus on axonal pathfinding and dendritic branching. In the last chapter I will briefly describe the spontaneous activity patterns that exist in the developing brain and will describe how retinal wave activity is generated and propagated in the visual system. Furthermore, I will illustrate the importance of retinal wave activity for early postnatal development of the visual system and highlight the open questions that still exist at present. The introduction chapter concludes with a description of the main objectives of my PhD thesis.

1.2 From the retina to V1: the first steps of visual processing

Light enters the eye through the retina, where photoreceptors translate information embedded in light photons into chemical signals that the nervous system is able to interpret. Retinal ganglion cells then transmit processed light information to different regions of the brain. Over forty subcortical brain areas receive projections from the retina. These brain areas are mostly part of non-image-forming circuits, which are not involved in the perception of sight. For visual perception, light information is transmitted through retinogeniculate connections to the dorsal Lateral Geniculate Nucleus (dLGN), from where it is relayed to the primary visual cortex (V1) through thalamocortical connections (Figure 1). V1 sends projections to the surrounding higher-order visual areas, which in turn send feedback projections to V1 and dLGN to modulate responses. In addition, the visual system receives multiple feedback projections from numerous other areas. Though this complex circuitry is characteristic of the mammal brain, it poses a challenge to decipher the contribution of each individual member of the visual system to visual perception. In this chapter I will provide a simplistic overview of the function of the areas involved in the first stages of visual processing: the retina, dLGN and V1. Furthermore, I will describe the gross anatomy of these structures and provide a simplistic overview of the feedforward projections interconnecting the different areas. I will thereby focus on the architectural and functional features that are relevant for the current thesis.

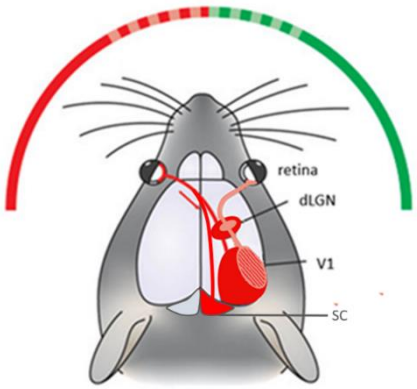

Figure 1 Axons from the retina project directly to the SC and indirectly through the dLGN to V1. In mice, as opposed to primates, the eyes are laterally positioned within the skull. The overlap in hemifields is therefore small (depicted in grated green and red zones). The majority of light information of the left hemifield is captured by the left retina and projects to the contralateral hemisphere. Important for visual perception is the indirect pathway from the retina to the primary visual cortex (V1) via the dorsal Lateral Geniculate Nucleus (dLGN). While the majority of retinal axons in the dLGN originate from the contralateral hemisphere, a small ipsilateral zone exists in which a small number of ipsilateral axons terminate. V1 can be divided into a larger monocular zone and a smaller binocular zone. Another important pathway for visual perception is the direct pathway from the retina to the superior colliculus (SC). The SC is essential for visual motion processing.

1.2.1 The cell types and circuits of the mouse retina: a brief overview

The retina consist of five major neuronal cell types which are organised in layers (Dunn and Wong, 2014) (Figure 2). This basic building plan is conserved across vertebrate species (Hoon et al., 2014). The processing of visual information begins with the rod and cone photoreceptors, which are organized in a single layer called the outer nuclear layer. Light-sensitive pigments in the photoreceptors are able to capture light photons and translate light information into a neurotransmitter response (Masland, 2012). Rod photoreceptors all express the same type of light-sensitive pigment, rhodopsin, which is able to detect a single photon. Rods are thus highly sensitive to light and henceforth specialized for dim-light vision. In contrast, the less abundant mice cone receptors contain one of the two low-sensitive light detecting pigments, each with a different spectral absorption. The existence of distinct chromatic pathways is at the basis of colour vision.

Photoreceptors synapse onto bipolar neurons located in the inner nuclear layer of the retina. These consist of two broad classes, the rod and cone bipolar cells, which are primarily contacted by respectively rod and cone photoreceptors. The responses of the bipolar cells are modulated by inhibitory horizontal cells (Hoon et al., 2014). Bipolar cells in turn synapse onto retinal ganglion cells and amacrine cells, the second inhibitory cell type of the retina. Amacrine cells provide direct feedforward inhibition of the retinal ganglion cells and provide feedback inhibition through their synapses onto the bipolar axons, thereby modulating activity patterns in the retinal ganglion cells. These are the output neurons of the retina, and project to numerous

brain regions, including the dorsal Lateral Geniculate Nucleus. Retinal ganglion cells (RGCs) are able to detect sensory input in only a part of the visual scene, its receptive field. The receptive fields of neighbouring RGCs are also located next to each other in the visual space.

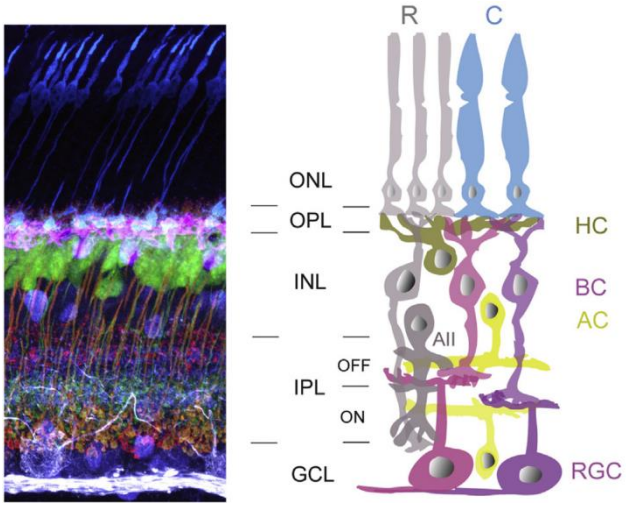

Figure 2 The basic architecture of the retina (Left) Immunohistochemical labelling of the major neuronal cell types in a cross section of the mouse retina reveal that the different cell types are organized in distinct layers. (Right) schematic representation of the building plan of the mouse retina. The deepest layer is the outer nuclear layer (ONL) in which the rod (R) and cone (C) photoreceptors are located. In the inner nuclear layer (INL) cell bodies of the bipolar cells (BC) and inhibitory amacrine cells (AC) are located. The retinal ganglion cells (RGC) are located in the ganglion cell layer (GCL). Synaptic connections between different cell types are located in the two plexiform layers, the outer plexiform layer (OPL) and inner plexiform layer (IPL). In the IPL there is a lamination visible of synaptic input from cells that depolarize in response to light increments (ON) and decrements (OFF). [Figure adapted from Hoon et al. 2017]

Anatomical and genetic sequencing studies have shown that the five major cell types of the retina can be subdivided into multiple subclasses of specialized cell types. For instance, 12 types of bipolar cells, 30 morphological distinct amacrine cells, and at least 30 different ganglion cells have been found in the mouse retina (Azeredo da Silveira and Roska, 2011; Rheaume et al., 2018; Sanes and Masland, 2015). The specialization of the retinal ganglion cells seem to revolve around the detection of distinct visual features (Sanes and Masland, 2015). A first classification of retinal ganglion cells (RGCs) can be made based on whether they increase firing rate in response to light increments, decrements or both presented in their receptive field centres: the ON, OFF and ON-OFF retinal ganglion cell types (Kerschensteiner and Guido, 2017). A fourth category for which so far one RGC type has been found, exhibit a high firing baseline which is suppressed by ON and OFF stimuli and therefore function as uniformity detectors. Furthermore, a large number of RGCs, the different direction sensitive RGC types (dsRGCs), are specialized for the detection of motion. For instance, the ON-dsRGCs display the highest firing rate to movement in a preferred direction (Sanes and Masland, 2015).

The different types of bipolar cells and retinal ganglion cells seem to be organized in local microcircuits dedicated to the specific task of the retinal ganglion cell (Azeredo da Silveira and Roska, 2011). Different types of ganglion cells thus provide higher visual areas with parallel information streams about distinct features of the visual scene.

1.2.2 The dorsal Lateral Geniculate Nucleus: more than just a relay station

The dorsal Lateral Geniculate Nucleus (dLGN) is part of the thalamus, a highly innervated region that lies in the diencephalon. The thalamus consist of multiple nuclei; activity in the so-called first-order thalamic nuclei are primarily driven by sensory information from the periphery, while higher-order thalamic nuclei receive driving input from predominantly cortical projections (Ghodrati et al., 2017). The dorsal Lateral Geniculate Nucleus (dLGN) is a first-order thalamic nucleus in which retinal ganglion axons (RGCs) innervate the excitatory thalamocortical neurons, which makes up roughly 90% of the dLGN, and to lesser degree the inhibitory neurons (Cox and Beatty, 2017; Evangelio et al., 2018). The inhibitory neurons of the dLGN, together with cortical feedback projections and input from the thalamic reticular nucleus, brainstem and superior colliculus, provide modulatory input to the thalamocortical neurons (Ghodrati et al., 2017). Thalamocortical neurons in turn send visual information to the primary visual cortex (V1) where the first stage of cortical processing takes place.

Historically, the dLGN was viewed as mere a relay station, passing on visual information to V1 in a linear way. Studies of the past decade however have demonstrated that the convergence of retinal input onto the thalamocortical (TC) neurons of the dLGN is greater than originally thought (Monavarfeshani et al., 2017). An innovative trans-synaptic tracing study by Rompani and colleagues (2017) found that three types of retinal input convergence can be defined. In the first type of convergence, the relay mode, TC neurons receive monocular input from a few RGCs of the same type (1-5). TC neurons belonging to the second category, the combination mode, receive monocular input from a larger number of RGCs from different types (6-36). Interestingly, they also found TC neurons that received binocular input from up to 90 RGCs belonging to different cell types. These findings strongly indicate that the dLGN performs visual input integration and is not simply passing on information to V1. Recent studies are starting to unravel the contribution of the dLGN to early visual processing, though a lot remains to be understood to date.

As opposed to higher mammals, the mouse dLGN lacks visible cytoarchitectural laminae (Monavarfeshani et al., 2017). Nevertheless, the terminations of retinal afferents are spatially organized in maps based on three functional principles which overlap with the functional organization principles in laminae of higher mammals: eye-segregation, retinotopic organization and cell-class specific lamination (Guido, 2018; Kerschensteiner and Guido, 2017; Monavarfeshani et al., 2017). The distinct functional regions in the dLGN are therefore often referred to as the hidden laminae of the dLGN (Reese, 1988).

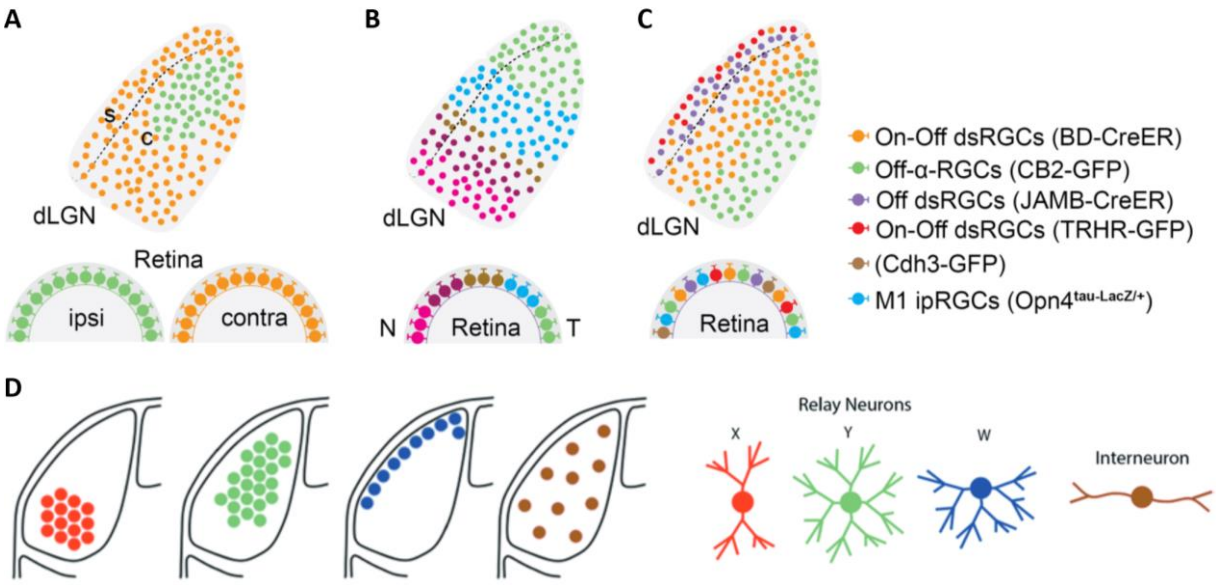

Figure 3 The functional lamination of the dorsal Lateral Geniculate Nucleus (dLGN) (A) The dLGN can be divided into a small ipsilateral zone (green) in which axons from the ipsilateral retinogeniculate cells (RGCs) terminate and a larger contralateral zone (orange). (B) Adjacent RGCs project to neighbouring thalamocortical (TC) neurons in the dLGN, thereby creating a retinotopic map of the visual scene. (C) Cell class lamination based on where axons from different RGC types terminate, reveals that the division into a shell and core (depicted with dashed line) can be further divided in several subregions. Direction-sensitive cells (dsRGCs) seem to be predominantly localized in the shell region. In figures (A) (B) and (C) the division of the dLGN into a smaller shell and a larger core is depicted with a dashed line. (D) a second cell class lamination is seen for the different classes of dLGN neurons. While interneurons (brown) appear to be evenly distributed across the dLGN, the different types of TC neurons, namely X, Y and W neurons seem to be localized in distinct regions. W cells are predominantly located in the shell region of the dLGN. [Based on adapted figures from Kerschensteiner and Guido, 2017; Monavarfeshani et al., 2017]

The first anatomical distinction is the segregation of retinogeniculate axons into distinct eye-specific regions (Figure 3A). Since the eyes of mice are laterally positioned within the skull, the binocular field of view is small. Therefore, only few ipsilateral afferents project to the ipsilateral dLGN (5-10%) (Kerschensteiner and Guido, 2017; Monavarfeshani et al., 2017). The majority of retinogeniculate terminals in the dLGN thus originate from the contralateral eye (Figure 3A). Although anatomical tracing studies have shown that retinogeniculate

arborizations are spatially organized in eye-specific regions, electrophysiological studies report that a subset of thalamocortical neurons receive binocular input (Rompani et al., 2017). Whether this means that the distinction in eye-specific regions is less strict than previously reported or whether the dendritic tree of these binocular neurons extend to both eye-specific regions remains to be determined.

The second functional principle by which the dLGN neurons are spatially organized is based on the topographic position of the retinogeniculate cells (RGCs) from which they receive input (Figure 3B). Neighbouring RGCs have receptive fields that are located next to each other in the visual space. This retinotopic representation is maintained in the dLGN and V1 as neighbouring RGCs project to neighbouring thalamocortical cells (TCs) and neighbouring TCs project to neighbouring V1 neurons. Interestingly, the input that binocular thalamocortical neurons receive from both eyes is also retinotopically matched, which further strengthens the notion that the retinotopic representation of the visual scene is an important aspect of early visual processing (Rompani et al., 2017).

In the nineties, researchers discovered that the dLGN could be divided into a dorsolateral shell region and a larger ventromedial core based on the input from morphological distinct retinal ganglion cells (RGCs) (Kerschensteiner and Guido, 2017). This finding together with the discovery of the existence of at least 30 types of retinal ganglion cells, raised the hypothesis that further hidden laminae could be defined in the dLGN based on the spatially restricted innervation pattern of different RGC types. Indeed, studies labelling a few of these specific retinal ganglion cell types, have shown that the class-specific lamination is actually more refined than the simple division into a shell and core (Monavarfeshani et al., 2017). The extent of this class-specific lamination is however not known as the majority of the RGC types have not yet been studied due to technical challenges in labelling these specific RGC types. Nevertheless, it appears that different RGC types terminate in discrete laminae (Figure 3C). For instance, the termination zone of most of the direction-sensitive RGCs (dsRGCs) studied, is located in the shell of the dLGN (Seabrook et al., 2017).

Different regions can also be defined based on the three morphologically distinct thalamocortical cell classes: X cells, Y cells and W cells (Figure 3D). The latter can be found mainly in the shell, while X and Y cells are located in the core. Though there is evidence that points to the existence of at least two different types of inhibitory neurons, it is currently unclear whether these neurons are preferentially located in specific regions of the dLGN.

The division into different functional subregions based on TC cell type and retinogeniculate innervation pattern also has implications for the thalamocortical projections to V1. It appears that segregated parallel information streams are send to V1 informing about different visual features (Seabrook et al., 2017). For instance, W cells located in the shell of the dLGN, receive strong convergent input from ON-OFF dsRGCs and OFF-dsRGCs informing about the directional features of the visual stimulus (Cruz-Martín et al., 2014). In addition, these W cells also receive strong retinotopically matched input from the superior colliculus, a region which is involved in stimulus motion processing and eye position. In turn, these W cells project to superficial layer 1 and layer 2/3. In contrast, non-directionally tuned information from the canonical centre-surround RGCs is sent to the X and Y neurons of the dLGN, which in turn project to layer 4, the canonical thalamocortical recipient layer of V1 (Cruz-Martín et al., 2014). These findings suggest that the regionally restricted TC cell types are part of parallel pathways carrying information about distinct features of the visual scene to the primary visual cortex.

1.2.3 The primary visual cortex: the first stage of cortical processing

The neurons of the primary visual cortex (V1) are structured in six horizontal layers, which are characterized by a different composition of cell types and wiring schemes. Anatomical and electrophysiological studies have revealed a canonical interlaminar circuitry in the cortex (Bannister, 2005). As visual information travels through the different layers, important processing steps take place. While thalamocortical (TC) innervation

of neurons is reported for all cortical layers, the majority of the TC axons terminate in layer 4 (L4) (Ji et al., 2016). In L4 of V1, thalamocortical axons from the core dLGN synapse onto the main excitatory cell type in L4, the pyramidal neurons. From L4, information is sent to pyramidal neurons located in layer 2/3, from where it travels to deeper layers 5 and 6. Corticothalamic feedback projections originate from these deep layers. Notably, GABA-ergic interneurons providing inhibitory feedback to pyramidal cells, modulates neuronal activity within this circuitry.

As is the case in higher mammals, thalamocortical recipient neurons in L4 of V1 can be divided into two broad groups based on their receptive field properties: simple and complex cells. Both cell types respond primarily to oriented edges and gratings. Yet, the receptive field of simple cells have separated ON and OFF subregions, while complex cells do not possess defined ON and OFF zones and are therefore spatial invariant in their response (Niell, 2015). As opposed to higher mammals, these complex cells are less abundant in mouse V1. Furthermore, with an average size of 14 degrees, the receptive fields of mouse V1 neurons are big in comparison (Hübener, 2003).

Besides a division in different subtypes based on the stimulus position in the visual field, V1 neurons are also specialized for processing different attributes of the stimulus, such as orientation and motion direction. While the number or orientation responsive cells are numerous in primate V1, mouse V1 is characterized by a large number of non-oriented cells, including neurons that have a typical centre-surround receptive field organization (Niell, 2015). Interestingly, neurons with distinct receptive field properties are predominantly localized in specific cortical layers (Hübener, 2003); neurons with centre-surround receptive fields are mostly found in layer 4 while oriented cells are most abundant in layer 2/3.

V1 neurons and their thalamocortical input are also organized in such a way that their firing pattern conveys information about their spatial relationship. As mentioned in the previous section, neighbouring TC neurons project to neighbouring V1 neurons, thereby conveying information about their spatial relationship. As a result, the V1 of both hemispheres provide multiple overlapping retinotopic maps, representing different features of the visual space of the contralateral visual field (Seabrook et al., 2017) (Figure 4).

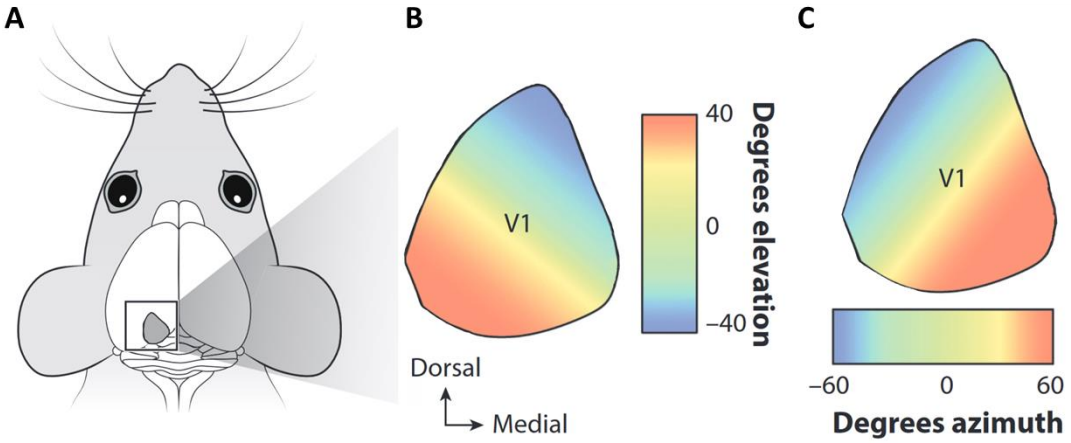

Figure 4 Retinotopic maps in mouse V1 (A) Location of the primary visual cortex (V1) in the mouse brain. (B) The retinotopic map of the visual space along the vertical axis (elevation) and (C) the horizontal axis (azimuth). [Adapted figure from Seabrook et al., 2017]

One of the hallmarks of the cortical architecture of higher mammals is the organization of neurons with similar response properties into columns, such as orientation preference and ocular dominance columns (Hübener, 2003). Mouse V1 lacks apparent orientation preference columns. Instead, orientation-selective cells are organized in a salt and pepper distribution. Since the input from the ipsilateral eye is limited in mouse V1, ocular dominance columns are also missing in mouse V1 (Seabrook et al., 2017). Instead, TC axons from the contralateral zone of the dLGN project to the entire primary visual cortex, while axons from the

ipsilateral eye terminate in a smaller subregion of V1, the binocular zone in which the majority of neurons is responsive to stimulation from either eye (Hübener, 2003). Even though it appears that a columnar organization of similar tuned neurons is lacking in mouse V1, evidence suggest that V1 might be to some extent modularly organized (Hübener, 2003; Ji et al., 2016). For instance, cell responses of neurons recorded in the same z-axis often have similar response characteristics including preferred orientation tuning. This result is more likely to be explained by the existence of some organisational principle then by mere chance. Furthermore, patches of neurons in L1 seem to receive clustered feedback and thalamocortical projections (Ji et al., 2016).

The primary visual cortex (V1) thus preserves the retinotopy outlined in the retina and dLGN, and performs cortical computations across layers that give rise to feature selectivity, including a preference of orientation, direction and/or spatiotemporal frequency. V1 in turn, sends information to higher visual areas where further visual processing takes place. Since the development of V1 is central to the main question of this thesis, the next chapter will discuss the developmental specification of pyramidal cell types of V1 and their wiring.

1.3 The developing brain: how the building blocks for vision are created

Early in embryonic development, undifferentiated neuroepithelial cells populate the ventricular zone (VZ), which is located in the telencephalic wall of the lateral ventricles. From this limited number of cells, the diverse glutamatergic neuronal and glial cell populations of the forebrain are generated (Lodato and Arlotta, 2015; Parnavelas, 2000; Woodworth et al., 2012). Apical radial glia in the VZ can self replicate in an asymmetric division, thereby producing an intermediate progenitor (IP) cell or a neuron. Most pyramidal neurons of the mouse cortex, however, are generated by the symmetric division of the IP cells, resulting in two neurons. The IP cells form a new germinal zone, called the sub-ventricular zone (SVZ). This second germinal zone persists during adulthood and is the largest region for neurogenesis in the adult brain. Next to IP cells, a second class of progenitors populate the SVZ, the basal radial glial. While these cells produce most of the cortical neurons in the human brain, only a few neurons in the mouse brain originate from these cells. The majority of the interneurons of the mouse brain are generated in distinct germinal zones called the medial and caudal ganglionic eminences (Batista-Brito et al., 2020).

The generation of the excitatory pyramidal neurons of the forebrain proceed in a precise temporal sequence starting at embryonic day 11.5 (E11.5) in the mouse (Hansen and Hippenmeyer, 2020; Kriegstein and Noctor, 2004; Nadarajah and Parnavelas, 2002). The pyramidal neurons that are generated first, migrate radially out of the VZ and SVZ and accumulate below the pial surface to form the preplate. The next group of post-mitotic pyramidal neurons migrate into the middle of the preplate, thereby dividing the preplate into a superficial marginal zone, the prospective Layer I of the cortex, and the deeper located subplate. The subplate is a transient developmental structure that assists in multiple developmental processes (Kanold and Luhmann, 2010). Next, pyramidal neurons of the deep layers of the cortex are produced, while neurons of progressively more superficial layers are generated subsequently during embryonic development (Figure 5A). These post-mitotic neurons migrate radially past the existing layers towards their appropriate laminae. In contrast, inhibitory neurons follow a distinct migratory route. They travel to their target location tangentially along corticofugal axon bundles from different laminae (Parnavelas, 2000). While at birth all cortical neurons have been born, neuronal migration towards the superficial layers of the cortex is still ongoing. At postnatal day 7 (P7) neuronal migration is completed and all cortical layers can be clearly distinguished in cross sections of the brain (Farhy-Tselnicker and Allen, 2018).

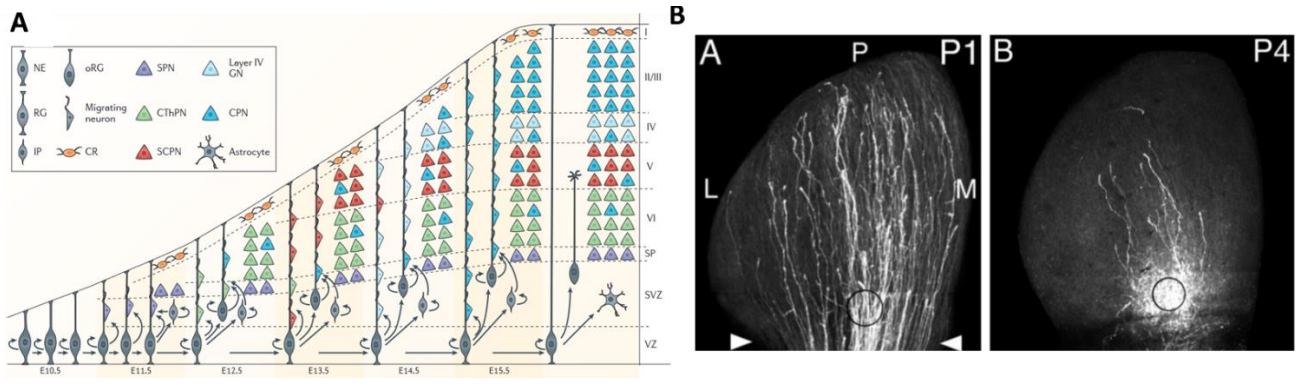

Figure 5 (A) Projection neurons of the different cortical layers are generated in an inside-out fashion, (B) axonal development is characterized by extensive arborization followed by the pruning of erroneous branches. (A) First neurons of the deeper layers are generated in the sub- and ventricular zone (SVZ and VZ), followed by subsequently more superficial layers. These neurons travel radially to their appropriate target layer with the help of radial glia cells (RG). SP = subplate, I-VI, layer 1 to 6. NE = neuroepithial cell, IP = intermediate progenitor, CR = Cajal-Retzius cells, SPN = subplate neurons. (B) Once axons have arrived at the target location, axons will start to arborize extensively. This is followed by a period of refinement in which aberrant branches are eliminated while correct connections are strengthened. [Figure adapted from Greig et al. (2013) and McLaughlin et al. (2003)]

The rise of distinct pyramidal subtypes is largely orchestrated by the activation of cell type specific transcription factors in the postmitotic neuron. While immature neurons migrate away from the germinal zone, the genetic profile of the neuron resembles more and more their adult genetic profile the closer it comes to its target region (Lodato and Arlotta, 2015). Interestingly, the functional input pyramidal neurons receive, seem to also exert influence on the cell-type specific genetic programs (Oishi et al., 2016; Pouchelon et al., 2014)

Once neurons have reached their appropriate location, dendrites and axons start to extend to form connections with appropriate target neurons. The developmental process of axon pathfinding has been extensively studied in the past decades. These studies have shown that the tip of the axon, the axonal growth cone, is equipped with specific receptors that can respond to extracellular cues. The axon is steered in the correct direction through the process of chemo attraction, chemo repulsion, contact attraction and contact repulsion (Aberle, 2019; Kolodkin and Tessier-Lavigne, 2011). Once arrived at the target location, axons start to branch and form immature synapses with neurons in their target region. During the process of axonal refinement, aberrant connections are eliminated while correct connections are strengthened (Oşan et al., 2011, see Figure 5B). Similarly, the dendritic structure is also refined through the process of both elongation and pruning of dendritic trees. Both the axonal and dendritic refinement seem to be regulated by activity-dependent processes (Lohmann et al., 2002; Ruthazer et al., 2003; Wong and Ghosh, 2002).

In the above section, I only provided a snapshot of the developmental processes that are central for the generation of a mature neuron from a progenitor cell. For detailed information on the process of neurogenesis, migration and cell-type differentiation I happily refer to some excellent reviews on these topics (Aberle, 2019, 2019; Greig et al., 2013; Kolodkin and Tessier-Lavigne, 2011; Kriegstein and Noctor, 2004; Lodato and Arlotta, 2015). In the sections below I will zoom in on two developmental processes that are central to this thesis. In the first section the process of thalamocortical axon ingrowth into the cortex is described. In the second section I will provide an overview of the available literature on the dendritic development of cortical neurons.

1.3.1 Thalamocortical axon ingrowth

Both thalamocortical projecting neurons as well as corticothalamic projections have to cross several so-called boundary zones on their path to their target regions. These boundary zones, including the diencephalic-telencephalic and the subpallial boundaries are characterized by distinct genetic expression profiles. Corridor neurons in the subpallium, guide the axons through gradients of axon guidance cues through these otherwise non accessible boundary zones (Hanashima et al., 2006). Furthermore, these secreted axon guidance gradients also initiate the sorting of the different thalamocortical axons from distinct thalamic nuclei in a rostral-caudal axis based on their cortical targets (López-Bendito, 2018). Further topographic sorting is achieved in the ventral telencephalon. A diverse set of axon guidance cues and ligand-receptor pairs have been found to be important for areal targeting of thalamocortical axons (López-Bendito, 2018). Among these are ephrins and ephrin-binding receptors (Gezelius and López-Bendito, 2017). Distinct cortical regions express a specific set of guidance molecules and membrane-bound molecules and release both specific repulsive and attractive factors. Axons from different thalamic nuclei express a distinct pool of receptors that can sense these guidance molecules along their path to their target region.

Besides the importance of the previously described attractive and repulsive factors, axon guidance cues and ligand-receptor interactions, growing thalamocortical axons also interact with certain cell populations they encounter along their long route to the cortex. These cell populations guide them in the correct direction and direct synaptogenesis with targeted neurons. One of the proposed interactions is that between thalamocortical axons and corticothalamic axons, which appear to be closely intermingled in the internal capsule. This hypothesis is known as the handshake hypothesis (López-Bendito and Molnár, 2003). The handshake hypothesis has been heavily debated since its proposal, driven by *in vitro* results demonstrating

that thalamocortical and corticothalamic axons repel each other (Bagnard et al., 2001). Recently however, it seems that some consensus have been reached on the matter (Deck et al., 2013; Dumoulin and Stoeckli, 2022; López-Bendito, 2018). A study by Chen and colleagues (2012) adopting conditional mutagenesis has shown that in absence of corticothalamic projections, thalamocortical axons are unable to cross the pallial-subpallial boundary. Evidence for a close interaction between both types of axons proposed in the original hypothesis was however not found. Instead, it appears that corticothalamic axons function as a corridor for thalamocortical axons in the otherwise non permissible pallial-subpallial boundary zone.

Another neuronal population that seems to be important in establishing correct thalamocortical connections, are the neurons of the subplate. The subplate is a transient layer below the embryonic cortical plate. Though the majority of subplate neurons have died at the end of the third postnatal week, a small fraction of subplate neurons survive and form layer 6b in the adult cortex (Kanold and Luhmann, 2010). The subplate is a conserved region across species, though the size of the subplate varies between species (Wang et al., 2010). Subplate neurons are among the first born neurons and electron microscopy have revealed that subplate cells already receive numerous synaptic contacts at E15 (Del Rio et al., 2000). The subplate plays an essential role in various developmental processes, including the guidance of thalamocortical axons to appropriate cortical target areas. Deletion of subplate neurons in the cat visual cortex by injecting the toxic kainic acid prevented the axonal ingrowth of dLGN axons into the visual cortex. Instead, thalamocortical axons continued their path in the internal capsule and passing the visual cortex in the process (Ghosh et al., 1990). In addition to its role in sorting thalamocortical axons to their corresponding projection area, subplate neurons are also part of a transient cortical circuit linking thalamocortical axons and L4 neurons together during embryonic development (Kanold, 2019; Molnár et al., 2020; Zhao et al., 2009). Upon reaching their target area, thalamocortical axons accumulate in the subplate before innervating the cortical plate. This axonal waiting period, is observed for multiple systems and in numerous species, though the length of the waiting period varies between species (Deck et al., 2013). In higher mammals, such as the cat and the primate, the waiting period lasts in the range from weeks to months, while in the rodent brain this period is much shorter (Ghosh et al., 1990; Herrmann et al., 1994; Miller et al., 1993; Molnár et al., 1998). Thalamocortical axons of the mouse brain are shown to accumulate around E15 and while a few axons already innervate the cortical plate at E16, the majority of axons wait two days before innervation (Del Rio et al., 2000; Deng and Elberger, 2003). Thalamocortical axons have been shown to form synaptic contacts with subplate neurons during the waiting period (Herrmann et al., 1994; Zhao et al., 2009). Similarly, many subplate neurons form excitatory synapses onto L4 neurons and L1 neurons, thereby forming a disynaptic pathway connecting first-order thalamocortical axons with their corresponding cortical target neurons (Kanold and Luhmann, 2010; Zhao et al., 2009). This transient circuitry has been found to be important in several developmental processes. Ablating the subplate neurons in the cat visual cortex through immunotoxin and kainic acid injections, have been shown to impair ocular dominance column formation and prevent the maturation of thalamocortical synapses onto L4 neurons (Kanold et al., 2003; Kanold and Shatz, 2006). Furthermore, subplate ablation prevents the maturation of the inhibitory network, thereby creating an imbalance in excitation and inhibition in the mature network (Kanold and Luhmann, 2010). Studies in the rat have found data in support of these findings (Dupont et al., 2006; Tolner et al., 2012). Overall, the data presented above suggest that the transient circuitry between thalamocortical neurons, subplate cells and targeted cortical neurons, may provide the cortical neurons with an instructive signal for thalamocortical and intracortical circuit integration (Kanold, 2019; Molnár et al., 2020).

Timeline of thalamocortical ingrowth

Since the aim of this thesis is to address the question how thalamocortical input affects the development of the primary visual cortex, insight into the developmental timeline of axon ingrowth is important. A number of studies have been performed in the early nineties, in a variety of species, to establish when thalamocortical axons innervate L4 of the cortex. These studies have mostly used the placement of DiI crystals in (part of) the

dorsal thalamus at various embryonic and postnatal ages to visualize the thalamocortical axons. The interpretation of these studies is challenging for several technical reasons. DiI crystals need to be placed in post-fixated tissue which needs to be kept in fixative solution for several weeks for the dye to travel along the entire length of the axon. This will likely affect the brain's structural integrity. In addition, the dorsal thalamus needs to be exposed for DiI placement, which requires the dissection of several brain areas covering the thalamus. Furthermore, once corticothalamic axons have arrived in the dorsal thalamus, these axons and their respective cortical neurons are also labelled in the cortex. Despite these limitations, these early DiI studies provide some insight into general thalamocortical development.

DiI placement in the dorsal thalamus of the cat have shown that axons arrive and wait in the subplate between embryonic day 38 (E38) and E50. In the following ten days axons start to invade the cortical plate. From E60 onwards, when L4 of the cat visual cortex is established, axons start to make elaborate terminals in L4 which progresses after birth (E65/P0) until the end of the first postnatal week (Ghosh et al., 1990). In rodents, both the waiting period and the period of ingrowth seem to be considerably shorter (Del Rio et al., 2000; Deng and Elberger, 2003; Miller et al., 1993; Molnár et al., 1998). For rats, with a gestational period of 21 days, a short waiting period of two days was reported until E19. Thereafter, axons start to penetrate the developing cortex (Molnár et al., 1998). Studies in the mouse brain reported a similar timeline of axonal ingrowth. At birth, axons started to detach from the subplate and grow into the cortical plate. By P3, all axons had lost their growth cones and axonal arbors started to form in L4. This axonal arborization expanded in the subsequent days (Auladell et al., 2000; Del Rio et al., 2000; Deng and Elberger, 2003). For DiI crystals placed in the ventral posteromedial nucleus (VPM), a first-order thalamic nucleus projecting to the somatosensory cortex, the barrels, a characteristic anatomical hallmark of the somatosensory cortex created by the organization of the thalamocortical axons, started to appear around P7 (Agmon et al., 1993; Deng and Elberger, 2003).

While most of the early DiI studies described above have focused on studying the thalamocortical innervation of L4, a study by Portera-Cailliau and colleagues (2005) have explored the timeline of ingrowth in L5a and L1 of the barrel cortex. Axons from the higher-order thalamic nucleus called the posterior medial nucleus, project to L5a and L1 of the mouse barrel cortex. In this study, thalamocortical axons were genetically labelled by the expression of the green fluorescent protein (GFP) and imaged *in vivo* in the barrel cortex with time-lapse two photon imaging between P5 and P19. Thalamocortical axons in L1 and L5a showed remarkable structural dynamics within the time period explored. The first week of postnatal development was marked by a rapid rate of TC axon arborization and retraction. For instance, at the end of the first postnatal week an axonal branch of around 800 micron was degenerated or retracted in a period of 24 hours, while new branches were simultaneously formed. The overall growth of axonal arbors outweighed the pruning events, leading to an increase in axon density during the first postnatal week. In contrast to the dynamic axonal branches formed in the first postnatal week, branches formed in the second postnatal week showed a lower rate of degeneration and retraction (Portera-Cailliau et al., 2005). This study therefore shows that thalamocortical axons and arborization can undergo major structural changes during the first week of postnatal development.

The above-described studies have been conducted in a variety of species looking at innervation patterns of the cortical plate in general, often not describing in which thalamic nuclei the DiI crystal was placed. Since neurons of distinct cortical regions and layers are characterized by different developmental trajectories (Bayer and Altman, 1991; Clancy et al., 2001; Ozkan et al., 2020), a comprehensive overview of the dynamics of thalamocortical ingrowth in specific regions of the mouse cortex, including the innervation of L4 of the visual cortex, is still missing. Nevertheless, the available studies provide a valuable impression of the course dynamics of axon ingrowth in the mammalian cortex.

1.3.2 Dendritic development of cortical neurons

At the same time that thalamocortical axons develop an elaborate arborization pattern in the cortex, cortical neurons are integrated in the thalamocortical and intracortical circuitry by extending their dendrites and forming synapses. Dendritic branching is next to axonal branching essential for circuit integration, as it determines the degree and nature of input the neurons receives. Furthermore, dendrites have an important function in filtering signals from multiple pre-synaptic neurons by integrating these signals into a single response, a process which is called dendritic integration (Branco and Häusser, 2011; Magee, 2000). In general, neurons display cell type-specific patterns of dendritic branching, underlying the fact that different cell types could be part of distinct circuitries and fulfil different tasks (McAllister, 2000). Furthermore, functionally-related input have been shown to cluster on common target dendritic branches (Ujfalussy and Makara, 2020; Winnubst et al., 2015).

Studies in the last decades adopting organotypic brain slice cultures, have revealed some of the molecular mechanisms that control the elemental dendritic architecture of cortical neurons during development. Dendritic outgrowth as well as the extension of the axonal projection commences once cortical neurons have arrived at their target location. A first step in dendritic differentiation in pyramidal neurons, is the extension of the apical dendrite towards the apical surface. The axon from a pyramidal projecting neuron grows towards the ventricle where the axons from multiple projecting neurons are organized in bundles. Surprisingly, one single signalling molecule, the semaphoring 3A (Sema3A), is responsible for the outgrowth of the apical dendrite towards the pial surface as well as the outgrowth of the axon in the opposite direction (Polleux, 1998; Polleux et al., 2000). A sufficient increase in intracellular cyclic guanosine monophosphate (cGMP) will cause the neuron to perceive Sema3A as a chemoattractant. Due to an asymmetric localization of the enzyme that regulates cGMP production in immature cortical neurons, Sema3A can act both as a chemorepellent as well as a chemoattractant to respectively the axon and apical dendrite of a neuron.

In addition, certain neurotropic factors have been shown to be important in regulating the development of the dendritic tree. Several neurotrophins have been shown to rapidly increase the dendritic complexity of pyramidal neurons, measured by an increase in total dendritic length and branchpoint number 24 hours after neurotrophin application (McAllister, 2000). Certain neurotrophins only affect the dendritic arbor development of neurons from specific layers. For example, L4 neurons are strongly affected by the presence of neurotrophin-3, displaying a rapid increase in dendritic complexity after exposure, while L5 neurons are unaffected. The Notch signalling pathway also strongly influences the dendritic architecture during development (Redmond et al., 2000). Notch signalling positively impacts the degree of dendritic branching, conversely total dendrite length and segment length are negatively influenced by Notch signalling. Furthermore, it appears that newly grown synapses influence the dendritic development of the neuron by selectively stabilizing the dendrites to which they have formed synapses on and by promoting the outgrowth of new branches (Cline and Haas, 2008; Niell et al., 2004). This so-called synaptotrophic growth, is likely to be regulated by calcium-dependent transcriptional programs (Cline and Haas, 2008).

While our understanding of the molecular mechanisms underlying general principles in dendritic development has grown, little data is available on how dendrites from distinct classes, layers and sensory regions develop over time. Several studies have been performed to study dendritic development of cortical neurons in the intact brain. A study by Callaway and Borrell (2011) explored the dendritic development of L4 neurons in the visual cortex (V1) of ferrets. The excitatory neurons of adult V1 in ferrets, as opposed to mouse V1, is composed of predominantly spiny stellate cells (80%) which are easily distinguished from the pyramidal neurons by their distinct dendritic morphology; pyramidal neurons have an apical dendrite which extends towards the pial surface of the cortex, which is absent in stellate cells. Surprisingly, the authors reported that all L4 neurons possessed an apical dendrite at early developmental stages, which the majority of cells lost during development to acquire the typical stellate morphology (Callaway and Borrell, 2011). This observation

was later also observed with two-photon imaging in the mouse somatosensory cortex (S1), which similarly to ferret V1 consists mainly of stellate cells (Nakazawa et al., 2018). While at P3 the majority of L4 neurons retained an apical dendrite, this was pruned at P6. Besides the major restructuring of the apical dendrite that occurred in mere days, they also observed a massive reorganization of the basal dendritic tree within the same time period. In the adult barrel cortex, the part of the somatosensory cortex associated with processing whisker stimulation, all L4 stellate cells have dendrites that extend asymmetrically within a single barrel. While basal dendrites displayed a symmetrical organization at P2, dendrites rearranged themselves within in the course of a few days to acquire the adult asymmetrical dendritic organization at P6 (Mizuno et al., 2014; Nakazawa et al., 2018). Furthermore, it appears that many of the developmental processes that lead to dendritic reformation, are influenced by spontaneous activity. This topic is covered in the subsequent subchapter.

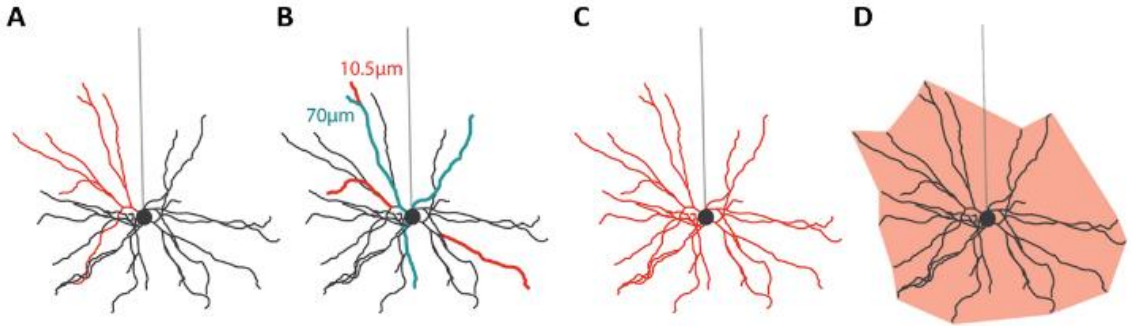

Figure 6 Example of commonly analysed dendritic parameters All figure panels show the same traced neuron but highlight distinct parameters that can be extracted from the image. The vertical grey line represents the orientation of the apical dendrite, which is not shown in the tracing. (A) in red a single dendrite, or dendritic tree is highlighted. (B) a dendritic tree consists of distinct segments (red). Different paths (blue) can be defined within a single tree, by following distinct segments at branch points. (C) in red, all individual dendrites, or the total dendritic tree is highlighted. The total arbor length is a sum of all individual segment lengths and is thus the length of the total dendritic tree. (D) one way to describe the complexity of a dendritic tree is by evaluating the volume of the tree. [adapted figure based on Richards et al., 2020]

The majority of studies on cortical dendritic development in the intact brain have explored dendritic changes of neurons in the somatosensory cortex. This is mainly because the developmental changes in dendritic morphology are easily captured in L4 S1 neurons, since adult S1 neurons are characterized by a distinct asymmetrical dendritic morphology. Adult V1 L4 neurons lack such a clear specification in dendritic organization. This probably contributes to the fact that the dendritic reorganization during development in mouse V1 is less studied. Nevertheless, a recent study by Richards and colleagues provided a detailed description of postnatal dendritic arbor development of pyramidal neurons from L2/3 in the mouse visual cortex (Richards et al., 2020). In this study they reconstructed Golgi-stained neurons in brain slices acquired at different timepoints between P7-P30. This encompasses a time period before eye opening (at P14) and the critical period after eye opening (±P21-P33, van Lier et al., 2020)). During this period, V1 displays an increased sensitivity and plasticity to environmental stimuli. Most parameters describing the basal tree, did not change significantly before eye opening (P7 and P12 timepoints), including the total arbor length, the segment length and the number of segments (see Figure 6 for description of parameters). Between P16 and P21 the total arbor length increased substantially, which is likely attributed to an increase in individual segment length. To capture the complexity of the basal arbor, they calculated the total volume of the arbor as well as the arbor density, which is the dendritic volume divided by the arbor volume. Arbor volume remained stable before eye opening and slightly increased at P16, while by P30 arbor volume had tripled. The arbor density showed interestingly a significant increase between P7 and P12, followed by a decrease at P16, which suggest that dendritic tree complexity could increase during early postnatal development and decrease thereafter.

While the main focus of this study was to map dendritic changes under the influence of stimulus-evoked activity, this study already provides some insight into the dendritic development of V1 L2/3 neurons before eye opening. Surprisingly, only minor changes were observed in dendritic parameters before eye opening. However, since neurons of different layers have distinct characteristics and generally specific patterns of dendritic branching (McAllister, 2000), L4 neurons could exhibit a different pattern of dendritic development. Given that L4 is the primary recipient layer of thalamocortical input, insight into the normal dendritic development of L4 neurons is important before studying the impact of spontaneous activity on thalamocortical and intracortical circuit integration of L4 neurons. Furthermore, placing dendritic development of L4 V1 neurons in the context of the development of thalamocortical innervation, will probably raise a hypothesis on if and when these developmental processes interact.

1.4 How (spontaneous) activity helps shape the brain

In the traditional view of neuronal development, the first rough organization of circuitry is laid out by innate genetic programs. The further refinement of these crude circuits into sophisticated neuronal networks underlying perception and complex behaviour was mostly attributed to activity-dependent plasticity mechanisms during the so-called critical period. A vast amount of evidence, however, has modified this strict segregation and has shown that an intersection exists between the genetic developmental programs and activity in the form of both stimulus-induced and spontaneously generated activity.

Spontaneously generated activity can be observed during development in a wide variety of species, including in the fly (Akin et al., 2019), rodent (Blankenship and Feller, 2010), cat (Sretavan and Shatz, 1984) and human brain (Tolonen et al., 2007). While spontaneous activity in higher vertebrates is mostly visible in the embryonic brain, spontaneous activity can still be observed in the postnatal brain in rodents and cats. Studies using these model species have shown that spontaneous activity is generated across the central nervous system, including in the spinal cord (Gonzalez-Islas and Wenner, 2006; Landmesser and O'Donovan, 1984), hippocampus (Ben-Ari et al., 1989; Garaschuk et al., 1998), thalamus (Xu et al., 2011), cerebellum (Watt et al., 2009), neocortex (Khazipov and Luhmann, 2006) and in developing sensory epithelia such as the retina (Sretavan and Shatz, 1984) and cochlea (Tritsch et al., 2007). In the somatosensory system of the rodent brain, spontaneously generated activity is generated by involuntary muscle twitches of the whiskers (Khazipov et al., 2004). Notably, these different forms of spontaneous activity are all characterized by the bursting of many neighbouring neurons, thereby encoding spatial information in the temporal firing pattern, followed by a refractory period (Blankenship and Feller, 2010; Kerschensteiner, 2014; Martini et al., 2018). This is in part due to evolutionary conserved mechanisms underlying the different types of spontaneous activity (Kerschensteiner, 2014). Furthermore, the patterned activity generated in the sensory periphery is transmitted to the sensory cortices through their respective first-order thalamic nuclei.

To better understand the influence of spontaneous activity on neuronal development, the mouse visual system and the associated spontaneous retinal waves has proven a useful model. Since retinal wave patterns persists after birth until eye opening, it is possible to study the influence of spontaneous activity on visual development largely without the interference of sensory experience (Martini et al., 2021). Furthermore, many important visual response features, such as direction selectivity and orientation selectivity already exist at eye opening (Rochefort et al., 2011; Thompson et al., 2017a). The developmental processes that take place within the first two weeks of postnatal development are thus crucial to prepare the visual system for the onset of vision. Notably, the concurrence of spontaneous activity within this same time period points to an instructive role for spontaneous activity in the development of the mouse visual system.

1.4.1 Retinal waves

Retinal waves are characterized by spontaneous bursts of action potentials in which adjacent retinal ganglion cells (RGCs) fire in sequence. As a result, a wave of depolarization travels across the retinal plane. Similar to other forms of spontaneous activity that occur during development, retinal waves and its main characteristics have been conserved across many species (Ford and Feller, 2012). For instance, retinal waves are initiated at random positions on the retinal plane and stop at distinct and dynamic borders. Furthermore, RGCs that participated in a retinal wave require a refractory period of around one minute before they can be part of a new travelling wave. For most species, retinal waves can be classified in subtypes based on the different molecular mechanisms that underly the generation of the spontaneous patterned activity.

In mice, retinal wave activity can be divided in three subsequent classes; stage I retinal waves can be observed from embryonic day 16 till day 18, while stage II and stage III waves are observed in the postnatal retina from respectively P0-P10 and P11-P14 (Bansal et al., 2000; Kerschensteiner, 2014). The mechanism underlying the generation and spatial-temporal properties of the spontaneous retinal wave activity of type II and III has been

extensively studied, in comparison, the study of type I waves has received little attention, which is probably due to its embryonic timing. Nevertheless, a recent study by Voufo and colleagues (2022) studied the mechanisms underlying the generation of stage I waves by applying different pharmacological inhibitors. Application of a gap junction antagonist reduced both the number of RGCs participating in a single wave as well as decreased overall wave frequency. Furthermore, application of an antagonist binding to multiple classes of nicotinic acetylcholine receptors (nAChR), abolished embryonic wave activity. In contrast, the specific antagonist for the β2 subunit of nAChRs, which is central in the generation of stage II waves, did not block retinal wave activity. These results suggest that both specific nAChRs and gap junction signalling is involved in the generation and propagation of retinal stage I waves (Voufo et al., 2022). Considering the early onset of stage I waves and its coincidence with several early developmental processes that are important for the correct wiring of the retinal circuitry, stage I waves could have a big impact on retinal development. Future studies on the molecular mechanisms underlying stage I waves and their influence on the development of retinal circuitry will therefore provide valuable insight for understanding how the normal as well as pathological retinal circuit is formed during early development.

The generation of stage II waves, or so-called cholinergic waves, depends on the rare spontaneous depolarizations of cholinergic starburst amacrine cells (SACs) in the developing retina (Ford et al., 2012; Maccione et al., 2014; Thompson et al., 2017b; Zheng et al., 2004). Through recurrent gap junction connections between the SACs, the depolarization wave spreads to the connected SACs, thereby inducing the release of acetylcholine (ACh) and GABA. This in turn activates nACh and GABA-A receptors of both SACs and RGCs. Early in development, GABA-A receptor activation acts depolarizing until GABA-A signalling matures at around P7 (Thompson et al., 2017a). As a result of the direct cholinergic input and excitatory input from SACs and GABAergic input, RGCs fire and a wave of depolarization spreads across the retinal plane. This spatial-temporal patterned activity is not limited to the retina, but can also be observed in the superior colliculus (SC), the dorsal Lateral Geniculate Nucleus (dLGN) and primary visual cortex (V1) (Ackman et al., 2012a; Hanganu et al., 2006). Studies that administered antagonists or used a genetic mouse model that affected specific subtypes of nAChRs, revealed that specific subunits of the nAChRs, α3 and β2, are essential for the cholinergic signalling underlying the spatial-temporal pattern of retinal II waves. The β2 knock out mouse model have been since extensively used in studies exploring the influence of stage II waves on visual circuitry development. Due to the developmental switch in GABA-signalling, cholinergic waves have slightly different characteristics during development. Cholinergic waves in the first postnatal week of development travel slowly, over large areas with only few neurons participating in a wave event while waves becomes smaller and recruit more neurons as GABA signalling matures in the retina (Maccione et al., 2014). Furthermore, retinal waves have a preferred temporal-nasal direction of travel during late cholinergic waves and early stage III waves (P8-P11) (Ge et al., 2021).

The transition from cholinergic waves, to stage III waves appears to be tightly linked; a disruption of stage II waves leads to a premature initiation of stage III waves, while abolishing stage III waves will extend the period in which cholinergic waves can be observed (Xu et al., 2016). The mechanism underlying this transition is currently not understood. Compared to cholinergic waves, stage III waves are smaller, more frequent, and appear to be confined to several preferred regions. Furthermore, as opposed to stage II waves, stage III waves are not initiated by the spontaneous firing of a cell in the retina. Instead the generation of stage III waves, or glutamatergic waves, are generated by the amplification of coincident membrane fluctuations in the retinal network (Kerschensteiner, 2016). Depolarization of ON cone bipolar cells induces the release of glutamate into the synaptic cleft. In response, ON cone bipolar cells that express ionotropic glutamate receptors (iGluRs), as well as amacrine cells fire. Other ON cone bipolar cells get activated through gap junction connections with iGluRs possessing bipolar cells and amacrine cells. In turn, OFF cone bipolar cells are activated through amacrine cells in response to an ON cone bipolar depolarization. This results in the lateral

propagation of depolarization in first RGCs that respond to light increments (ON), followed by activation of RGCs that respond to light decrements (OFF (Kerschensteiner, 2016)).

Though direct evidence is lacking, several observations indicate that glutamatergic retinal waves are relayed to V1 (Gribizis et al., 2019; M. Siegel et al., 2012). Yet, it appears that glutamatergic waves drive the cortex less than the earlier cholinergic waves (Gribizis et al., 2019; M. Siegel et al., 2012). The onset of glutamatergic waves coincide with the time that the first light responses can be observed in RGCs (Tiriac et al., 2018). It therefore can be expected that light exposure can influence the glutamatergic waves. Indeed, light stimulation through the close eye lids in the days preceding eye opening elicited a glutamatergic wave in 50% of the cases (Tiriac et al., 2018). These induced retinal waves did not differ in properties from spontaneously generated glutamatergic waves. It is important to note that while light exposure does increase the occurrence of spontaneous glutamatergic waves, no stimulus induced visual processing can be observed (Rochefort et al., 2011). Thus, activity in the different areas of the visual system is predominantly spontaneous in nature before eye opening.

1.4.2 The influence of retinal wave activity on eye-segregation and retinotopic map formation

As both eye-segregation and retinotopic map formation emerge through the sorting of projections from RGC axons during stage II waves (Ackman and Crair, 2014), both are natural candidates of visual features that could be affected by retinal wave distortion. With the knowledge about the mechanisms underlying the generation of the retinal waves, several tools have been developed to disrupt retinal wave generation and/or propagation, including pharmacological manipulation *in vitro* and the generation of mouse mutants. A widely used mouse model in studies on retinal wave influence has been the Chrnb2 mutant ($\beta2^{-/-}$) mouse (Bansal et al., 2000; Leighton and Lohmann, 2016). This mouse model lacks the β2-subunit of the nicotinic ACh receptor which disrupts both the frequency and spatial-temporal pattern of cholinergic retinal waves in the first week of postnatal development and thereby, the information that is encoded and transmitted to the superior colliculus (SC) and dorsal lateral geniculate nucleus (dLGN). Importantly, visual response features of retinal ganglion cells (RGCs) are seemingly not altered in the $\beta2^{-/-}$ mouse, as $\beta2^{-/-}$ RGCs demonstrate normal spatial resolution, ON/OFF segregation and direction selectivity (Bansal et al., 2000; Elstrott et al., 2009; Rossi et al., 2001).

While visual response features in the RGCs appear to be normal, retinal axonal termination zones in the SC are enlarged and elongated in the $\beta2^{-/-}$ mouse, especially along the visual azimuth. This impacts the receptive field size of SC neurons, which are greatly enlarged (Chandrasekaran, 2005; McLaughlin et al., 2003; Mrsic-Flogel, 2005). As a result, a fine retinotopic map is lacking in the SC of β2-/- mice. The retinal termination zone in the dLGN of $\beta2^{-/-}$ animals is also enlarged and more diffuse, especially along the temporal-nasal axis of the visual axis, though the impact on the receptive field size of dLGN neurons in the $\beta2^{-/-}$ is less severe compared to the SC. Correspondingly, while the gross structure of the retinotopic map is intact, the fine-scale retinotopy is distorted, notably along the azimuth (Grubb et al., 2003). This biased retinotopic defect likely arises from the preferred temporal-nasal direction of travel of retinal waves.

Since spatial-temporal patterned activity generated in the retina travels to the primary visual cortex (V1) through the dLGN, retinotopic map distortions are also present in V1. Geniculocortical projections terminate in larger areas within V1, resulting in a defective anatomical and functional receptive field organization in V1 at P8 (Cang et al., 2005) (Figure 7A). Again, this defect was most pronounced along the azimuth. Surprisingly, a later study by Wang and colleagues (2008) demonstrated that receptive field properties, including spatial structure and direction and orientation selectivity, were unaffected in V1 of adult β2-/- mice. Furthermore, $\beta2^{-/-}$ mice performed similarly well as wildtype mice in various visual behaviour tests tasking cortical functions (Wang et al., 2010). As receptive field properties in mouse V1 are not yet matured at the end of the first

postnatal week, glutamatergic retinal waves activity could be responsible for the restoration of receptive field properties by potentially rewiring the geniculocortical circuitry (Kerschensteiner, 2016; Xu et al., 2016).

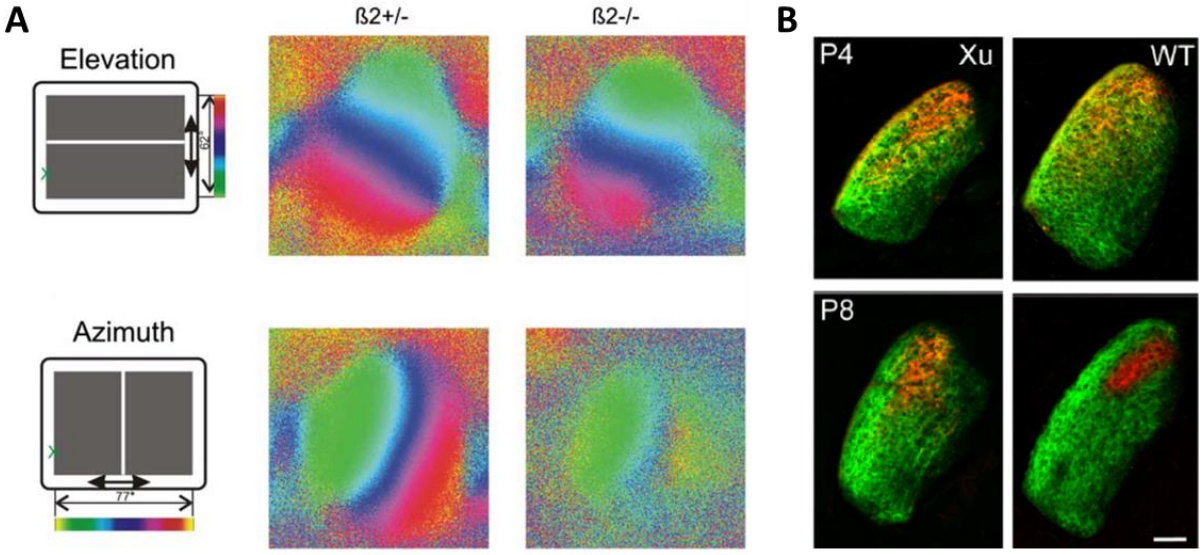

Figure 7 $\beta2^{-/-}$ mice show a defect in retinotopic map formation and eye segregation (A) The fine retinotopic map in the primary visual cortex of $\beta2^{-/-}$ mice is distorted compared to heterozygous littermates. The defect in the azimuth axis of the visual scene is more severe compared to the elevation axis. (B) At P4 retinal ganglion axons have not yet been segregated into distinct anatomical regions in the dorsal Lateral Geniculate Nucleus. At P8, axons are segregated in the wildtype mouses (WT), but not in the $\beta2^{-/-}$ mice (Xu). [Figure is adapted based on images shown in Rubin et al., 2011 and Cang et al., 2005]

In addition to the reported changes in retinotopy, studies exploiting the $\beta2^{-/-}$mutant mouse have reported altered eye segregation in the SC, dLGN and V1 (Burbridge et al., 2014; Rossi et al., 2001; Rubin et al., 2011). For instance, retinogeniculate axons fail to segregate in distinct zones in the dLGN Figure 7B). Furthermore, the binocular field of V1 in $\beta2^{-/-}$ mice is enlarged and the border with the monocular visual cortex is less well defined (Rossi et al., 2001). This can be explained by the observation that in $\beta2^{-/-}$ mice significantly more coincident retinal waves occur in both eyes compared to wildtype mice (Burbridge et al., 2014). As a result, spontaneous activity does not solely synchronize with adjacent retinal ganglion cells within a single eye, but also with the other eye, thereby disrupting the eye-specific association embedded in the pattern of retinal wave activity, resulting in a defect in eye-segregation (Burbridge et al., 2014; Rossi et al., 2001; Zhang et al., 2017). While eye-segregation is established during the period of cholinergic waves, glutamatergic waves also affect eye-segregation. Optogenetic stimulation of retinal ganglion cells in both eyes can disrupt the previously established eye-specific segregation as well as the retinotopic map (Kerschensteiner, 2016).

In addition, both the SC and dLGN display a functional organization in $\beta2^{-/-}$ mice of ON-selective and OFF-selective neurons, which isn't observed in wildtype mice (Chandrasekaran, 2005; Grubb et al., 2003). Normally, SC neurons respond to both light increments (ON) and decrements (OFF). In $\beta2^{-/-}$ mice however, SC neurons demonstrate selectivity. Furthermore, ON-centre and OFF-centre dLGN neurons in $\beta2^{-/-}$ mice are spatially segregated while this doesn't occur in wildtype mice. Potentially, these observations could be explained by the earlier presence of glutamatergic waves in the $\beta2^{-/-}$ retina. While normally glutamatergic waves appear after P10, glutamatergic waves appear at P8 in the $\beta2^{-/-}$ retina (Bansal et al., 2000). Given the subsequent activation of ON and OFF RGCs in the glutamatergic waves, it can be hypothesized that the segregation of ON and OFF visual properties that are observed downstream of the retina in $\beta2^{-/-}$ mice are based on the same bursting-time-dependent plasticity rules underlying eye-segregation. This hypothesis however, remains to be tested (Kerschensteiner, 2016).

Retinal waves in the $\beta2^{-/-}$ mouse model demonstrate both a reduced frequency as well as altered spatial-temporal properties. It was therefore impossible to determine whether defects in retinotopic map formation

and eye segregation are caused by changes in the spatial-temporal pattern of retinal wave activity, on overall activity level, or a combination of both. Furthermore, the studies described above have adopted the global β2 knockout mouse model. Since the β2 subunit of cholinergic receptors is widely expressed in the brain and the eye, defects observed in the $\beta2^{-/-}$ mice could thus be originating from other defects than solely a distortion of retinal wave activity. In recent years, the use of conditional transgenic mice and tailored optogenetic tools has helped to discern the relative influence of the retinal wave's frequency and its spatial characteristics on retinotopic map formation and eye segregation (Kirkby *et al.*, 2013; Leighton and Lohmann, 2016). These studies have shown that the frequency of retinal spontaneous activity is essential for the developmental process of eye segregation in the SC and dLGN (Arroyo and Feller, 2016; Xu et al., 2016). In contrast, the spatial-temporal property of retinal waves encodes information on the spatial relation between neurons and is therefore important for the refinement of retinotopic maps in the SC, dLGN and primary visual cortex (V1) (Ackman and Crair, 2014; Cang et al., 2005; Grubb et al., 2003; Huberman et al., 2008; Kirkby et al., 2013).

1.4.3 The impact of spontaneous activity on the molecular identity, morphology and electrophysiological properties of cortical neurons

As is described in the previous section, a vast number of studies have been conducted to study the impact of retinal wave activity on the development of eye-segregation, retinotopic map formation and the acquisition of receptive field characteristics. The impact on these visual features is attributed to a defect in wiring upstream of the primary visual cortex (V1). Yet surprisingly few studies have been conducted on how spontaneous activity from the periphery influence the functional integration of L4 neurons in local cortical circuits, which depend on the morphology and electrophysiological properties of single cortical neurons. Furthermore, currently no data is available that explored these questions in the visual system. Most of the studies have been conducted in the primary somatosensory cortex (S1), which differs from V1 in some important aspects (BOX 1). Despite these differences, data from studies that explored the influence of (spontaneous) activity in early postnatal development of S1, can provide clues on how spontaneous activity from the periphery influence the development of V1 L4 neurons.

Recent studies in the primary somatosensory cortex (S1) have shown that the molecular identity, morphology and functional properties of postmitotic L4 neurons can change at late stages of differentiation (De la Rossa et al., 2013). Furthermore, it appears that thalamocortical input is instructive for defining L4 cell identity (Oishi et al., 2016; Pouchelon et al., 2014). In a study by Pouchelon and colleagues (2014), the ventrobasalis nucleus (VB), the first-order thalamic nucleus that projects to L4 in S1, was genetically ablated to study the impact of thalamocortical input on S1 development. At P4 all VB neurons had died eliminating all thalamocortical axons. Instead, axons from the posterior nucleus, a higher-order thalamic nucleus that normally only projects to L4 of the secondary somatosensory cortex (S2), grew into L4 of S1. This restructured thalamic input induced changes in the genetic identify of L4 neurons in S1; neurons repressed the expression of typical S1 L4 genes and acquired an expression profile that resembled L4 S2. More importantly, these genetic changes induced by aberrant thalamic input also led to functional response differences compared to wildtype L4 S1 neurons. While normally L4 neurons of S1 only respond to tactile input, L4 S1 neurons of animals in which the VB was ablated now responded to noxious sensory input as well (Pouchelon et al., 2014). A later study by Oishi and colleagues provided additional evidence that cell-type specific genetic programs of L4 S1 neurons are under the control of thalamocortical input. Knockdown of the L4-specific gene Protocadherin 20 (Pcdh20) led to a mislocalization of prospective L4 neurons in L2/3. Furthermore, this misplacement led to a decrease in several L4 marker genes at P2, such as Rorb, while the expression of L2/3 specific genes increased. Furthermore, electrophysiological and morphological properties resembled properties of wildtype L2/3 neurons instead of L4 neurons. This suggest that the environment a neuron is exposed to influences its cell fate. The input a neuron receives is one of the environmental factors that could

contribute to the switch in genetic profile. To study the effect of thalamocortical input on L4 cortical cell fate acquisition, the authors explored expression profiles in Pcdh10 (also known as OL-protocadherin or OL-pc)-knockout mice, in which the number of thalamocortical axons is severely decreased. The expression of L4 specific genes was markedly decreased in these mice while expression of L2/3 markers increased (Oishi et al., 2016). The results from Oishi and colleagues (2016) and Pouchelon and colleagues (2014) therefore strongly indicate that thalamocortical input is instructive in the acquisition of genetic and functional cell fate of L4 in S1.

BOX 1 Not all sensory regions are the same

For interpreting studies on the impact of thalamocortical activity on cortical development, it is important to note that while distinct sensory regions such as the primary visual cortex (V1) and the primary somatosensory cortex (S1) share some common features, they also differ in several important characteristics. First, S1 and V1 differ in cell composition in the adult brain; while pyramidal neurons makes up 99% of the excitatory cell population in V1, stellate cells are the predominant excitatory cell type in S1 (Scala et al., 2019). Likewise, the somatostatin-positive (SOM+) interneurons in L4 of V1 are mostly (92%) characterized as Martinotti cells, sending axons to L1 of V1. In contrast, SOM+ interneurons in L4 of S1 are mostly (96%) terminating in L4 and are defined as non-Martinotti cells. Therefore, the intracortical circuitry likely differs between both sensory regions. Another important difference lies in the timing of developmental processes. The anterior located S1 develops in an earlier time-window than the posterior located V1 (Bayer and Altman, 1991; Clancy et al., 2001; Ozkan et al., 2020). Furthermore, mouse S1 is characterized by the presence of cytoarchitectonic clusters of neurons in L4 called barrels, in which the dendrites of L4 stellate cells are asymmetrically organized. In contrast to S1 no cytoarchitectonic structures are distinguishable in L4 of V1. Instead, adult L4 neurons in V1 appear to have a symmetric organisation of dendrites (Scala et al., 2019). Another important difference between V1 and S1 is that spontaneous activity in V1 can be studied largely independent of stimulus-induced activity. In the developing S1, stimulus-induced whisker activation already commences at birth and therefore stimulus-induced activity exist next to the spontaneously generated activity induced by involuntary whisker twitches. In contrast, spontaneous activity in V1 can be studied largely independent of stimulus-induced activity, as eyelids remain closed until the end of the second postnatal week. During this period, light stimulation through the closed eyelids does not result in visual processing of stimulus features but instead induce a retinal wave (Tiriac et al., 2018).

An important factor for determining how a cell is integrated in the thalamocortical and intracortical circuitry is the dendritic structure of the neuron. Both the length of a neuron's dendrites and the extend of dendritic branching regulates from which area and therefore from how many neurons a neuron is able to receive information. The strength and number of synapses of course also influences this. While the study of Pouchelon and colleagues (2014) reported a change in genetic profile when changing the nature of thalamocortical input they did not explore morphological changes that could underly the functional response difference they reported. While Oishi and colleagues (2016) did explore morphological changes in post-mitotic L4 neurons that were mislocalized to L2/3 after Pcdh20 knockdown, they didn't assess the morphology of L4 neurons in which thalamocortical input was lacking. Furthermore, in both studies, the reported changes in genetic profile and associated changes in functional response properties and morphology, could arise from the lack of, or aberrant thalamocortical input of both structural and/or functional input. Therefore, the exact contribution of (spontaneous) thalamocortical activity for instructing cell-specific genetic programs is currently not known.

A few studies have been conducted to study the influence of thalamocortical activity on the dendritic morphology specifically. Most of these studies have studied L4 neurons in the barrel cortex of the mouse. Adult L4 neurons have a characteristic asymmetric orientation of the dendritic tree, which they acquire around P6 (see Dendritic development of cortical neurons). Dendrites of neurons located at the border of a barrel are facing the inside of the barrel, where thalamocortical axons accumulate (Mizuno et al., 2014). Eliminating the N-methyl-Daspartate (NMDA)-type ionotropic glutamate receptor (NMDAR) in the cortex affects part of the signalling pathway by which thalamocortical as well as intracortical input influence a neuron. In the cortical NMDAR1 knock out mouse, the dendrites of the L4 neurons are symmetrically orientated at P16 (Mizuno et al., 2014). The average dendritic length of NMDAR1 KO neurons was not significantly different from wildtype neurons. Two-photon imaging between P4 and P6 confirmed the histological results. Furthermore it revealed that the development of the dendritic tree is a dynamic process in which periods of elongation and retraction alternate quickly (Mizuno et al., 2014; Nakazawa et al., 2018). More importantly, NMDAR1 KO neurons appeared to be more dynamic, indicated by a higher change in dendritic length compared to control cells. As the knockout of NMDA receptors affect the signalling pathway both used by intracortical and thalamocortical input, a study by Nakazawa specifically explored the influence of thalamocortical activity by cutting the infraorbital nerve (ION) at P0 which eliminates sensory input from the whiskers. Two-photon time-lapse imaging of L4 neurons between P3 and P6 revealed that the dendritic branches of neurons in the ION severed mice failed to orient themselves towards the barrel at P6. Furthermore, they reported that the number of eliminated, and newly formed trees was significantly smaller in the ION-severed mice compared to L4 neurons located at the edge of the barrel in control mice. Instead, tree dynamics were similar to L4 neurons located inside the barrel, which do not possess an asymmetrical tree organization, but smaller compared to neurons located at the edge. These results suggest that the spatial biased thalamocortical input a neuron receives at the edge of a barrel is required for the asymmetric refinement of the dendritic structure. This restructuration is achieved not by an increase in the number of overall dendritic trees, as this remains stable between P3 and P6, but by retracting existing trees and the biased growth of new trees towards the barrel (Nakazawa et al., 2018).

While the above presented studies indicate that functional thalamocortical input may play a major role in L4 neuronal development of the somatosensory cortex in mice, they cannot differentiate between the role of stimulus-induced activity and spontaneous activity from the periphery. While retinal wave spontaneous activity and stimulus-induced activity in the visual cortex occur in largely segregated periods during development, no study to date have explored the impact of thalamocortical activity on L4 V1 development in mice. The generalization of the results reported in the somatosensory cortex to other systems, suggest that thalamocortical activity including spontaneously generated activity could instruct morphological changes. This hypothesis still remains to be tested.

1.5 Dissertation project

In the developing brain, the first rough organization of circuitry is laid out by innate genetic programs, mediating cell differentiation and guiding the growing axons to their appropriate targets through gradients of molecular guidance cues (Goodman and Shatz 1993; Sperry 1964, reviews: Flanagan 2006; McLaughlin and O'Leary 2005). The further refinement of these crude circuits into refined neural networks underlying perception and complex behaviour, has been shown to depend on activity-dependent plasticity mechanisms. The extent to which spontaneous neuronal activity plays a role and when it exerts an influence, is however not precisely known and is heavily debated.

To better understand the influence of spontaneous activity on neuronal development, the mouse visual system and the associated spontaneous retinal waves has proven a useful model since the period of spontaneous retinal activity and stimulus-evoked activity are largely segregated by eye opening at P14. Furthermore, functional maps such as eye-segregation and the retinotopic map, as well as many important visual response features such as direction selectivity and orientation selectivity, already exist at eye opening (Rochefort et al., 2011; Thompson et al., 2017a). This raises the hypothesis that spontaneous activity from the periphery could be instructive in establishing these visual features. Indeed, several studies using transgenic mouse models, drugs and optogenetic tools have shown that retinal spontaneous activity is essential for the developmental process of eye segregation and retinotopic map formation in the superior colliculus, dorsal Lateral Geniculate Nucleus and primary visual cortex (V1) (Ackman and Crair, 2014; Cang et al., 2005; Grubb et al., 2003; Huberman et al., 2008; Kirkby et al., 2013; Xu et al., 2011).

Major open questions, however, are how the retinal wave pattern interact with gene expression to steer molecular developmental programs underlying the functional and anatomical changes required for normal V1 function and circuit integration. Next to axonal arborization, the dendritic structure of a neuron is an important morphological feature that contributes to circuit integration. Despite its importance, only a few studies to date have described normal dendritic development of neurons in cortical layer 4, the neurons that receive the strongest input from axons of first-order thalamic nuclei. Even fewer studies have explored the contribution of spontaneous activity to this process. These studies have shown that the dendritic structure is rapidly and markedly restructured during early development (Mizuno et al., 2014; Nakazawa et al., 2018). Furthermore, eliminating thalamocortical input strongly affected the developmental dendritic restructuring indicating that functional thalamocortical input may play a major role in L4 neuronal development.

Since these studies were conducted in the somatosensory system, in which spontaneous and stimulus-evoked activity coexist during early development, the specific contribution of spontaneous activity to dendritic development is currently still not known. Therefore, the central aim of my PhD is to understand how spontaneous activity from the periphery affects the dendritic development of L4 neurons in V1.

Driven by this question, the aims of my PhD research are the following:

1. Establish a viral method to allow for targeted and early expression of transgenes in the dLGN of neonatal mice.
2. Identify important timepoints in L4 cortical development based on the normal developmental timeline of thalamocortical ingrowth and dendritic development.
    a. Identify the developmental timing of thalamocortical axon interactions with L4 neurons by fluorescent labelling of thalamocortical axons through stereotactic viral injections.
    b. Identify morphological changes in sparsely labelled L4 pyramidal neurons during early postnatal development.
3. Assess the impact of functional input from TC axons on L4 morphological development by silencing dLGN neurons through stereotactic viral injections.

Each of the results chapters is centred around one of these aims. In addition, to provide a complete picture of the timeline of L4 pyramidal development, the second chapter of the Results section will also include data on the development of activity patterns in V1 that were obtained by my colleague Dr. Susanne Falkner.

2. Results

2.1 Preface

The following chapters describe the results related to the various aims of my PhD thesis. The work presented in these chapters has been carried out in close collaboration with several people. Below, I will describe the individual contributions of the people involved.

The surgical protocol for targeted stereotactic injections in the dLGN of neonate mice, described in chapter 2.2, has been developed and optimized by my own efforts. The input and experience from Dr. Susanne Falkner proved invaluable for establishing and optimizing the protocol.

To study thalamocortical axon ingrowth, described in chapter 2.3.2, I performed all stereotactic surgeries and most of the perfusions and antibody stainings. For some samples, I received assistance from our lab technicians, Caroline Bornmann and Sabrina Innocenti. The subsequent image acquisition and analyses were executed by me. The data describing the synchronous activity patterns during early development, presented in chapter 2.3.3 was acquired through the sole efforts of Dr. Susanne Falkner.

All data related to the study of morphological development, including the description of the normal developmental timeline of L4 morphology (chapter 2.3.4) and the data describing how L4 morphology is affected by thalamocortical silencing (chapter 2.4), were acquired through the joint effort of Shirley Dixit and myself. Specifically, I performed all stereotactic injections for the data presented in chapter 2.4 and cut most of the brains. Shirley Dixit perfused most of the animals in assistance with Sabrina Innocenti. Brain sections were stained and imaged by Shirley Dixit. Morphological tracings were performed by us both, though Shirley Dixit traced the majority of the neurons while I performed the final evaluation and correction of all tracings. Moreover, I extracted the dendritic parameters and performed the respective statistical analyses.

Finally, I received help in cloning the numerous plasmids used for my research from Dr. Dietmar Schreiner. Our lab technician Caroline Bornmann produced all the viruses that were used for the stereotactic injections.

2.2 Targeted stereotactic injections in the dLGN of neonate mice

2.2.1 Introduction

With the use of cell-type specific transgenic mouse lines, the injection of viral vectors or a combination of both, the expression of transgenes can be introduced into a specific population of cells. The expression of these transgenes allows the researcher to visualize and monitor certain cell populations through the expression of fluorescent proteins, or to increase or decrease activity in certain neurons by expressing molecular manipulators of activity. A widely used approach to express transgenes in specific cell populations in the mouse brain is the Cre/loxP binary system (Harris et al., 2014). This system is based on the principle of Cre-lox recombination in which the expression of the enzyme Cre recombinase leads to recombination of a target sequence, the transgene, located between two Lox sites. The expression of Cre can be regionally or cell-type specifically controlled by using selective promoters and even temporal control can be achieved with the availability of the Cre^{ERT2} variant, which is only activated after tamoxifen administration. Through interbreeding of a Cre driver mouse line and a reporter transgenic line the preferred transgenic mouse line can be generated. More and more Cre-driver lines have become available; in the Allen Brain Atlas, the transgenic characterization of over 2,000 Cre driver lines can be found. Among these is the Rorb-IRES2-Cre driver line, a line that results in transgene expression in neurons expressing the RAR related orphan receptor B (Rorb) protein, which displays a laminar expression in the cortex and is found predominantly in pyramidal layer 4 neurons and cortical stellate cells. The disadvantage of Cre-loxP transgenic mouse lines, it that it is typically time-consuming. An alternative faster option is to inject a recombinant virus into a transgenic mouse, or even to co-inject Cre driver and reporter recombinant viruses into a wildtype mouse to achieve spatial and cell-type specific control of transgene expression. However, the spatial and cell-type specific control of all these Cre-loxP based strategies depend on the availability of selective promoters for the region and/or cell population of interest. Furthermore, Cre-loxP based strategies often lack specificity with regard to specific sub-regions and brain nuclei. For instance, the use of the Rorb-IRES2-Cre line results in transgene expression in pyramidal L4 neurons of various sensory cortices. Targeted expression in one of the sensory cortices specifically, is thus not possible using the Rorb-IRES2-Cre line.

For expression in the thalamus, only a few Cre-driver lines are available, of which none lead to expression of the transgene specifically in the dLGN. One of these is the $Gbx2Cre^{ERT}$ mouse line, which is used by the Lopez-Bendito lab to introduce the expression of Kir2.1 in several thalamic nuclei, including the dLGN (Jones and Rubenstein, 2004; Moreno-Juan et al., 2017). For the present study however, the use of this mouse line isn't an option since it would be hard to grasp the influence of dLGN activity on the development of L4 neurons in V1, when the effect of silencing also extends to numerous other thalamic nuclei (Jones and Rubenstein, 2004). Therefore, we have to resort to viral injections targeted specifically to the dLGN to achieve region-specific expression of the transgene.

The use of a viral delivery strategy has however its limitations and poses significant challenges to overcome to achieve region specificity of transduction at an early age. First of all, viral delivery has a limited cell-type specific control of expression dictated by the type of virus used and the type of promoter that controls transgene expression. Furthermore, the spatial control of expression is determined solely by the precision of the injection. For this reason, existing viral delivery methods in neonates, such as injecting into the ventricle (Kim et al., 2013) or into the transverse sinus (Hamodi et al., 2020), aren't an option for the present study as these techniques lead to whole-brain expression. Therefore, the only method available to accomplish transduction specifically in the dLGN is to resort to precise localized stereotactic injections into the neonate brain. While this is commonly performed in adult mice, there were no reports for stereotactic injections in neonates at the start of the PhD project and still today only a handful of studies can be found (Ho et al., 2020; Olivetti et al., 2020). Furthermore, these studies often still relied on the Cre/loxP system to achieve region

specific transgene expression in a small brain region. Performing localized stereotactic injections in neonates poses a significant challenge considering the small size of the pup and the flexibility of the skull, making positioning into a stereotactic frame more prone to variability. Achieving spatial control of transduction is therefore challenging, especially when targeting a small structure such as the dLGN.

Another concern was that infection with viral vectors is known to require several days (1-2 weeks) for the transgene to be sufficiently expressed in the adult mouse brain. This is a limiting factor when studying axonal development within the first week after birth and when the goal is to silence feedforward activity from the dLGN to V1 at the end of the first postnatal week. However, studies adopting intraventricular and transverse sinus injections in neonates both report early transgene expression. While these studies did not inject directly into the brain, they provide evidence for the general notion that viral delivery in neonates leads to an earlier onset of transgene expression in the brain than can be seen in the adult brain. Nevertheless, to ensure an adequate level of transgene expression is achieved before the time window of interest, viral delivery need to be performed as early as possible, ideally the day the animal is born at postnatal day 0 (P0).

To overcome the challenges presented above, the first goal of my project was to establish a reproducible and reliable surgical protocol for viral injections in P0 mice that specifically target the dLGN, while keeping transgene expression in surrounding thalamic nuclei to a minimum. As a first step in establishing this protocol I explored at postnatal day 5 (P5), the cell-type specific expression of the green fluorescent protein (GFP) packaged in three different AAV serotypes, namely AAV1, AAV8 and AAV9. The serotype with the highest proportion of neurons transduced was subsequently used to test which of the tested promoters, the CMV early enhancer/chicken β actin (CAG) promoter, the human elongation factor-1 alpha (ef1α) promoter, and the human synapsin 1 (syn) promoter, had the earliest onset of expression of the fluorescent protein tdTomato. After identifying the best serotype and promoter for our purpose I moved on to further fine-tune the protocol to ensure that viral spread to adjacent regions was limited while dLGN neuronal transduction ratio was maximized. The results of these different steps are described in the following sections. In the last part of this chapter, I will highlight how the availability of this protocol in combination with methods such as two-photon imaging and cleared brain imaging opens up a new and exciting possibilities to explore previously unanswered questions.

2.2.2 The use of AAV serotypes 9 and 8 led to a high percentage of dLGN neurons transduced at P5

Different AAV serotypes are characterized by different cellular specificity, transduction efficiency and tissue tropism based partly on the different properties of their capsids (Cearley et al., 2008). We therefore wanted to explore which AAV serotype is best suited for transduction of dLGN neurons and to see if indeed the neonatal brain is able to express the transgene early after viral injection.

To test the neuronal transduction ratio of dLGN neurons at postnatal day 5 (P5) I injected three different AAV viruses carrying GFP under the control of the promoter CAG; AAV serotypes 1, 8 and 9. We opted to use the promoter CAG as it is known to be a strong ubiquitous promoter, leaving us with the possibility to compare the transduction specificity and efficiency of the different serotypes. A volume of 100nl of the respective viruses was injected with a Hamilton syringe into the dLGN of pups at P0 (for details see chapter 4.3 Stereotactic injections). Pups were transcardially perfused at P5 with a 4% paraformaldehyde (PFA) in phosphate buffered saline (PBS) solution. Brains were dissected and sectioned according to the protocol described in the Material and Methods sections. Brain sections were subsequently stained for DAPI to visualize cell nuclei and with an antibody reactive to GFP to visualize infected cells (see 4.4.4 Antibodies). In addition, slices were stained for NeuN, a neuron-specific nuclear protein, and for the presence of glia-specific protein S100 to visualize glia. Other brain slices were stained for an antibody reactive to oligodendrocyte transcription factor 2 (olig2), which is an oligodendrocyte marker. Image stacks were taken with a confocal

microscope at a 25x magnification (0.80 NA). For the quantification of the number of GFP+ neurons, the z-plane was selected with the best GFP signal to manually annotate cells, neurons and infected cells. For the quantification of the number of infected oligodendrocytes and glia cells respectively, the z-plane was selected which showed the best signal.

Surprisingly, we found that a large population of cells (40-60%) in the dLGN were expressing GFP at P5, four and a half days after injection (Figure 8D). This demonstrates that viral transduction in neonates indeed comply to different metabolic dynamics than viral injections in the adult brain, which requires often 10 days before sufficient expression of the transgene can be observed. As can be seen in Figure 8E as well as in in the image panels presented in Figure 8A-C, all three serotypes had a relatively high transduction ratio of neurons. Serotype AAV1 performed worst with an infection ratio of around 60%. Serotype AAV9 performed best, infecting more than 80% of the neurons identified within the optical slice.

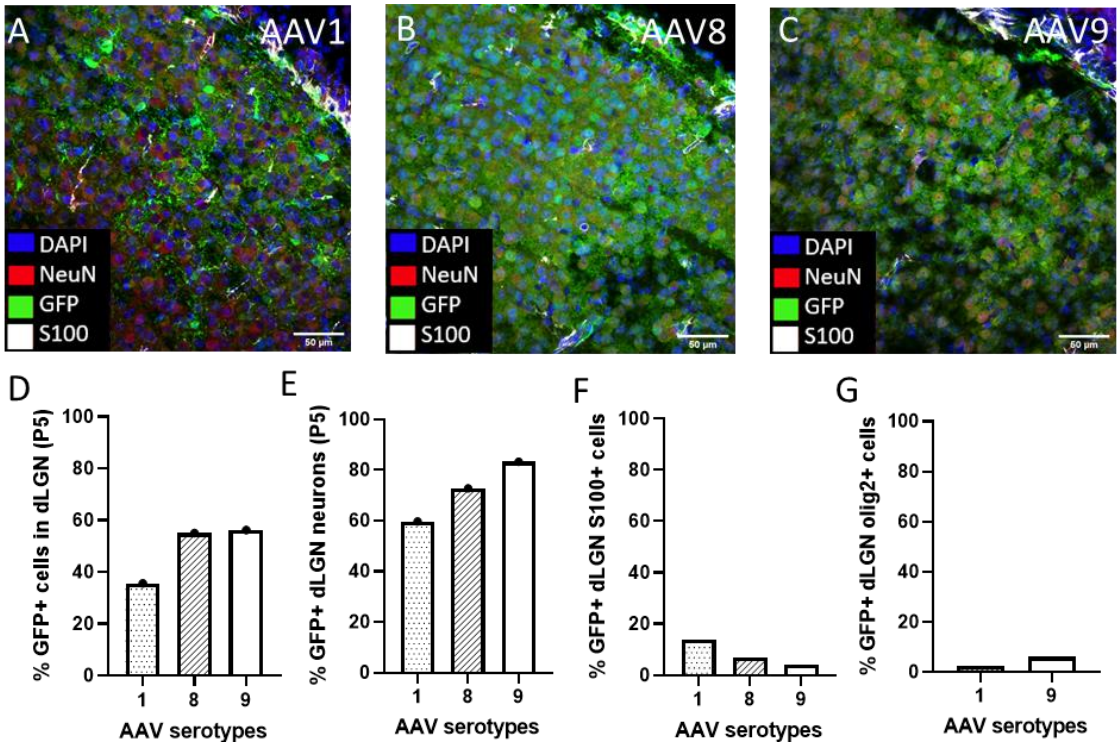

Figure 8 AAV serotypes 8 and 9 led to a high percentage of neurons transduced at P5. (A-C) single confocal optical sections at 25x magnification (0.80 NA) within the dLGN of brains injected with either AAV serotype 1, 2 or 9 provides a glimpse of how efficient the different serotypes are in transducing neurons (NeuN) and glia cells (S100). (D) Quantification of the number of GFP^+ cells within the dLGN for the different serotypes. The quantification of the number of GFP^+ neurons (E) shows that serotype 9 is most successful in transducing neurons in the dLGN, with 83% of the neurons expression GFP. The number of GFP^+ glia cells (F) and oligodendrocytes (G) were relatively low for all serotypes tested. Scale bar denotes 50µm. Number of animals: n=1 for all viruses. Number of cells counted: AAV1 n=690, AAV8= 710, AAV9=754. Viral titer: AAV1 $4.0*10^{11}$ GC/ml, AAV8 $8.0*10^{12}$ GC/ml and AAV9 $3.0*10^{12}$ GC/ml.

Though our primary aim was to maximize neuronal transduction ratio, a low infection ratio of other cell types was also preferred. This to minimize interfering effects of silencing other cell types when injecting a molecular silencer of activity into the dLGN. As can be seen in the images shown in Figure 9A-C we could observe multiple GFP^+ cell structures resembling the morphology of glia cells in the AAV1 and AAV8 injected brain slices. Indeed near 14% of the counted $S100^+$ cells were quantified as GFP^+ for serotype 1 (Figure 8F). For

serotype 9 this percentage was 4.1%. Though serotype 1 showed the highest infection ratio of glia cells compared to other serotypes, it had a low tendency to infect oligodendrocytes (Figure 8G).

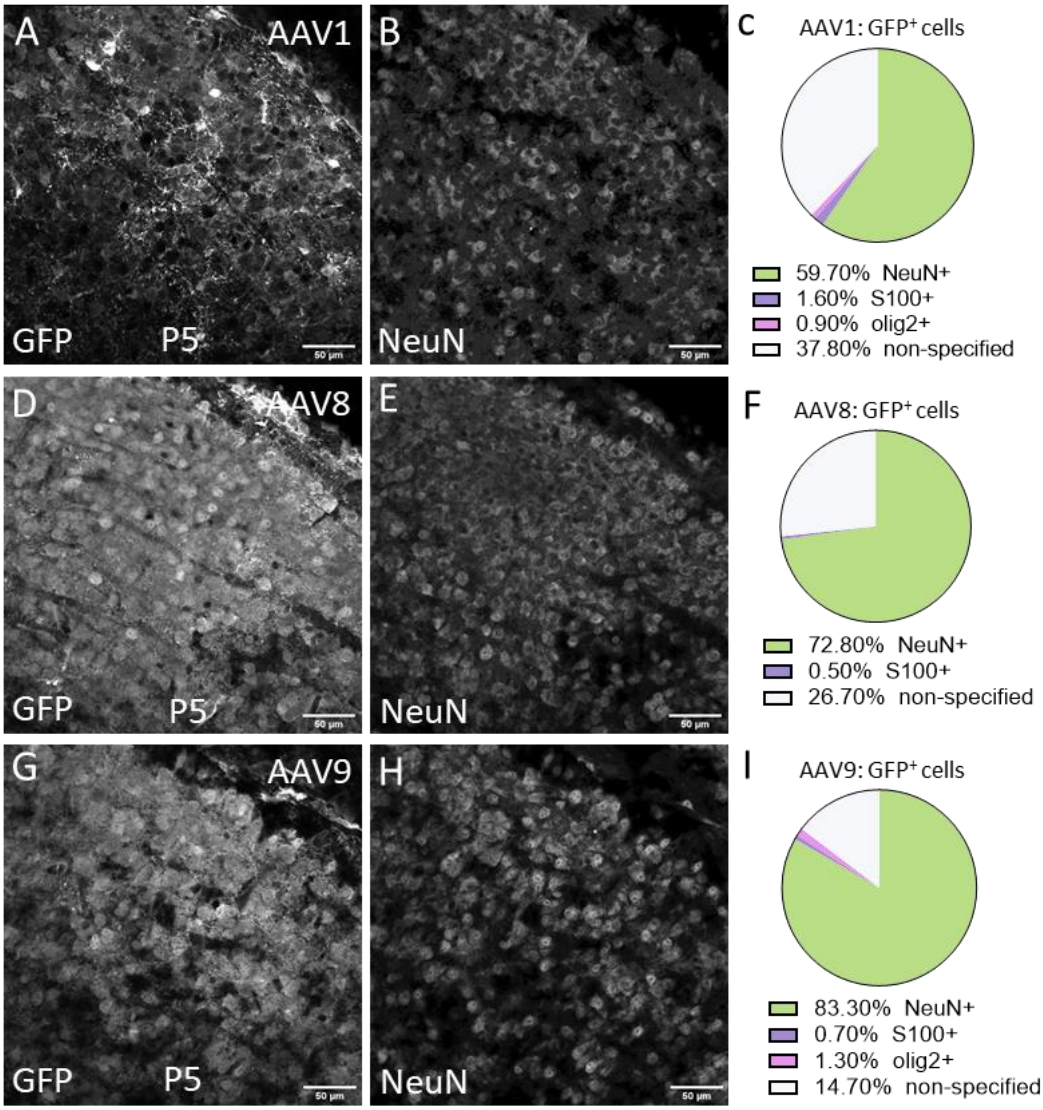

Figure 9 Injection with serotype 9 leads to the highest percentage of NeuN$^+$ GFP$^+$ cells. GFP signal in the dLGN of P5 mice that were injected with either serotype 1 (A), serotype 8 (D) or serotype 9 (G). (B, E, H) NeuN signal in the same optical sections as presented respectively in A, D and G. The composition of GFP$^+$ cells for a brain injected with serotype 1 (C), 8 (F) and 9 (I) demonstrate that serotype AAV9 has the highest number of NeuN$^+$ transduced cells. Note that a substantial number of cells could not be identified as belonging to either one of the categories: neurons (NeuN$^+$), glia cells (S100$^+$) and oligodendrocytes (olig2$^+$). Scale bar denotes 50µm. Number of animals: n=1 for all viruses. Number of cells counted: AAV1 n=690, AAV8= 710, AAV9=754. Viral titer: AAV1 $4.0*10^{11}$ GC/ml, AAV8 $8.0*10^{12}$ GC/ml and AAV9 $3.0*10^{12}$ GC/ml.

We also looked at the ratio of GFP$^+$ cells that were either found to be NeuN$^+$, S100$^+$ or olig2$^+$. Quantification of infected neurons and oligodendrocytes proved to be challenging as NeuN and olig2 are both nuclear markers while GFP is expressed only in the cytoplasm of infected cells. As a result, the quantification yielded a relatively high number of GFP$^+$ cells which could not be identified as being either a neuron, a glia cell or an oligodendrocyte (Figure 9C, F and I). Taking the general cell composition of the dLGN into account, the majority of these infected cells are most likely to be neurons. Therefore, the number of NeuN$^+$ GPF$^+$ cells presented in the pie charts in Figure 9 will most likely be higher in reality. Despite that, serotype 9 already displayed a high number of NeuN$^+$ GFP$^+$ cells (80%), demonstrating that serotype 9 has a strong specificity towards infecting neurons.

Using targeted stereotactic injections in the dLGN of neonate mice, we demonstrated that viral transduction in neonatal mice exhibits an early onset of transgene expression for all tested serotypes, with serotypes AAV8 and AAV9 performing best by transducing 60% of the cells in the dLGN at P5. Serotype 9 demonstrated the highest ratio of neurons being transduced (80% of neurons) and showed a low transduction rate of oligodendrocytes and glia cells. Therefore, we decided to adopt serotype AAV9 for further injections.

2.2.3 The use of promoters CAG, ef1α and synapsin all led to early expression of the transgene at P4

After having established the best serotype to use in terms of expression onset and specificity we wanted to test how different promoters influence the dynamics of transgene expression. We set out to test two ubiquitously expressing promoters, namely the CMV early enhancer/chicken β actin (CAG) promoter and the human elongation factor-1 alpha (ef1α) promoter and tested the neuronal-specific promoter human synapsin 1 (syn). When using a viral strategy to silence activity in neurons, the use of a neuronal specific promoter is preferred to avoid unexpected interfering effects from other cell types being transduced. However, since AAV serotype 9 showed a high transduction specificity towards neurons, a ubiquitously expressing promoter might be preferred when it possesses more favourable expression dynamics.

To test the dynamics of the promoters CAG, ef1α and synapsin, we created three AAV9 viruses in which tdTomato was expressed under the control of one of these promoters and injected the virus in the dLGN of neonate mice at P0. For these injections a volume of 100nl was injected with a Hamilton syringe (see 4.3 Stereotactic Injections for detailed description of procedure). Mice were sacrificed at P4, and brains were processed as described in the Material and Methods section. An antibody reactive to tdTomato (rabbit αRFP) was used to visualize transduced cells. Cells and tdTomato$^+$ cells were manually annotated in ImageJ Fiji.

As can be seen in the images presented in Figure 10, the use of all promoters resulted in substantial tdTomato expression within the dLGN. At P4, 66.2% and 62.4% of the cells were transduced for respectively the ubiquitous promoters CAG and ef1α (see Figure 10J). The use of synapsin as a promoter led to a lower number of transduced cells, namely 38.5%. Though the difference in number between the non-cell type specific promoters and synapsin can be partially explained by the lack of infected glia and oligodendrocytes, given the cell type composition of the dLGN it is likely that CAG and ef1α are also able to transduce more neurons compared to the use of synapsin at this timepoint. Therefore the choice between either a ubiquitous promoter such as CAG or synapsin depend mainly on the importance of neuron-specific transduction and on practical considerations such as timing and the length of the construct to be packaged into the AAV which is known to impact transduction efficiency (Wu et al., 2010); ef1α and CAG are substantially bigger than synapsin, being respectively three and four times as big.

For the study of thalamocortical ingrowth into V1 in neonate mice, it is important to have as many axons of the dLGN labelled as early as possible (as early as P3). Therefore, for this purpose we opted to use the ubiquitous promoter CAG to express tdTomato in the dLGN. To silence activity in dLGN neurons, we wanted to assure that as many neurons as possible were silenced at the timepoint at which spontaneous activity in V1 reaches a peak (P9) (see 2.3.3 Spontaneous synchronous events in V1 increase in frequency during early postnatal development). For this purpose and considering packaging restraints we choose to use the synapsin promoter to introduce the concomitant expression of Kir2.1 and tdTomato in the dLGN.

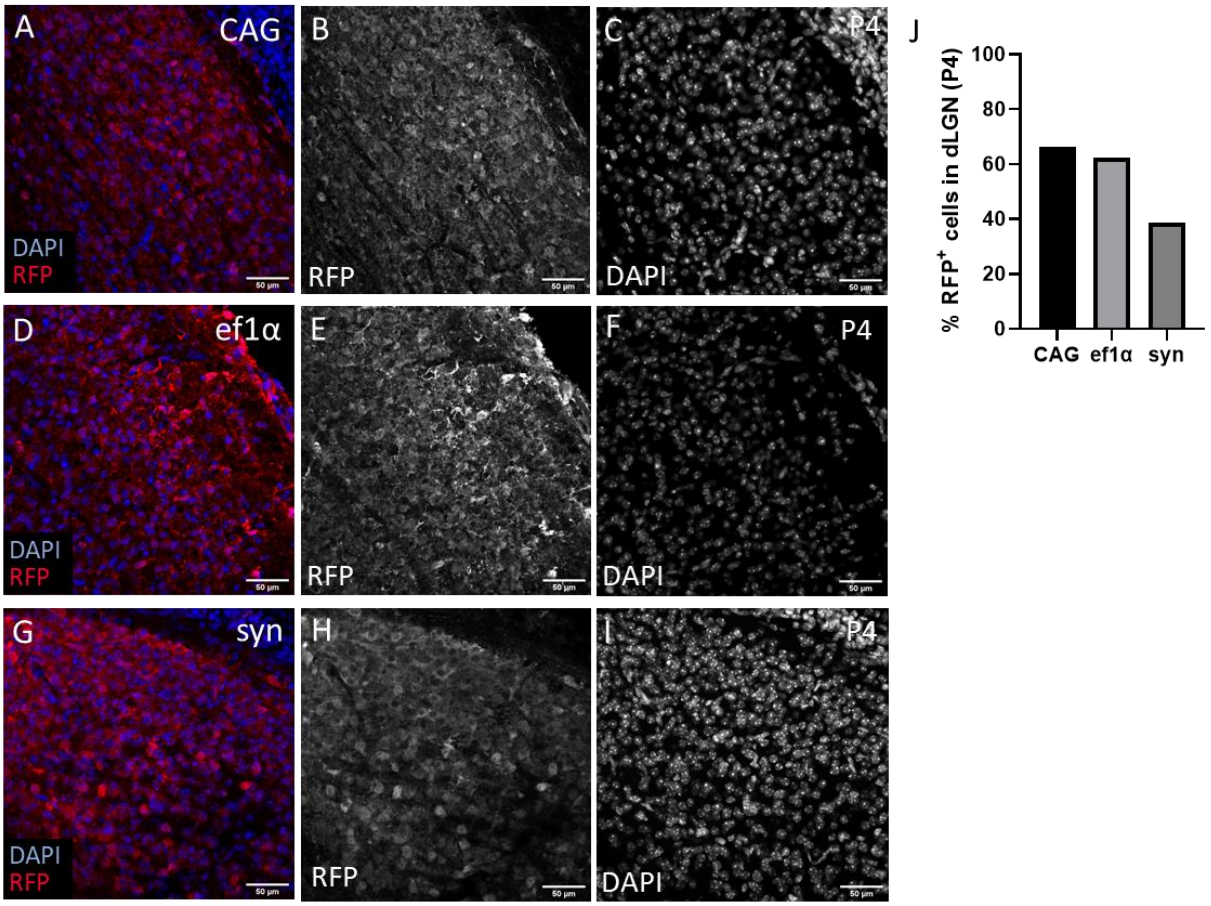

Figure 10 The use of promoters CAG, ef1α and synapsin all lead to early transgene expression in the dLGN at P4. (A-C) single optical section taken at 25x magnification (0.80 NA) in the dLGN of P4 mice, showing the tdTomato expressing cells (RFP^+) in (B), cell nuclei (DAPI) in (C) and the overlay in panel (A) for a mouse injected with AAV9 CAG-tdTomato. Similarly, single optical sections of the dLGN of a P4 mouse injected with AAV9 ef1α-tdTomato and AAV9 syn-tdTomato are depicted in respectively (D-F) and (G-I). (J) Quantification of the number of RFP^+ cells in the dLGN for the three different promoters shows that the ubiquitously expressing promoters have more cells transduced than synapsin at P4. Even though the use of synapsin excludes the possibility of transducing non-neuronal cells, given that neurons are the predominant cell type in the dLGN it is likely that a higher number of neurons are transduced at P4 when using the CAG and ef1α promoter compared to synapsin. Scale bar denotes 50µm. Number of animals: n=1 for all viruses. Number of cells counted: CAG n=610, ef1α n=622, syn n=868. Viral titer: AAV9 CAG-tdTomato $3.2*10^{12}$ GC/ml, AAV9 ef1α-tdTomato $4.4*10^{12}$ GC/ml and AAV9 syn-tdTomato $3.6*10^{12}$ GC/ml.

2.2.4 Fine-tuning the protocol: decreasing variability and limiting viral spread

After having identified the best AAV serotype and promoter to use for our different purposes we moved on to further optimize the surgical protocol. I will describe the protocol in short to highlight the different optimization steps we performed to decrease the variability between injections and to limit viral spread to other regions than the dLGN. A detailed description of the protocol can be found in the Material and Methods section (chapter 4.3.1 Surgical protocol for stereotactic viral injections targeted to the dLGN of the neonate mouse).

To maximize viral expression time, we choose to inject as early as possible. At the day of birth, at P0, the surgery was performed when a clear milk belly was visible to assure the pup had enough nutrition to sustain itself during the surgery and recovery time. The pup was placed into a stereotactic frame using the blunt ear bars to fixate the skull (Figure 11A and B). As opposed to the adult brain, the skull of the neonate mouse is soft and therefore will indent when fixating the head into the frame. The amount of pressure placed on the skull will therefore create variability for the injections in the X and Z coordinate; pressing the skull in more than a previous time will result in an injection lateral and above the dLGN, whereas pressing the skull in less

than a previous time will lead to an injection medial and below of the dLGN. This factor is hard to control objectively. We documented the curvature of the skull after placement by taking a picture and tried to be as constant as possible. However, we found out that the best method to be consistent in the placement is to perform these surgeries regularly.

Figure 11 Pups were placed in a stereotactic frame to perform viral injections; the main blood vessels were used to determine injection coordinates. (A and B) surgeries were performed at postnatal day 0 at which the head was fixated in a stereotactic frame using blunt ear bars. The amount of pressure applied by the ear bars will determine how much the flexible neonatal skull will indent and therefore how much the brain is reshaped. This will create variability between animals using the same injection coordinates. (C) image depicting the main blood vessels of the brain. The intersection of the transverse sinus and superior sagittal sinus, the so-called confluence of sinuses was used as a setpoint for both the X and Y coordinates. The Z coordinate was set to 0 at X=1.2 and Y=1.0.

After placement in the stereotactic frame, a small incision was made to expose the intersection of the transverse sinus and the superior sagittal sinus, the confluence of sinuses. Since the sagittal sutures of the neonate skull are barely visible at this age, we used the main blood vessels to determine the coordinates of injection. The confluence of sinuses was set as 0 for the X and Y coordinates (Figure 11C). Though we expect that using these main blood vessels of the brain to navigate might be less consistent between animals as opposed to using the skull sutures in the adult brain, using the same coordinates for different pups resulted in injections with similar target locations. At the appropriate X and Y coordinates a small craniotomy was made with a 30G needle. While direct penetration was possible using the injection capillary, we felt that the indentation needed to penetrate the skull led to too much damage based on initial trials using this technique. After making the craniotomy, the Z-coordinate was set at 0 at the surface of the brain. Since it was often hard to assess when the injection capillary hit the surface, we observed that a correct and constant determination of the Z axis was also a critical factor for hitting the dLGN. After multiple trial injections, we established the coordinates of X 1.2, Y 1.0 and the Z coordinate of -1.9 as target coordinates for the dLGN.

Using an injection volume of 100nl we observed that multiple thalamic nuclei were expressing the transgene using the AAV9 CAG-GFP virus at a viral titer of $3.2*10^{12}$ GC/mL. A limited viral spread is especially important when wanting to silence activity in the dLGN. In order to understand its effect on the L4 neurons in V1 it's important to minimize the effect of silencing as much as possible to the dLGN specifically, as it is likely that silencing other thalamic nuclei will lead to unwanted side effects making it difficult to interpret the data. However, there is a trade-off between limiting viral spread to adjacent regions by decreasing the injection volume and the chances of hitting the dLGN. Therefore, we set out to see what the lower limit of injection volume was while still maintaining a reasonable success ratio. We decreased the injection volume step wise, going from injecting 100nl, 15nl to eventually 8nl (Figure 12A, B and C respectively). With the injection volume of 8nl the viral spread was substantially decreased. Besides the dLGN, only small parts of adjacent thalamic nuclei expressed the transgene (Figure 12D). These include the ventral posterior medial nucleus (VPM), the posterior nucleus (PO), the lateral posterior nucleus (LP), the ventral lateral geniculate nucleus (vLGN) and the intergeniculate leaflet (iGL). We used the Allen Brain Atlas – Mouse Connectivity to see if any of these nuclei project to the primary visual cortex (V1) or in other ways could complicate the interpretation of our silencing experiments. The VPM is a so-called first-order thalamic nuclei as it projects to a primary

sensory region, the primary somatosensory cortex (S1). The vLGN and iGL are highly reciprocal connected to each other and with the superior colliculus. PO and LP are both higher-order thalamic nuclei sending information to secondary sensory cortices; PO sends projections to the secondary somatosensory region and LP to secondary visual areas. Though the majority of the thalamocortical axons project to higher visual areas, there are also few projections to V1. However, these are primarily located in L1 of V1. Therefore, we concluded that the limited spread to these adjacent thalamic nuclei would not pose a problem for the interpretation of dLGN silencing experiments.

When performing these surgeries regularly, I obtained a success ratio of hitting the dLGN in 50-70% of the cases using an injection volume of 8nl. We concluded that this was a good trade-off between decreasing viral spread to adjacent regions while not impacting the success rate of hitting the dLGN too much.

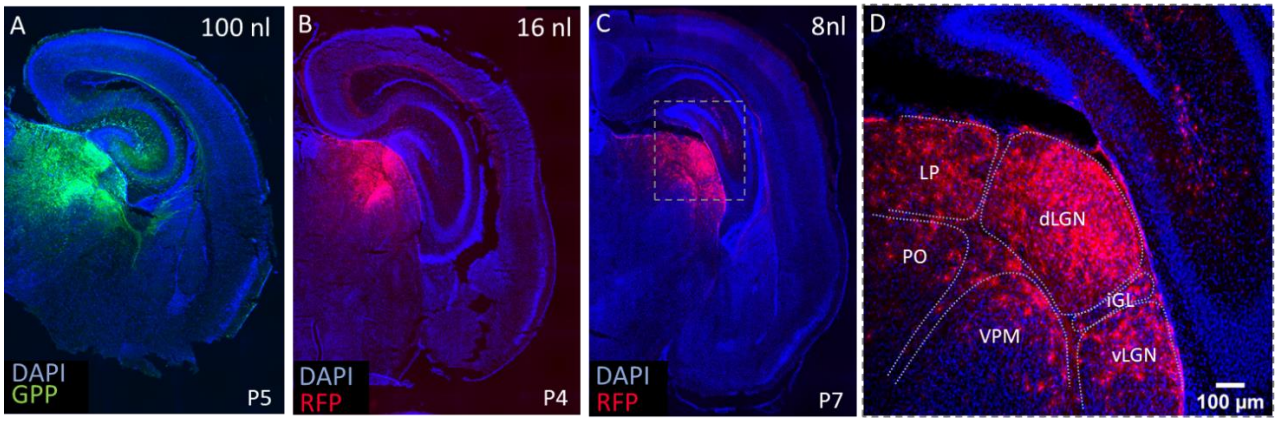

Figure 12. Viral spread for different injection volumes targeted to the dorsal Lateral Geniculate Nucleus (dLGN). (A) An injection volume of 100nl of the AAV9 CAG-GFP virus ($3.0*10^{12}$ GC/mL) resulted in transgene expression in the majority of the diencephalon as well as to expression in the hippocampus (HPC). (B&C) Injecting a smaller volume of 16nl (B) and 8nl (C) of the AAV9 CAG-tdTomato virus ($3.2*10^{12}$ GC/mL) decreased the spread. (D) For an injection volume of 8nl targeted to the dLGN, transgene expression could be observed in the Lateral Posterior Nucleus (LP), posterior nucleus (PO), the ventral posterior medial nucleus (VPM), the intergeniculate leaflet (iGL) and the ventral Lateral Geniculate Nucleus (vLGN). Little expression was observed in the HPC.

In some instances, we could also observe transgene expression in the hippocampus (HPC) (Figure 12A and C). These observations were made for injections using different injection volumes, which therefore suggest that this observation does not depend on the injection volume. We posed two hypotheses that could explain this observation. Either the injection capillary has virus on the outside of the capillary in between the injections or the virus spreads to the hippocampus as a result of capillary pressure and the speed by which we retract the capillary is the variable factor that dictates whether we observe transgene expression in the hippocampus or not. To rule out the first hypothesis we implemented a cleaning protocol in between injections in which the capillary is cleaned with 70% EtOH and 0.9% NaCL before injecting. To explore the latter, I retracted the capillary slowly in some injections while maintaining a normal speed for other injections and compared injection sites. While we could observe minimal transgene expression in the HPC for some injections for both retraction speeds, retracting the needle more slowly seemed to have a higher chance of minimizing transgene expression in the HPC. Notably, we also experienced that the titer of the virus influenced the spread of transduction, a titer of 10^{13} GC/mL led to more spread compared to viruses with a titer of 10^{12} GC/mL. Since we optimized our injection volume using a virus with a titer of 10^{12} GC/mL, we decided to perform all stereotactic injections with a viral titer of 10^{12} GC/mL

As the above discussed challenges illustrates there are many factors within this protocol that have an impact on the outcome of the injections. The developed strategies detailed above try to control these factors as much as possible.

2.2.5 Possible applications

We explored whether the innate fluorescent protein expression level would be high enough to allow for structural imaging of the thalamocortical axons in V1 in two pilot experiments. Brain clearing methods, allow the volumetric imaging of the intact circuitry at sub-cellular resolution using Light-sheet microscopy (Tainaka et al., 2018; Ueda et al., 2020). This will provide valuable insight into the development of thalamocortical circuitry that might be missed with classical immunohistochemistry performed in selected brain sections. We therefore set out to test this application in the neonate virally injected brain.

Successful brain clearing was achieved using an adapted version of the Cubic L clearing protocol described in Tainaka et al. (2018) (see Material and Methods: 4.5 Clearing protocol for the neonate brain). The images presented in Figure 13F and G were acquired through Lightsheet microscope imaging at 5x magnification (0.16 NA). As can be seen in the figure, the thalamocortical axons can be tracked from the dLGN to V1. A disadvantage of cleared brain imaging is that it only provides an impression of the thalamocortical circuitry at a given timepoint during development. Though *in vivo* two-photon structural imaging can only study the thalamocortical axon ingrowth in the V1 itself, it does provide the ability to longitudinally study the development of these projections in the intact brain. As is shown in Figure 13B and C, the fluorescent expression level in the dLGN was sufficient to image the thalamocortical axons in the different layers of the visual cortex at high spatial resolution using two-photon imaging.

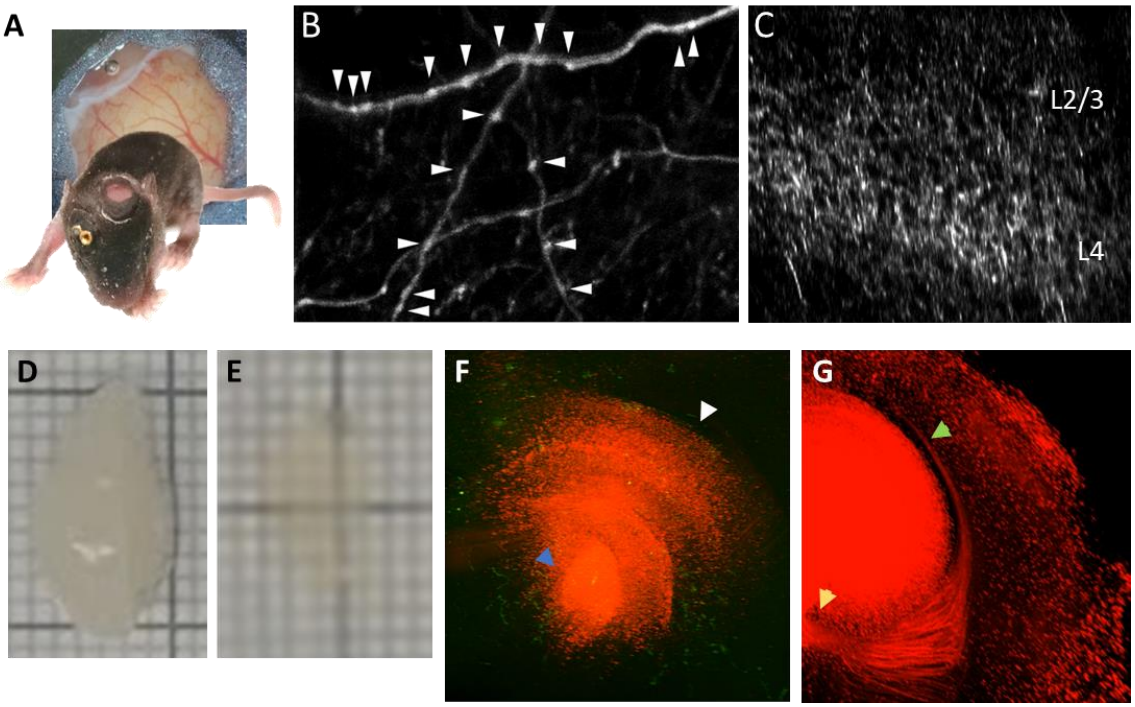

Figure 13 Thalamocortical axons imaged with two-photon *in vivo* structural imaging and Light-sheet imaging of the cleared brain. Injection of the AAV9 CAG-tdTomato (titer 10^{12} GC/mL) virus led to sufficient tdTomato expression to allow for the structural imaging of thalamocortical (TC) axons using structural *in vivo* two-photon imaging (A-C) and whole-brain Light Sheet imaging of the cleared brain (D-G). (A) a glass window was implanted above V1 at P5 to allow structural imaging at P9. (B) Axonal boutons could be distinguished in L4 (arrows). (C) Enrichment of TC axons was visible in L4 of V1. Using the Cubic L clearing protocol, a perfused brain (D) was made transparent (E) allowing Lightsheet imaging of TC connections (F and G). The blue arrow denotes the injection site in the diencephalon. The white arrow points at the cortex. You can see axons growing out of the thalamic nuclei (yellow) growing towards the cortex in bundles (green arrow). Note that for this brain sample a bigger injection volume of 50nl was used. Therefore, transgene expression can be observed in multiple thalamic nuclei.

Notably, the injection protocol can be used to introduce the transgene expression of a variety of proteins. For instance, besides introducing the fluorescent protein in the cytoplasm of neurons, specific synaptic proteins could be tagged with a fluorescent protein to study thalamocortical synapse development.

Furthermore, the activity of transduced neurons can be manipulated by the expression of so-called molecular manipulators of activity that either increase or decrease thalamocortical activity.

2.2.6 Conclusion

We developed a reproducible and reliable surgical protocol for viral injections in P0 mice to specifically target the dLGN, while keeping transgene expression in surrounding thalamic nuclei to a minimum. A high transgene expression level of the fluorescent protein was already visible as early as P3, making it possible to detect thalamocortical axons in the visual cortex through immunohistochemistry staining in brain slices. For injections in the dLGN, serotype AAV9 proved to be the most efficient in transducing dLGN neurons. The ubiquitously expressing promoters tested, the CMV early enhancer/chicken β actin (CAG) promoter and the human elongation factor-1 alpha (ef1α) promoter, showed an early onset of expression and were able to transduce around 65% of the cells in the dLGN. The neuronal-specific promoter human synapsin 1 (syn) transduced 39% of the dLGN neurons. Taken the cell type composition of the dLGN into account, it is likely that the CAG and ef1α promoter are able to transduce more neurons compared to the use of synapsin at this age. The choice between using either a ubiquitous promoter or synapsin will thus depend on the importance of neuron-specific transduction and on practical considerations such as timing and the length of the construct to be packaged into the AAV.

The degree of viral spread to thalamic nuclei adjacent to the dLGN depend on the injection volume and viral titer. Using an injection volume of 8nl of a virus with a titer of 10^{12} GC/mL injected over ten minutes using a pressure injection system, the viral spread was minimized while maintaining a sufficient transgene expression level in the dLGN. Several factors that impacted the success ratio of hitting the dLGN were hard to control, such as the placement of the head in the stereotactic frame. However, performing the surgeries on a regular basis decreased this variability and led to a success ratio of 50-70% using the injection coordinates X1.2 Y1.0 and X1.9. Importantly, the success ratio did not depend on the experimenter performing the surgeries as the protocol was also successfully executed by others.

In this chapter, we have shown that the innate fluorescent protein expression level is sufficient to perform immunohistochemistry on brain sections as early as P3. Furthermore, the expression level is also sufficient to allow for *in vivo* two-photon structural imaging. Using a CUBIC L clearing protocol in combination with a Light Sheet imaging microscope, the axonal projections could be traced from the injection site to the cortex. Notably, besides the expression of fluorescent proteins, the injection protocol can be used to introduce the transgene expression of various proteins, including the expression of molecular manipulators of activity. This will provide the experimenter with a spatial precision of manipulation that was previously impossible to achieve with existing methods in the neonate brain. Furthermore, a big advantage of the newly developed surgical protocol is that spatial precision of transgene expression does not depend on the Cre/loxP expression system, leaving the option open to use this system for other applications.

Overall, the novel neonatal viral injection method described in this chapter opens up new strategies to answer questions that were previously difficult to study due to technical challenges. We have used this technique to study the timeline of thalamocortical axonal ingrowth in V1 through the expression of a fluorescent protein in the dLGN, and to study the impact of spontaneous activity on the dendritic development of Layer 4 pyramidal neurons in V1 by introducing the expression of a molecular silencer of activity in the dLGN. The respective data is described in chapter 2.3.2 and 2.4.

2.3 Early V1 postnatal development is characterized by parallel changes in thalamocortical ingrowth, dendritic complexity, and synchronous activity

2.3.1 Introduction

At birth, the visual system of the mouse is set up in a crude way in which the first rough organization is laid out predominantly by innate genetic programs. The visual circuitry however is still immature; photoreceptors are still unresponsive to light (Tian and Copenhagen, 2003), retinogeniculate axons have not yet reached the dorsal Lateral Geniculate Nucleus (dLGN), and thalamocortical axons still need to find their way to the primary visual cortex (V1), where they will form synapses onto the dendrites of their target L4 neurons. Nevertheless, many visual response features, such as orientation and direction selectivity, are functional at eye opening around postnatal day 14 (P14) (Rochefort et al., 2011; Thompson et al., 2017a). The developmental processes that take place within the first two weeks of postnatal development are thus crucial to prepare the visual system for the onset of vision.

Mapping these developmental processes, is therefore important to understand their relationship. Three developmental processes are of interest:

1. When do thalamocortical axons arrive in L4 of the primary visual cortex (V1)?
2. How is neuronal activity in L4 of V1 characterized in the first two weeks of postnatal development?
3. What is the normal developmental timeline of dendritic morphology of L4 V1 neurons?

Early studies in the nineties have addressed this first question, by providing a coarse impression of the dynamics of axon ingrowth in the cortex. Based on studies in rats and cats, it appears that thalamocortical (TC) axons arrive at the appropriate cortical area during prenatal development well before their target cells have migrated to their appropriate location (Ghosh et al., 1990; Molnár et al., 1998). TC axons accumulate in the subplate and wait for several days before they start to grow into the cortical plate around the age of birth (Ghosh et al., 1990; Herrmann et al., 1994). Though most of the studies have been performed in a variety of species, including in cat, hamsters and rats, only a few studies exist for mice (Agmon et al., 1993; Auladell et al., 2000). Furthermore, these studies can be difficult to interpret as they often do not research a specific population of thalamic projections. Therefore, even though the current literature does provide an impression of how thalamocortical axons develop over time, they do not provide a clear overview of when structural innervation of L4 in V1 takes place. With the development of the surgical protocol detailed in the previous chapter, I have created a tool to directly target the dLGN neurons at P0 with viral injection. By injecting a virus encoding for a fluorescent protein I can directly assess the development of dLGN projections to L4 of V1 during early postnatal development. The results of this analysis are presented in the first part of this chapter.

Despite growing interest in understanding how spontaneous activity generated in the retina affect visual circuitry, little attention has gone to map the spatial-temporal characteristics of these spontaneous waves in areas upstream of the retina, such as V1. A study by Ackman and colleagues (2012) was the first to record retinal wave activity in V1 by calcium widefield-imaging and reported that spontaneous waves became apparent at P5 (Ackman et al., 2012b; Ackman and Crair, 2014). A later study by Gribizis and colleagues (2019) compared activity patterns between the time period of P5-P8 with ages P10-P13. Later in development, waves became more frequent but were shorter in duration compared to P5-P8. The disadvantage of wide-field imaging, however, is that it only captures activity on a mesoscopic scale, summing the activity of multiple neurons over several cortical layers. By recording the activity on a neuronal scale in L4 specifically, we can better understand how the dynamics of spontaneous wave activity evolves over time in this specific population. To address the second question, our lab therefore performed longitudinal two-photon calcium imaging of L2/3 and L4 in V1. In the second part of the chapter, I will summarize the data of my colleague Dr.

Susanne Falkner, thereby providing an overview of how synchronous activity patterns in V1 evolve during early postnatal development.

Thalamocortical activity is relayed to Layer 4 pyramidal neurons through post-synaptic receptors located primarily on their dendrites. While dendritic morphology is a determinant factor for a neuron's function, much remains to be understood on how the dendritic tree is formed and reshaped during development (Richards et al., 2020). A study in the primary visual cortex (V1) of ferrets, in which cortical development evolves on a slower timescale, reported that dendritic complexity increased most between P14 and P26 (Callaway and Borrell, 2011). More interestingly it appeared that both stellate cells and pyramidal cells of layer 4 of V1 possess an apical dendrite in early development and that stellate cells lose this apical dendrite at P22 to acquire their typical stellate dendritic configuration. This developmental process was later also reported to occur in the somatosensory cortex of mice, in which stellate cells had lost their apical dendrite at P6 (Nakazawa et al., 2018). Further studies on L4 stellate cells of the mouse barrel cortex revealed that major structural changes occur between P2 and P6, in which the symmetric basal tree of stellate cells evolves into an asymmetric tree that extends within a single barrel (Mizuno et al., 2007; Nakazawa et al., 2018). These studies demonstrate that dendritic morphology can change rapidly and markedly during early postnatal development. Nevertheless, to date little information is available on dendritic development of L4 neurons of mouse V1 specifically. In the last part of this chapter, I will present the results that I obtained together with my colleague Shirley Dixit to explore morphological changes in L4 pyramidal neurons at distinct time points in early development.

2.3.2 Thalamocortical axon arborizations in V1 continue to evolve during the first two weeks of postnatal development

To study how thalamocortical projections to layer 4 (L4) of the primary visual cortex (V1) develop during early development, we choose to adopt a viral labelling strategy marking axons from the dLGN and evaluating their projection patterns at different ages during the first two weeks of postnatal development. To this end, we expressed the fluorescent protein tdTomato in thalamocortical axons by performing injections with CAG-tdTomato virus (titer 10^{12} GC/ml) into the dLGN at postnatal day zero (P0) (for a description of the protocol see previous chapter as well as Materials & Methods). Pups were subsequently transcardially perfused at various ages ranging between P3 and P14, the day of eye opening (see Perfusion, cryostat sectioning and immunohistochemistry for details on perfusion and sample processing). Forty-micron sections were stained with an α-RFP (red fluorescent protein) antibody, which shows reactivity to various red fluorescent proteins including tdTomato. In addition, we also stained with an antibody reactive to vesicular glutamate transporter 2 (vglut2). Vesicular glutamate transporters are proteins that are found in excitatory presynaptic vesicles and are tasked to transport the neurotransmitter glutamate into the vesicle. Type 2 is predominantly found in thalamocortical synapses and vglut2 is therefore a commonly used marker for thalamocortical synapses. Finally, sections were stained with DAPI to visualize cell bodies.

As a first step, the locus of injection was evaluated by taking a 10x image (0.45 NA) of the diencephalon centred around the dLGN with a confocal microscope (Figure 14, top row). Furthermore, stitched images of the entire slice, acquired with a slide scanner microscope (at 10x, 0.45 NA) were used to evaluate the spread of viral transduction to other thalamic nuclei. Injections that did not show sufficient expression levels of the fluorescent protein tdTomato in the entire span of the dLGN were excluded from further analysis. Furthermore, injections that showed extensive labelling in other regions that would make it difficult to distinguish the origin of the thalamocortical axons, such as the hippocampus, were also excluded (see Figure 12, and section 2.2.4 Fine-tuning the protocol: decreasing variability and limiting viral spread, for the description of the thalamic nuclei). For injections passing the inclusion criteria, a 10x (0.45 NA) confocal image of the visual cortex encompassing all cortical layers was acquired (Figure 14, middle row).

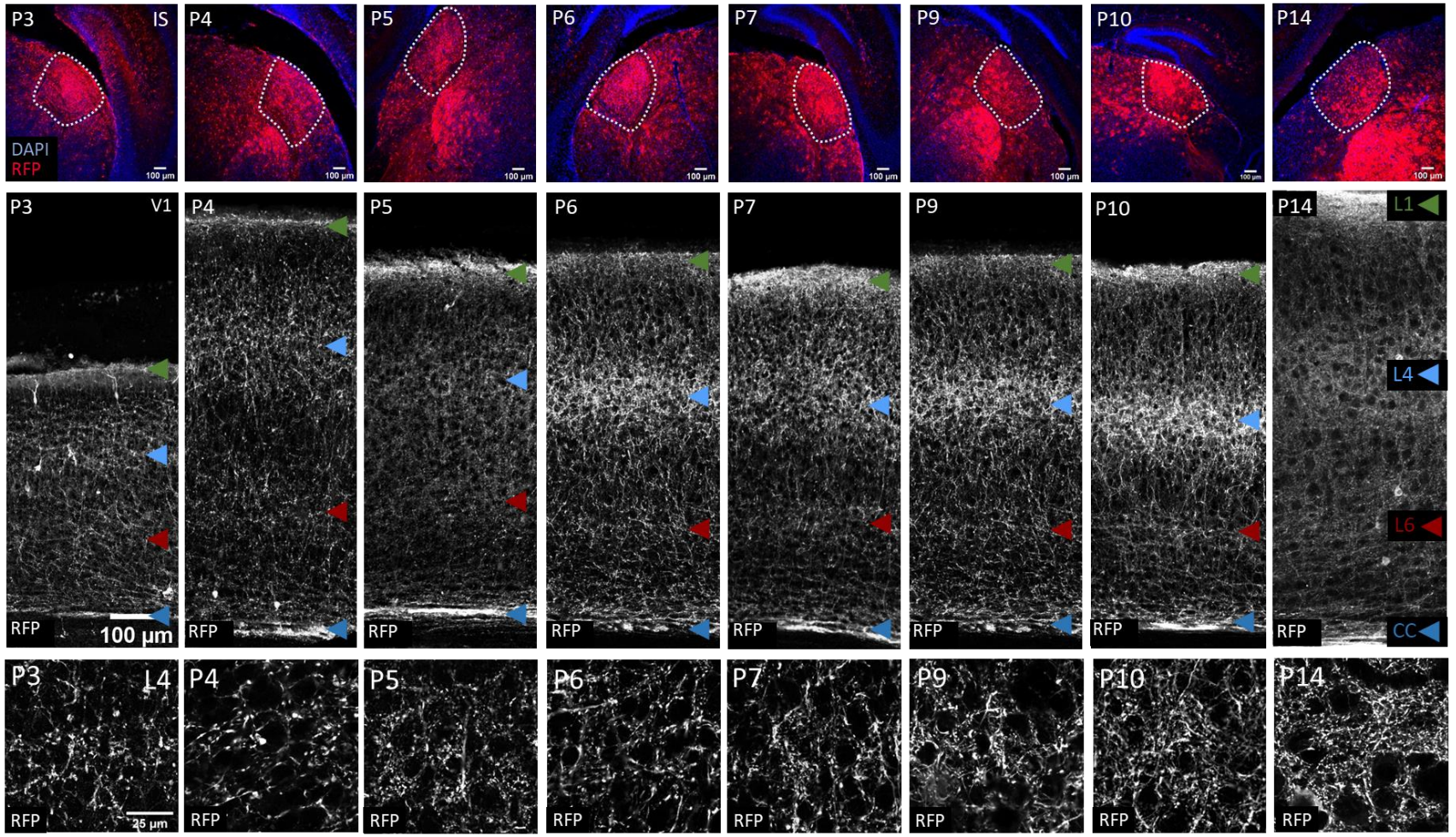

Figure 14 Axonal ingrowth in V1 during the first two weeks of postnatal development Thalamocortical axons were visualized by introducing the fluorescent protein tdTomato in dLGN neurons through targeted localized stereotactic injections with a CAG-tdTomato virus (titer 1012 GC/ml). Figures that are organized within a single column show data from a single injection corresponding to different ages (e.g., the first column shows data acquired at P3, the last from P14). On the top row the 10x (0.45 NA) image of the respective injection site is displayed. The dorsal Lateral Geniculate Nucleus (dLGN) is highlighted with a dashed white line. In the second row the 10x (0.45 NA) confocal images can be found that were taken in V1, showing only the RFP signal in grey. The coloured arrows points to different layers of the cortex, L1 (green), L4 (blue), L6 (red), and to the corpus callosum (dark blue). The last row shows single optical sections that were acquired with a 63x (1.40 NA) magnification in L4. For each timepoint data from a single injection was chosen as a representative of the group. The number of replicates for each timepoint is denoted in the figure. Based on visual evaluation it appears that axonal ingrowth into V1 is not yet complete at birth, but that the number of axons/axon arborizations appear to increase during early postnatal development. Furthermore, when comparing the 63x images of L4 between age P10 and P14 it appears that a finer mesh of axonal arborizations arise.

A 63x (1.40 NA) confocal image was then taken in L4 to provide a more detailed view of axonal ingrowth during early postnatal development (Figure 14, bottom row).

As can be seen in Figure 14, only subtle changes are visible at the 10x magnification (0.45 NA) during the first two weeks of postnatal development. Already at P3, axons from the dLGN are visible in all layers of the visual cortex and appear to be slightly concentrated in Layer 4 (L4) and Layer 1 (L1). At P6, L4 becomes apparent as a dense layer of axonal arborizations. At P14, the cortex has expanded in size and layers 1, 4 and 6 have an increased number of axons arborizations compared to the other layers of the visual cortex. Looking at the 63x magnification (1.40 NA) images taken within L4, it can be observed that indeed axonal ingrowth in V1 is not yet complete at P3. Axonal arborizations seem to increase gradually during the first two weeks of postnatal development. Moreover, axonal varicosities at younger ages appear to be bigger in size compared to later in development. Furthermore, when comparing the images for P10 and P14, it appears that a finer mesh of axonal arborizations arise between these two timepoints.

Quantification of axonal ingrowth in L4 of V1

To objectively confirm the above observations, we developed an algorithm to quantify the axonal ingrowth in L4 of V1. The algorithm defines the so-called area of axonal coverage, that is, the percentage of RFP+ pixels within a given image. A detailed description of the method, programmed in ImageJ Fiji can be found in the Material and Methods section. In short, the algorithm defines a threshold for each individual image based on the distribution of pixel intensities across the entire image. Since the signal threshold is not an absolute number, the benefit of our approach is that the algorithm is less sensitive to differences in intensity levels between images recorded across experiments and is more sensitive to detect axonal structures, even in images with low signal-to-noise quality.

The quantification results depicted in Figure 15 confirm our observations. First, axonal ingrowth and arborization occurs in a gradient and is not yet complete at birth. Furthermore, it appears that the largest increase in axonal coverage, defined as the percentage of RFP^+ pixels within an image, occurs within the first postnatal week of development until postnatal day 9. Between P9 and P14 axonal area increases only slightly.

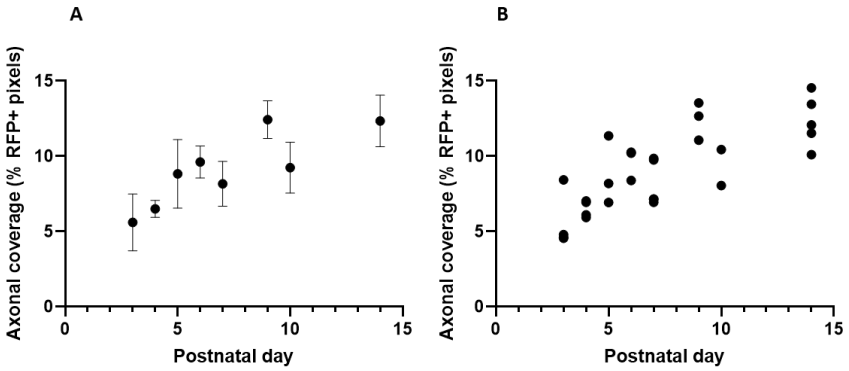

C

Postnatal day	Nr of replicates	Nr of animals	From nr of litters
3	4	3	2
4	4	2	1
5	3	3	2
6	3	2	2
7	5	3	3
9	3	3	2
10	2	2	2
14	5	4	3

Figure 15 Quantification of axonal ingrowth in layer 4 (L4) of the primary visual cortex (V1) during the first two weeks of postnatal development (A) graph depicting the mean value and error bars of axonal area, defined as the percentage of RFP+ pixels within a given image, at different ages during early postnatal development. In (B), individual replicates are denoted. Note that we considered a successful viral injection in the dLGN of one hemisphere as a replicate. Consequently, two replicates can be derived from the same animal. Table (C) provides information on the identity of the replicates shown in (A) and (B).

Many axonal varicosities colocalize with vglut2

Since we could observe axonal varicosities already at postnatal day 3 (P3), we were interested to see whether these varicosities would colocalize with vglut2, which would add evidence that these varicosities are presynaptic structures. Therefore, sections were stained with an antibody reactive to RFP, visualizing the thalamocortical axons that express tdTomato, and with an antibody reactive to vlgut2 to visualize the presynaptic vesicles.

As mentioned before, at P3 thick axonal varicosities could be observed (Figure 16). Many of these varicosities did colocalize with vglut2 suggesting that they are indeed pre-synaptic structures. At later timepoints, the varicosities became smaller in size. Furthermore, it appeared that the number of axonal varicosities colocalizing with vglut2 increased throughout development. Nonetheless, since we did not perform quantification, we cannot provide objective support for this observation.

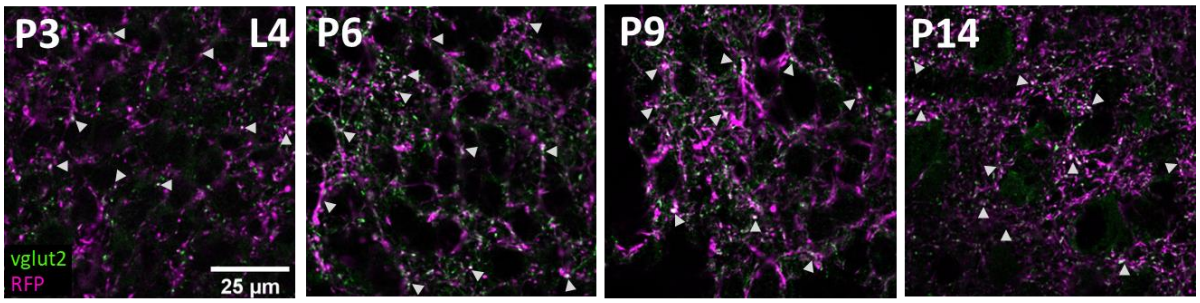

Figure 16 Many thalamocortical axonal varicosities colocalize with vglut2. Many axonal varicosities (magenta) colocalize with vglut2 (green) throughout development, which will appear as white in the image. Several points of overlap are indicated by a white arrow, though many more points of colocalization can be observed in the images. Already at P3 many axonal varicosities colocalize with vlgut2, indicating that they are pre-synaptic structures. Furthermore, it appears that throughout development, the number of these pre-synaptic structures increases. Images are representative single optical sections from confocal images acquired with a 63x magnification.

2.3.3 Spontaneous synchronous events in V1 increase in frequency during early postnatal development

In addition to mapping changes in thalamocortical input to the primary visual cortex (V1) during early postnatal development, our lab also explored the activity pattern of V1 neurons throughout this same developmental time window. Two-photon calcium imaging detects rapid changes in intracellular free calcium caused by neuronal activity. The genetically encoded fluorescent calcium indicator GCaMP6f is a member of a family of ultra-sensitive and fast-responding protein calcium sensors and is shown to reliable detect single action potentials in the soma (Chen et al., 2013). Therefore, at present, two-photon calcium imaging is considered a powerful method to monitor activity of multiple distinct neurons *in vivo*. Dr. Susanne Falkner performed two-photon calcium imaging in V1 of Cux2-CreERTxGCaMP6f mice between the ages of P6 and P13. In these mice GCaMP6f is expressed in neurons expressing Cux2 (Cut like Homeobox2). Cux2 shows a layer-specific expression in the cortex and is enriched in layer 2/3 (L2/3) and to a lesser degree in layer 4 (L4) of sensory regions (see Allen in situ Atlas and Figure 17A). Therefore, it was possible to record both in L2/3 as well as in L4 of V1.

At postnatal day 5 (P5), a cranial glass window was placed above the primary visual cortex together with a fixation screw (Figure 17A). After a recovery period, imaging sessions commenced at P6 and were repeated daily until P13, resulting in a developmental timeline of neuronal activity in the same population of neurons. Since we are interested primarily in activity changes caused by changes in thalamocortical input during development, we explored parameters of synchronous events in the visual cortex. These events are reported to be predominantly spontaneously generated in the periphery during the first week of postnatal development (Gribizis et al., 2019). A synchronous event,

or so-called spontaneous wave referring to the spatial-temporal characteristic of the event, was defined as a minimum of 5% of the cells within a field of views (FoV) being active within a time bin of 0.165ms. For each FoV the average frequency of waves was calculated and plotted across time (Figure 17B). Furthermore, for each timepoint the average fraction of neurons that were active in all wave events was calculated (Figure 17B).

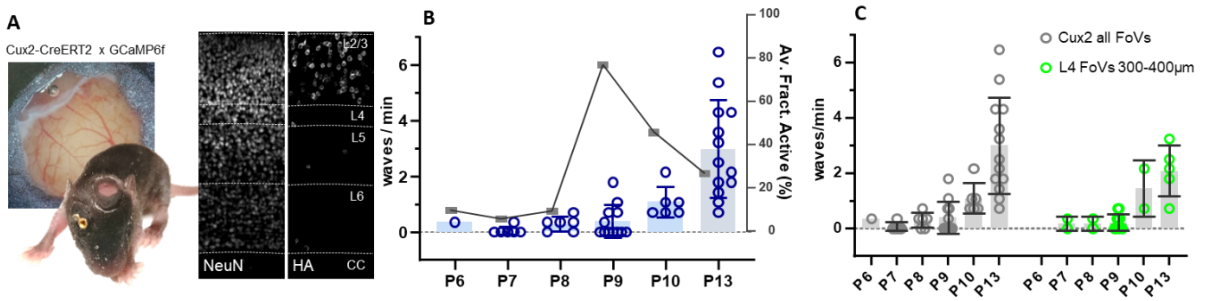

Figure 17 Two photon calcium imaging reveals that the number of synchronous events increase throughout early postnatal development. A) Two-photon calcium imaging was performed in Cux2-CreERTxGCaMP6f mice. Cux2 is a widely used layer 2/3 (L2/3) marker gene and results in specific expression in L2/3 and to lesser degree in L4 of the cortex as can be seen in the image. For this image, a Cux2-CreERTxRpl22-HA line was stained with a NeuN-antibody, a neuronal nuclear antigen, to characterize the different cortical layers and an antibody against the HA-tag to characterize Cre-expression in this mouse line. Indeed, HA was detected predominantly in L2/3 and to lesser degree in L4. At postnatal day 5 (P5) a cranial glass window was placed above V1 together with a fixation screw. After a short recovery period imaging started at P6 until P13. B) The number of waves per minute (waves/min) was defined as the number of synchronous events (in which at least 5% of the neurons were active within a time bin of 0.165ms) recorded in each field of view (FoV) over a course of one minute. The frequency of spontaneous synchronous events increased steadily during early postnatal development up until the day before eye opening at P13. For every FoV and every synchronous event, the percentage of active cells that participated in each event was also calculated. The average fraction of active cells across all events, recorded in all FoVs, is depicted in the line graph. It peaks at P9 and decreases in the next days. C) The frequency data depicted in (B) is shown again in grey, encompassing all recorded FoVs located in L2/3 and L4 of V1. In green the data is shown for the FoVs located solely in 4 and shows a similar trend in increase in frequency.

Synchronous events rarely occurred within the first postnatal week (see Figure 17). From P8 onwards, the wave frequency increased steadily resulting in an average occurrence of three waves per minute at P13. Relatively few neurons, 10 percent, participated in a synchronous event at the ages P6 to P8. This peaked at P9 to roughly 80% and dropped again a day later to 40%. At the day of eye opening the percentage of neurons participating in a wave event decreased to 20%.

The data presented in Figure 17B is based on recordings of several FoVs per mouse spanning 150 to 400µm depth, encompassing L2/3 as well as L4. Since the focus of this thesis is to understand the effect of thalamocortical activity on L4 V1 neurons, we were interested to see whether L4 neurons might show a different pattern in wave frequency increase throughout early postnatal development. To this end data from FoVs recorded in L4 were separately plotted (Figure 17C). Similarly, to the data of all FoVs combined, L4 data showed a steady increase in wave frequency starting at P8.

2.3.4 The dendritic structure of L4 neurons of V1 undergoes major changes within the first week of postnatal development

Thalamocortical activity is relayed to L4 pyramidal neurons through post-synaptic receptors located primarily on their dendrites. Given that dendritic morphology, along with the degree of axonal arborization, is an important factor that determines to which thalamocortical neurons L4 V1 neurons are connected and at which strength, we lastly set out to describe the process of L4 V1 dendritic morphological development.

While Cre-dependent lines enable scientists to zoom in on a subset of cells that are genetically defined as a specific cell population, the combination of a Cre-dependent line and a sparse labelling strategy enables the researcher to explore the morphology of a cell belonging to a specific cell population. One of the tools to sparsely label a subset of cells from a genetically-defined cell population, is the mononucleotide repeat frameshift type 3 (MORF3) mouse line (Veldman et al., 2020). In these mice, the expression of the genetically engineered V5 tag is depending on a rare and stochastic mutation that will transform the out-of-frame sequence into an in-frame sequence leading to expression. By combining the MORF3 mouse line with a Rorb-Cre mouse line, expression of the membrane-associated V5 tag is limited to less than 5% of the $Rorb^{+}$ neurons, which mainly consists of L4 pyramidal neurons. Since V5 is membrane-bound, the entirety of axonal and dendritic processes belonging to a sparsely labelled L4 neuron is visible with fluorescent microscopy after immunohistochemistry.

In collaboration with Shirley Dixit, I explored the dendritic morphology of L4 neurons of the primary visual cortex (V1) at different ages during the first two weeks of postnatal development. Based on the data of the axonal ingrowth analysis and functional analysis of L4 neuronal activity, we defined the following timepoints of interest: 1) P5, when structural and functional thalamocortical (TC) innervation of V1 is minimal 2) P10, when structural TC innervation is almost completed, and finally 4) P15, the day after eye opening. Since the onset of vision is associated with a switch in cortical processing, we choose to include this last day to account for effects on morphology related to this event (Colonnese et al., 2010). We later also decided to include P13, when TC ingrowth has plateaued and (spontaneous) wave frequency is at its peak, to represent the end state before eye opening. Data collection of P13 is still ongoing and is therefore not presented in this chapter.

We sacrificed pups from the MORF3xRorb-IRES-Cre mouse line at these specified ages with the perfusion protocol described in the Methods and Materials. Forty-micron sections were cut with a cryostat and subsequently stained with anti-V5 to visualize the sparsely labelled L4 neurons and their morphology (for more details, see 4.4 Perfusion, cryostat sectioning and immunohistochemistry). Additionally, since Rorb expression is not solely limited to L4 but is also expressed in a subpopulation of L5 and L6 pyramidal neurons of the cortex, we also stained for Er81, a commonly used L5 marker to differentiate L4 neurons from adjacent $Rorb^{+}$ L5 neurons.

All L4 neurons were imaged at 60x magnification (1.30 NA) in the anterior region of the primary visual cortex with a spinning disk confocal microscope (see 4. Material and Methods for details). We choose to only image neurons that showed minimal overlap with other labelled neurons. This, to decrease the chance of wrongfully attributing intersecting dendrites of neighbouring cells to the neuron being traced. Furthermore, neurons that showed Er81 reactivity were excluded from further analyses (see Figure 18 for an example). Images were then stitched offline to acquire tiled images of the entire neuron which were used for tracing using the software Neurolucida 360. Given the section thickness of 40µm it was not uncommon to observe premature cut-offs of dendrites. Neurons that showed extensive cutting were therefore excluded from further analyses. Since the apical dendrite and its bifurcations were often cut, we decided to focus our analyses on the basal dendritic tree.

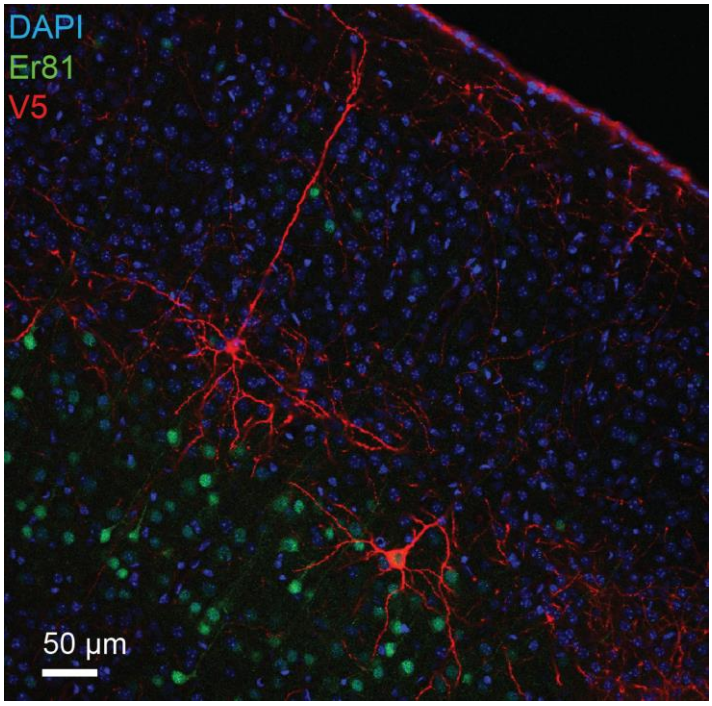

Figure 18 Sparsely labelled pyramidal Rorb$^+$ neurons in the anterior region of the primary visual cortex (V1). Example of two sparsely labelled Rorb$^+$ pyramidal neurons in V1. The dendritic structure, cell body as well as the axon of two sparsely labelled neurons are visualized through V5-antibody staining (red). One of the neurons shows reactivity for Er81 (green) and is thus a Layer 5 pyramidal neuron. This neuron is therefore excluded from further analysis. The second is Er81$^-$ and is therefore a Layer 4 pyramidal neuron. Note that in this example the apical dendrite of the neuron is still intact, extending towards the pial surface. Since the dendritic structure of this neuron only shows minimal overlap with adjacent labelled neurons, this neuron surpasses the inclusion criteria for further analysis (i.e. dendritic tracing).

A visual evaluation of the traced neurons at different timepoints already reveals that the morphology of L4 neurons undergoes major changes during the first two weeks of postnatal development (Figure 19). At P4, the dendritic tree surrounding the soma is small. In contrast, at P10, the dendritic tree seems to have expanded and is more complex, covering a larger volume surrounding the cell body with seemingly more bifurcations. At P15, this complexity seems to have decreased, as the dendritic branches seem to cover less space in comparison to P10. Notably, some heterogeneity can be observed between L4 neurons of the same age.

Dendritic parameter analyses reveal that early postnatal development of L4 morphology is characterized by both pruning and growth events

In order to objectively and quantitatively describe the morphological changes observed in the reconstructed neurons across early postnatal development, we extracted various parameters that are commonly used to describe the dendritic morphology using the software Neurolucida Explorer.

Though not all developmental changes reached significance, several interesting trends are emerging when evaluating the results presented in Figure 20. First of all, both the average segment length (B) as well as the total dendrite length (C) increased significantly between P4 and P10 (see Figure 6, for definitions used in describing dendritic morphology). Between P10 and P15, the average segment length showed a tendency to further increase. Thus, there is a phase of overall dendrite expansion between P4 and P15.

The examination of branch points suggested an increase between P4 and P10, followed by a decrease at P15, though this did not reach statistical significance in the current dataset. Thus, it appears that dendritic branching is more extensive at P10 and decreases around eye opening. Interestingly, this increase and subsequent decrease in dendritic complexity seems to be caused by a parallel trend of increase and decrease in the number of secondary and tertiary dendrites, as the number of primary dendrites does not seem to change during early postnatal development.

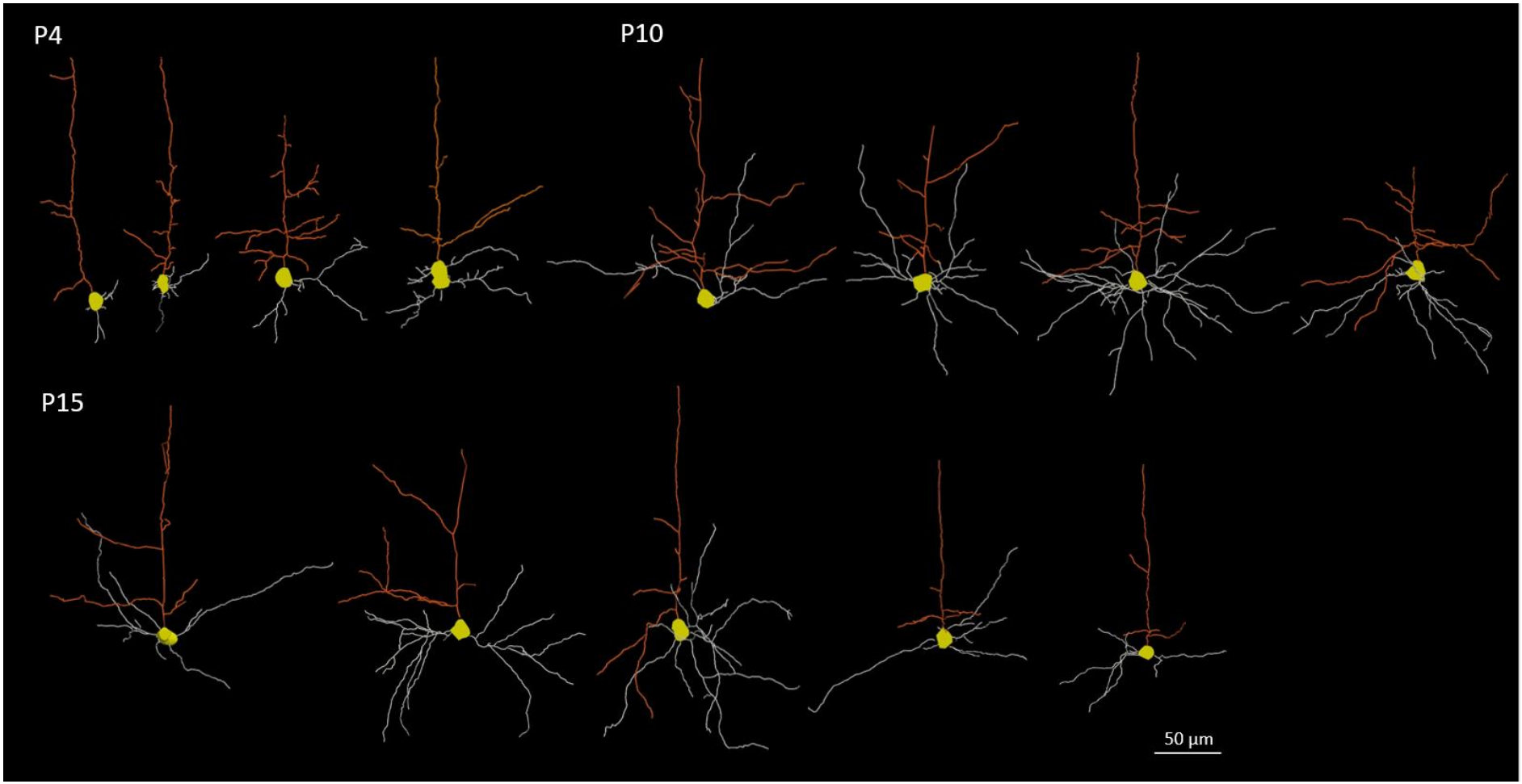

Figure 19 Morphological reconstruction of Layer 4 (L4) neurons of the primary visual cortex (V1) at postnatal day 4 (P4), P10 and P15 suggest that the basal dendritic morphology undergoes major changes during early postnatal development. Basal dendrites are depicted in grey, the apical dendrite in orange and the cell body in yellow. Note that despite the heterogeneity in dendritic morphology of neurons of the same age, several trends are emerging to describe the development of basal dendritic morphology of L4 V1 neurons. At P4 the dendritic tree is small, encompassing only a small volume surrounding the cell body. At P10 dendrites have extended and the dendritic tree has become more complex, with seemingly more bifurcations. At P15, the dendritic tree appears to be less complex compared to P10. Morphological tracings are based on stitched 60x (1.30 NA) images acquired with a spinning disk confocal microscope.

A

	P4	P10	P15
Nr of replicates	4	4	5
Nr of animals	2	3	3
From nr of litters	2	3	3

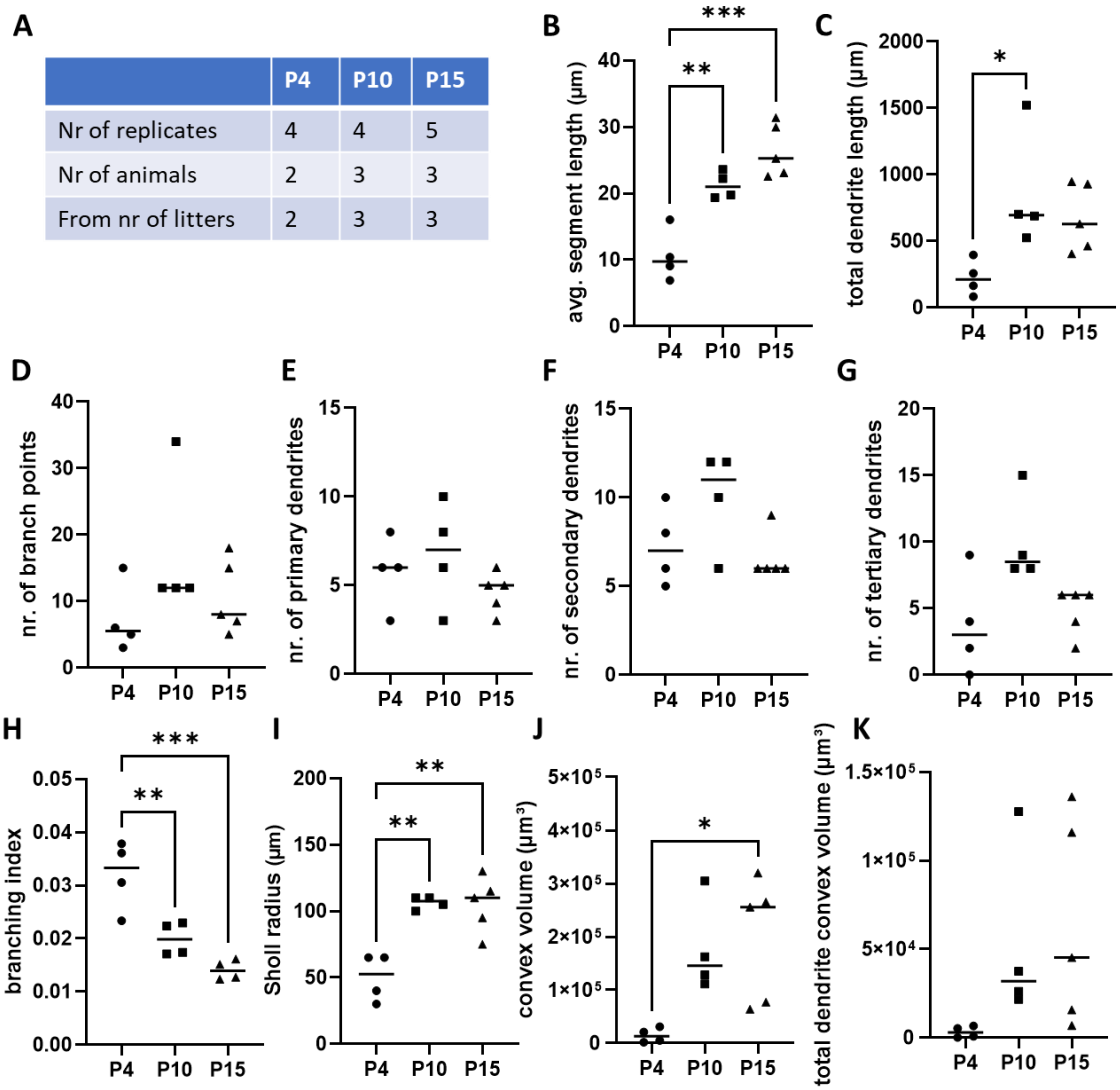

Figure 20 Parametric analyses at different timepoints reveal that early postnatal development of the basal dendritic morphology of L4 V1 neurons is marked by both growth and pruning events. avg = average, nr = number, * p<0.05, ** P<0.01, *** p<0.001. (A) table summarizing the origin of the data. (B-K) graphs depicting the values of different parameters that describe the dendritic morphology of L4 V1 neurons of the control at different ages during early postnatal development, at postnatal day 4 (P4), 10 (P10) and 15 (P15). Given the heterogeneity in morphology within conditions and the small dataset we choose to depict the median value instead of the mean. (B) the average (avg.) segment length as well as the total dendritic length of neurons within the same group (C) significantly increased between P4 and P10 (avg. segment length, one-way ANOVA with p<0.005 for P4-P10 and p=0.0001 for P4-P15 comparison, total dendrite length one-way ANOVA with p=0.0351 for P4-P10). While the total dendrite length did not appear to change between P10 and P15, a trend of a small increase was apparent for the average segment length (one-way ANOVA, P10-15 p=0.1151 vs. P=0.6476 for total dendrite length P10-P15). For the number of branch points, no significant results were reported. However, the trend emerges that there is slightly more branching at P10 compared to both P4 and P15. Since the number of primary dendrites appear to have overlapping distributions of variability, it can be hypothesized that the apparent increase and subsequent decrease in branching is attributed to the change in the number of secondary and tertiary dendrites, as these show a parallel trend (nr of secondary dendrites: Kruskal-Wallis test, P4-P10 p=0.3763, P10-P15 p=0.189, P4-P15 p>0.999, nr of tertiary dendrites: Kruskal-Wallis test with p=0.0827 for P4-P10, p=0.1235 for P10-P15 and P>0.999 for P4-P15). The branching index which is calculated by dividing the nr of branch points by the total dendrite length of the neuron, shows less variability and is therefore also able to capture the significant decrease between P4 and P10 (one-way ANOVA, p=0.0085) and P4 and P15 (p=0.0006) (P10-P15, p=0.1889). This decrease in branching index is driven by the relatively large increase in dendrite length (C). The Sholl radius (I) was significantly increased as well between P4 and P10, implying that the reach of the neuron is increased (one-way ANOVA P4-P10 p=0.002, P10-P15 p=0.99. P4-P15 p=0.0016). This is also reflected in the significant increase in convex volume drawn across the entire dendritic tree (J), as well as the trend of increase seen for the summed convex volume for individual dendrites (K) (Kruskas-Wallis test for (J), P4-P10 p=0.0548, P4-P15 p=0.0385 and P10-P15 p>0.999, and one-way ANOVA for (K), P4-P10 p=0.3185, P4-P15 p=0.1731 and P10-P15 p=0.9368).

The branching index (H) is a measure which is often used to describe the relation between the degree of branching relative to the dendritic length (Redmond et al., 2000) and is calculated by dividing the number of branch points by the total dendritic length of the neuron. The branching index parameter showed less variability in our dataset compared to the individual parameters as it counteracts the premature cut-off of some dendrites that are observed while sectioning. The branching index significantly decreased between P4, P10 and P15. This decrease in branching index occurs despite the increase in branch points that is observed between P4 and P10 and the subsequent decrease between P10 and P15. This is caused by the relatively large expansion in dendritic length that occurs during these developmental stages.

Other methods to describe the complexity of dendritic morphology is to define the Sholl radius, the radius of the sphere that is encompassing the longest dendrite of the dendritic tree, and to calculate the dendritic volume. Both the Sholl radius (I) and convex volume (J) significantly increased between P4 and P15, of which the first increased the most between P4 and P10. This suggest that the so-called reach or connective zone of the neuron is increased during early postnatal development and stabilizes between P10 and P15.

2.3.5 Conclusion

Overall, the data presented in this chapter indicate that early V1 postnatal development is characterized by parallel changes in thalamocortical ingrowth, synchronous activity patterns and dendritic morphology.

First of all, thalamocortical axon ingrowth is not yet complete at birth but continues until postnatal day 10 (P10), as is indicated by an increase in the axonal coverage in images acquired in layer 4 (L4). Though axonal coverage remains relatively constant up until eye opening at P14, a finer mesh of axonal arborizations seem to arise based on visual evaluation of the 63x magnification images. In addition, the number of axonal varicosities that colocalizes with the presynaptic marker vlgut2 appear to increase in parallel, which suggests that the number of presynaptic structures increases during early postnatal development.

Though structural thalamocortical input to L4 is already present at P4, it appears that thalamocortical activity is rarely able to drive synchronous firing in V1 within the first postnatal week, as two-photon calcium imaging in L2/3 and L4 cells detected a low frequency of spontaneous synchronous events (once every five minutes). The occurrence of synchronous events in V1, which is most likely to originate from spontaneous activity from the periphery within the explored time window, increased up until eye opening. Interestingly, there was a sharp peak visible in the number of neurons that participated in a given synchronous event around P9, which steadily decreased until eye opening at P14.

The dendritic structure of L4 neurons in V1 also undergoes major changes during early postnatal development. While the dendritic tree is only small at P4, encompassing a small volume in the cortex with only few branches, the dendritic tree significantly increases its complexity and reach as is indicated by an apparent increase in the number of bifurcations (i.e. branching points) and a significant increase in Sholl radius. Though the dendritic length tends to continue to increase between P10 and P15, complexity appears to decrease as the number of secondary and tertiary dendrites, and thus the number of branch points, decreases. The high heterogeneity of dendritic structures of pyramidal neurons, which was also previously reported for L2/3 pyramidal neurons in V1 by Richards and colleagues (2020), posed a challenge to capture these changes statistically. We are currently expanding the dataset to increase the statistical power to account for the high variability.

In conclusion, we can identify several ages as crucial timepoints in the development of thalamocortical-L4 interactions based on the results presented in this chapter:

- P4, at which structural thalamocortical input to L4 is limited and functional input is absent
- P9-P10, at which the number of thalamocortical axons/axonal arborizations have stabilized and at which synchronous firing events in V1 are characterized by a peak in neuronal participation ratio.
- P13-P15, the days around eye-opening which are characterized by a peak in synchronous event frequency, an apparent restructuration of axonal arborizations and a decrease in dendritic branching complexity.

Given that developmental changes in dendritic morphology occur in the same time window at which we see changes in structural and functional thalamocortical input, the question arises whether the morphological changes reported in L4 V1 neurons are directly influenced by this input.

2.4 The influence of spontaneous activity on the morphology of L4 neurons in V1

Having identified crucial timepoints in the development of structural and functional thalamocortical input to layer 4 (L4) neurons, and having explored L4 morphological changes during early development, a next step is to assess the relationship between the two developmental processes. With the establishment of a surgical protocol for targeted viral injections in the dLGN of neonates, we can introduce molecular silencers of activity to markedly reduce activity from the periphery from an early age in transgenic MORF3-Rorb-IRES-Cre mice in which L4 neurons of the cortex are sparsely labelled by V5 expression. We therefore have the tools available to assess the influence of functional input from the dLGN on L4 morphology in V1. Since a neuron's morphology is one of the factors that is determining the degree of circuit integration, these results will provide insight in if, and to what extent spontaneous activity from the periphery is instrumental for circuit integration during development.

Several molecular silencers aimed to silence or decrease neuronal activity are available to date. Often used molecular silencers include the overexpression of the Kir2.1 channel, expression of Tetanus neurotoxin (TeNT), and expression of the inhibitory DREADD (Designer Receptors Exclusively activated by Designer Drugs) hM4Di, which is only active when an agonist, such as clozapine N-oxide (CNO) is bound. The use of each of these molecular silencers are characterized by several advantages and disadvantages depending on their underlying molecular mechanism. The overexpression of TeNT blocks synaptic vesicle release trough cleavage of synaptobrevin, one of the proteins that is essential for vesicle fusion (Sweeney et al., 1995). This prevents neurotransmitter release, but also blocks neuropeptide release, causing unwanted side effects. Furthermore, unpublished results from our lab by Dr. Ying Yin Lee have indicated that the expression of TeNT *in vivo* can cause gliosis. Overexpression of the Kir2.1 channel and DREADDs act both through increasing the firing threshold of a cell by decreasing the resting membrane potential through an increase of potassium efflux (Roth, 2016; White et al., 2011). As a result, firing is markedly decreased. The use of DREADDs in combination with CNO has the advantage over both Kir2.1 and TeNT, in that it provides temporal control of silencing effect. However, concern has been raised in recent years over unwanted side effects that are caused by the degradation products of CNO (Raper et al., 2017; Roth, 2016; Thorn et al., 2018). Among these degradation products, is clozapine, a commonly used antipsychotic drug. Even though promising new agonists have been developed recently, more research is needed to map the actions of these agonists and the side effects of their degradation products on the nervous system.

While the different advantages and disadvantages attributed to the different molecular silencers of activity all need to be considered before choosing the optimal strategy for our experimental purpose, the most important prerequisite is that the applied silencing strategy does not interfere with thalamocortical axon development, as this will affect both the structural and functional thalamocortical input to L4 neurons. Since a previous study reported that Kir2.1 overexpression in olfactory sensory neurons led to a delay in axon ingrowth in the glomeruli (Yu et al., 2004), it is important to exclude gross effects on thalamocortical ingrowth in V1 when implementing any of the silencing strategies. I therefore performed a pilot experiment in which I explored the pattern of axons/axonal arborizations for all three molecular manipulators, visualized by the concomitant expression of the cell filler mCherry, at postnatal day (P) 9 after viral injection at P0.5. A visual comparison of axonal coverage with the CAG-tdTomato injected brain suggested that axonal ingrowth is largely unaffected for all three molecular silencers (data not shown).

Since the fluorophore mCherry has different spectral properties than the fluorophore tdTomato in the control condition, a direct and quantitative comparison of axonal coverage between conditions prove to be difficult. Furthermore, a delay in ingrowth could be apparent at an earlier timepoint and be corrected at P9, therefore a direct comparison of tdTomato expression at an early timepoint was warranted.

Though the initial pilot experiment did not reveal marked differences in axonal ingrowth for all three molecular silencers compared to the control condition, we decided to move forward with Kir2.1 for the quantitative evaluation of axonal ingrowth, since we considered Kir2.1 as the most appealing candidate for several reasons. First, to silence activity, Kir2.1 channels do not require the administration of a ligand as is the case for hM4Di. Though it therefore does not allow for temporal control of activity, it does provide a practical advantage; there is neither need to expose the animal to repeated CNO injections nor to perform a functional analysis to establish the appropriate dose and related duration of the silencing effect. More importantly, Kir2.1 overexpression is a widely accepted molecular tool to silence activity and has previously been used and validated in neonatal mice to suppress activity (Mizuno et al., 2007; Moreno-Juan et al., 2017).

2.4.1 Overexpression of the Kir2.1 channel does not significantly grossly impair structural thalamocortical input

We compared thalamocortical axon ingrowth in V1 at P4 between animals that were injected at P0.5 with the AAV9 virus carrying either the syn-tdTomato or the syn-kir2.1-2a-tdtomato construct. With the use of the 2A protein coexpression system, the expression level of the fluorescent protein tdTomato is linked to the expression level of Kir2.1. We choose to adopt the neuron-specific synapsin (syn) promoter instead of the previously used ubiquitous CAG promoter to minimize confounding factors created by Kir2.1 expression in other cell populations such as glia and astrocytes. Animals were sacrificed at P4 through transcardial perfusion and brains were processed as described previously in detail in the Material and Methods chapter. By staining with a red fluorescent protein (RFP) antibody, which shows reactivity to various red fluorescent proteins including tdTomato, thalamocortical axons were visualized in the primary visual cortex (V1).

Visual evaluation of the higher magnification images (63x, 1.40 NA) did not reveal gross changes in thalamocortical axon ingrowth in layer 4 of V1 (Figure 21A and B). To objectively confirm this observation, we quantitatively assessed axonal ingrowth by using the same algorithm as is described in section Quantification of axonal ingrowth in L4 of V1 in chapter 2.2. This algorithm defines the area of axonal coverage, that is, the percentage of RFP^+ pixels within a given image. The results of this analysis are shown in Figure 21D. Though the statistical test did not reach significance, it does appear that the expression of Kir2.1 results in a slight reduction of axonal coverage. However, five out of the eight datapoints in the syn-tdTomato group were obtained from injections in which a 10 times higher viral titer was used by mistake (10^{13} instead of 10^{12} GC/ml). Given the effect of viral titer on expression level, it is likely that the higher mean of axonal coverage for the syn-tdTomato group was driven by these injections. Indeed, 4 out of the 5 datapoints in which the higher titer was used had a relatively high axonal coverage of 8%. This was also higher than the mean axonal coverage at P4 for CAG-tdTomato injected brains of 5.6%, (presented in Figure 15). Based on these considerations we therefore concluded that overexpression of Kir2.1 in the dLGN does not lead to major defects in thalamocortical axon ingrowth into V1 at P4. While defects on a smaller scale cannot be excluded, such as differences in axonal branching or in synaptogenesis, we believe that the exclusion of gross structural changes is sufficient to differentiate the functional effects of thalamocortical input on morphological development of L4 V1 neurons from the influence of structural input.

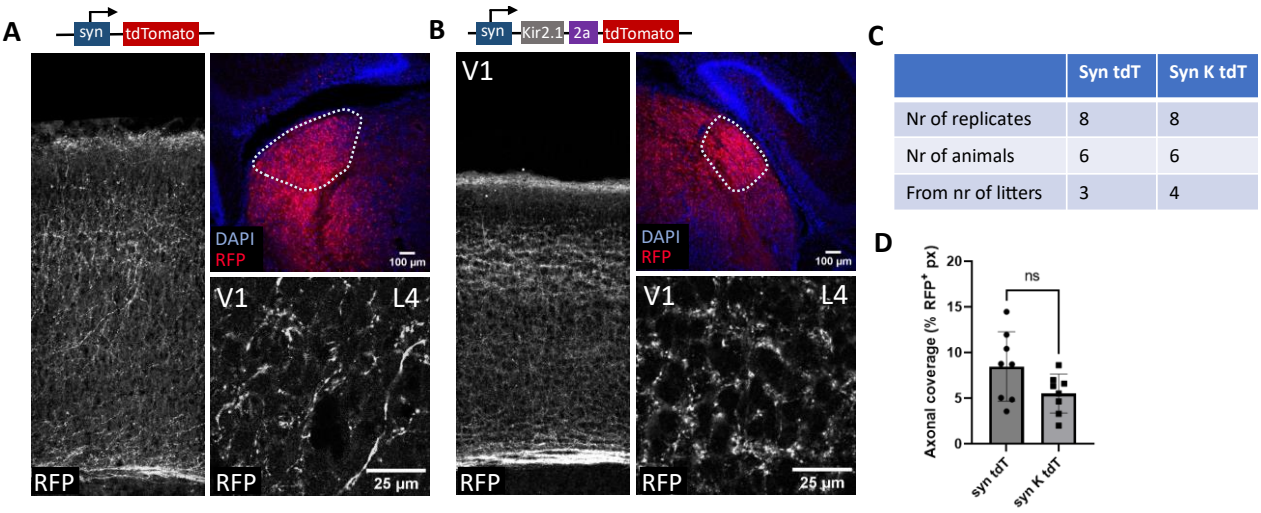

	Syn tdT	Syn K tdT
Nr of replicates	8	8
Nr of animals	6	6
From nr of litters	3	4

Figure 21 Kir2.1 expression in the dLGN does not significantly alter thalamocortical ingrowth in the primary visual cortex (V1) at postnatal day 4 (P4) We compared red fluorescent protein (RFP) expression levels in layer 4 (L4) of V1 at P4 between animals that were injected with either AAV9 syn-tdTomato ($3.6*10^{12}$ GC/ml and $2.0*10^{13}$ GC/ml) (A) or AAV9 syn-Kir2.1-2A-tdTomato ($3.0*10^{12}$ GC/ml) ((B) by defining the axonal coverage (D), that is, the percentage of RFP^+ pixels (px) in a given image. Injection site (IS) was visually evaluated across multiple sections on the anterior-posterior axis. Only injections that did show sufficient tdTomato expression across the entire dorsal lateral geniculate nucleus (dLGN) were included in the analysis (top right of A and B). Visual evaluation of the data did not reveal gross changes in thalamocortical ingrowth on the 10x (0.45 NA) overview pictures of V1 (left of A and B) nor on the 63x magnification (1.40 NA) images (bottom right A & B). The quantification presented in (D) confirms this observation, though there is a trend visible of a small reduction in expression level in the syn-Kir2.1-2A-tdTomato (syn K tdT) group (t-test, p=0.0739). This higher mean axonal coverage for the syn-tdTomato (syn-tdT) group could be explained by the higher viral titer used for most of these injections (10^{13} instead of 10^{12} GC/ml). We therefore believe that the gross thalamocortical ingrowth in L4 of V1 is intact for dLGN neurons expressing Kir2.1.

2.4.2 Visual evaluation of the preliminary results does not reveal gross differences in L4 dendritic morphology upon silencing thalamocortical activity

After establishing that Kir2.1 expression does not grossly impact structural thalamocortical input, we set out to study the influence of thalamocortical input on morphological development of L4 pyramidal neurons in V1. Since several interesting differences in morphology between P10 and P15 were reported in the previous chapter 2.3.4, we decided to evaluate morphological differences between experimental conditions on the day of eye opening at P13 to capture the influence of predominantly spontaneous thalamocortical activity. To this end, we injected MORF3xRorb-IRES-Cre P0 pups from the control group with the AAV9 syn-tdTomato virus, and pups from the experimental group with the AAV9 syn-Kir2.1-2a-tdTomato virus. Animals were sacrificed at P13 through transcardial perfusion as described in detail in the Material and Methods section. Sections were stained with an antibody reactive to V5 to visualize the morphology of $Rorb^+$ neurons and with an Er81 antibody, a L5 and L6 pyramidal cell marker. Based on Er81 reactivity, we could distinguish $Rorb^+$ L4 neurons from $Rorb^+$ L5 and L6 neurons. Only L4 neurons that showed minimal overlap with other labelled neurons located in the anterior region of V1 were imaged as previously described in chapter 2.3.4 to facilitate accurate morphological tracing. Again, neurons in which multiple primary dendrites were cut by sectioning were excluded from the analyses. The compressed stitched 60x (1.30 NA) images were used for anatomical tracing in Neurolucida 360. A reconstruction of the traced neurons for both the control group (A) and the experimental group (B) are presented in Figure 22.

As can be seen in Figure 22 the dendritic structure of L4 V1 neurons within the same group demonstrates already a substantial degree of variability. Gross changes in basal dendritic morphology as were reported for L4 stellate cells in the somatosensory cortex (Mizuno et al., 2007; Nakazawa et

al., 2018), are not apparent in neurons in which thalamocortical activity was silenced by Kir2.1 expression. Nevertheless, some dendrites appear to be more extended in animals injected with the syn-Kir2.1-2a-tdTomato virus compared to dendrites of the control condition in our preliminary dataset. Furthermore, dendrites from neurons of the experimental group appear to have a higher degree of branching. However, it must be noted that the small dataset in combination with the high degree of variability poses a challenge to capture these subtle changes in dendritic morphology between conditions.

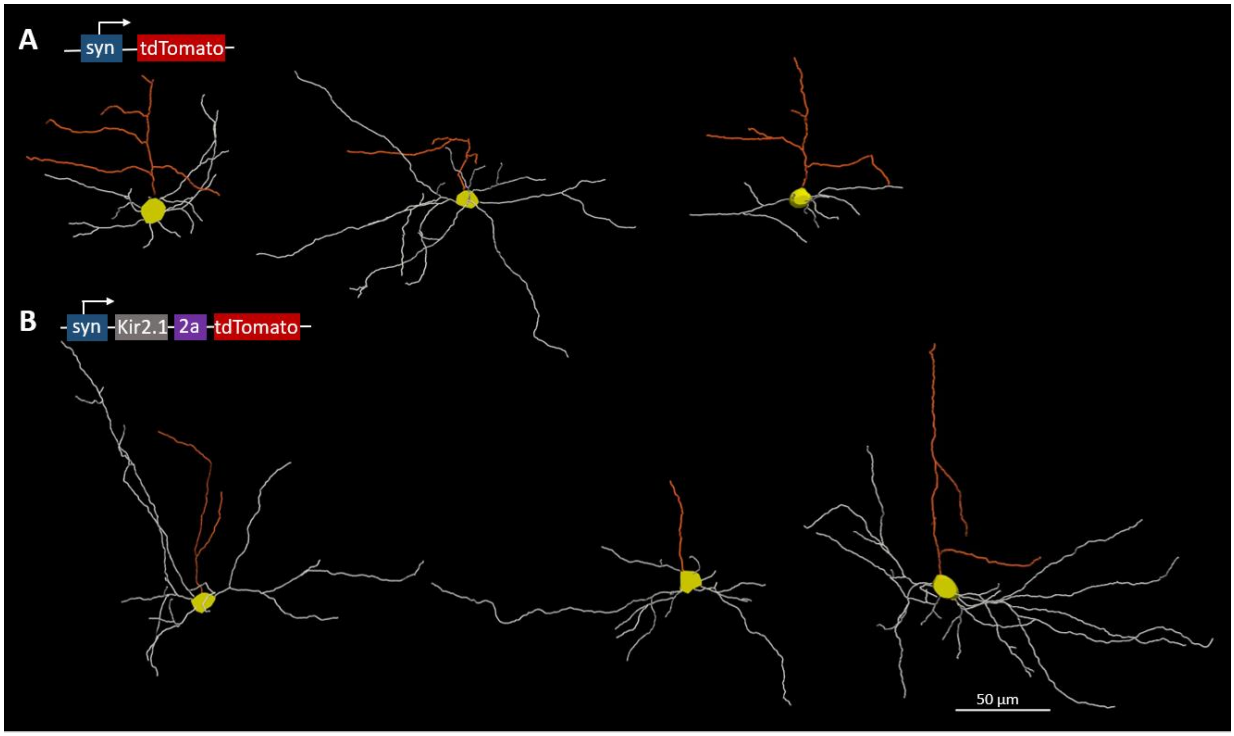

Figure 22 Morphological reconstruction of layer 4 (L4) neurons of the primary visual cortex (V1) at P13 show subtle changes upon silencing of thalamocortical activity. Reconstructed neurons of animals injected with the control AAV9 syn-tdTomato virus ($3.6*10^{12}$ GC/ml) (A) and AAV9 syn-Kir2.1-2A-tdTomato virus ($3.0*10^{12}$ GC/ml) (B). The apical dendrite, which is often cut, is depicted in orange, the basal dendrites are depicted in grey. Neurons in the experimental condition seem to branch more. Furthermore, some individual dendrites seem to extend over a longer area, while this cannot be observed in the control condition. Morphological tracings are based on stitched 60x (1.30 NA) images acquired with a spinning disk confocal microscope.

2.4.3 Preliminary dendritic parameter analyses suggest that L4 morphology is subtly affected by silencing thalamocortical input

Given the relatively large heterogeneity in L4 morphology and the small dataset of n=3, it is hard to capture changes in dendritic morphology associated with silencing thalamocortical activity. We therefore described the basal dendritic morphology for both conditions by exploring the same dendritic parameters as were used in the previous chapter to capture subtle differences in morphological characteristics. Though several trends emerge when evaluating the data presented in the graphs of Figure 23, caution must be taken when interpreting these results considering the small sample size. Further rigorous testing is required to verify the observations and hypotheses described below.

As can be seen in Figure 23, secondary dendrites appear to branch more in the experimental condition compared to the control condition, as the number of tertiary dendrites (G) appeared to be higher. This is the probable cause of the apparent increase in the number of branch points (D), which supports the

A

	Syn tdT	Syn Kir tdT
Nr of replicates	3	3
From nr of hemispheres	2	2
Nr of animals	2	1
From nr of litters	1	1

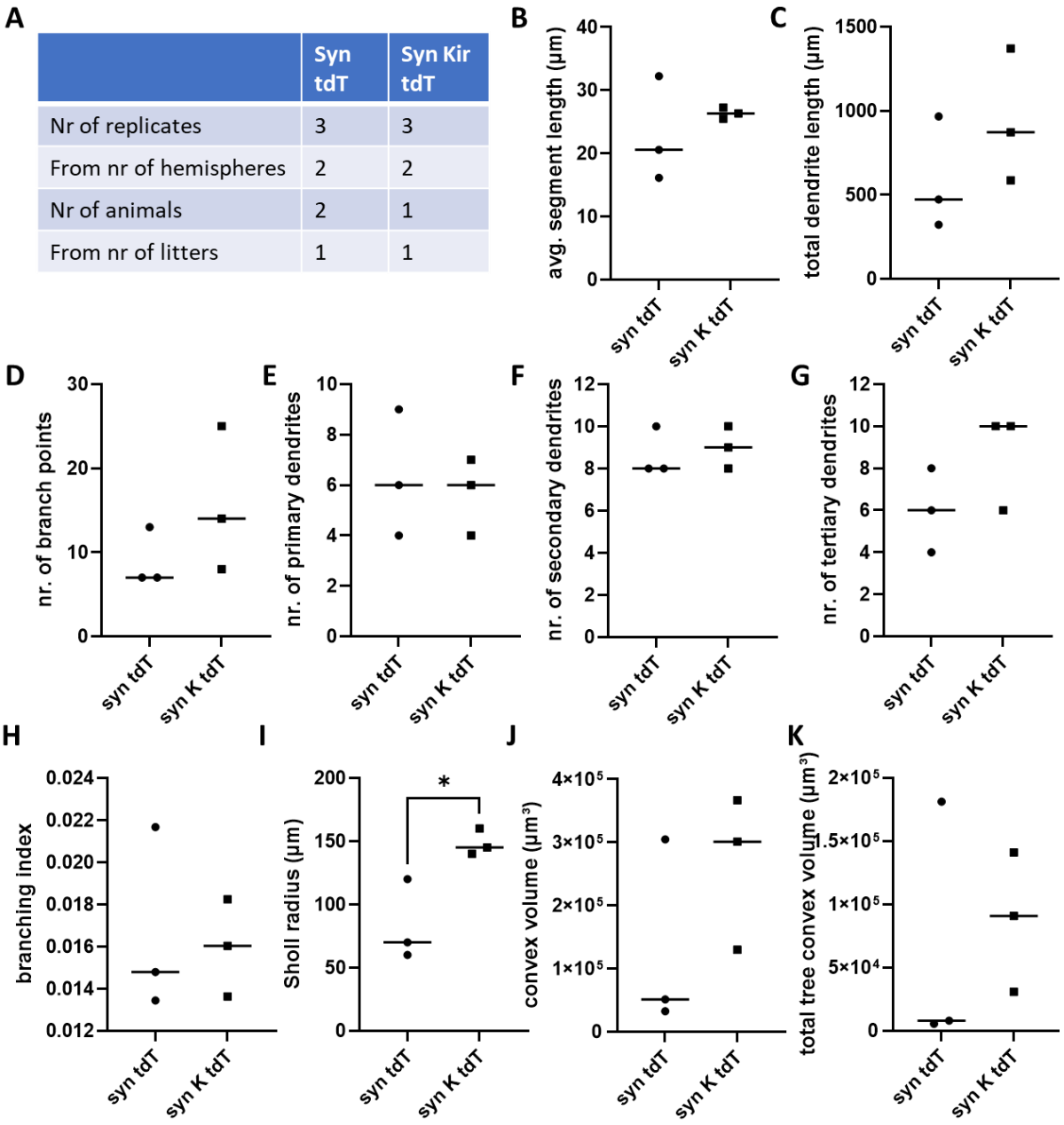

Figure 23 Parametric analyses of basal dendritic morphology of L4 V1 neurons at P13 of animals injected with either AAV9 syn-tdTomato (syn tdT) or syn-Kir2.1-2A-tdtomato (syn K tdT) viral titer: syn tdT $3.6*10^{12}$ GC/ml, syn K tdT $3.0*10^{12}$ GC/ml (A) table summarizing the origin of the data. Nr = number. (B-K) depicting the values of different parameters that describe the dendritic morphology of L4 V1 neurons of the control (syn tdT) and experimental condition (syn K tdT). Given the heterogeneity in morphology within conditions and the small dataset we choose to depict the median value instead of the mean. (B) the average (avg.) segment length as well as the total dendritic length of neurons within the same group (C) appeared to be higher in the experimental condition (unpaired t-test, p=0.2715 and p=0.3021). In animals injected with syn K tdT, the basal dendrites tended to show more branch points (D) which is likely attributed to an increase in the number of tertiary (G) dendrites as the number of primary (E) and secondary (F) dendrites did not change (Mann-Whitney test, p =0.200 for (D), p=>0.999 (F), unpaired t-test with p=0.6667 (G) and 0.7149 (E)) . The branching index (H) showed a slight increase in median in the experimental condition (unpaired t-test, p=0.8289). The Sholl radius (I) was significantly increased as well (unpaired t-test, p=0.0291), implying that the reach of the neuron is increased. This is also reflected in the apparent increase in convex volume for the total dendritic arbor (J), as well as the summed convex tree volume (K) (unpaired t-test, p=0.2928 and Mann-Whitney test, p=0.700).

visual observation made in the previous section. In addition, the segment length averaged per neuron (B) as well as the length of the entire basal dendritic tree (C) tends to be higher in animals injected with syn-Kir2.1-2a-tdTomato (syn K tdT). Therefore, it seems that not only there are more branches

at P13 when silencing thalamocortical functional input, but also that these tend to be longer. The branching index, a parameter that can be used to capture the complexity of the dendritic tree by dividing the number of branching points per neuron (D) by the total dendritic length (C), also reflect this trend; neurons of the experimental group appear to have a higher branching index (H). Taken together, these results suggest that the basal dendritic complexity is increased when thalamocortical activity is markedly reduced.

Furthermore, the significant increase in the Sholl radius (I) and the apparent increase in convex volume, in respect to both the total basal dendritic tree (J) and the individual dendrites (K), imply that the reach of L4 neurons is increased in absence of thalamocortical functional input. This suggests that the connective zone, a term posed by Sholl to describe the region in which synapse formation is possible, is enlarged when spontaneous activity from the periphery and dLGN is silenced.

2.4.4 Conclusion

Despite the requirement of dataset expansion, we believe that the data presented above raise some interesting hypotheses about the influence of thalamocortical input on dendritic morphology of L4 V1 neurons during early postnatal development. First of all, the observation that silencing thalamocortical activity tends to increase branching, specifically tertiary branching, and increase dendrite length and dendritic reach, suggest that the overall dendritic complexity is increased. Considering the role attributed to activity-dependent genetic programs in dendritic pruning, the hypothesis is raised that the observed increase in dendritic complexity is caused by a decrease in pruning in absence of spontaneous thalamocortical activity. Alternatively, the results could also be explained by a higher turnover of dendritic branching with an imbalance towards the growth of new branches.

Overall, the preliminary data presented in this chapter cautiously suggest that thalamocortical input may regulate the dendritic morphological development of L4 pyramidal neurons in V1 through either transcriptional programs or local signalling regulation. Since we did not find a difference in the gross thalamocortical structural input upon the expression of Kir2.1 in neurons of the dorsal lateral geniculate nucleus, we believe that the absence of synaptic transmission from the dLGN and periphery is responsible for the observed changes in dendritic morphology. Nevertheless, rigorous testing is required to statistically support the observations on dendritic morphological changes made in this chapter. These experiments are currently ongoing.

3. Discussion

Intricate neuronal circuits are at the base of several vital functions and complex behaviours. The correct functioning of these networks relies foremost on the precise formation of these circuits during development. However, much remains to be understood about the mechanisms underlying normal brain development, knowledge that is essential for studying neurodevelopmental disorders such as autism. The current thesis set out to provide insight into one of the open questions, by studying how spontaneous activity from the periphery impacts the dendritic morphology of layer 4 (L4) pyramidal neurons of the primary visual cortex (V1) during the first two weeks of postnatal development. First, I described the normal developmental timeline of axonal ingrowth from the dorsal Lateral Geniculate Nucleus (dLGN) into L4 of V1 to understand when structural thalamocortical input matures. Furthermore, two-photon calcium imaging data acquired by Dr. Susanne Falkner provided information on how functional thalamocortical input evolves during early postnatal development. Since the eye lids of mice remain closed until postnatal day 14 (P14), activity recorded in V1 is largely driven by spontaneous activity from the periphery. In addition, we explored how the basal dendritic tree of L4 neurons is shaped during early postnatal development by tracing sparsely labelled neurons in the MORF3xRorb-IRES-cre mouse line at distinct ages. These analyses provide a valuable description of each of these developmental processes and reveal that early postnatal development is characterized by parallel changes in thalamocortical axon ingrowth, synchronous activity in V1 and basal dendritic structure. Finally, we aimed to explore the relation between two of these developmental processes. By silencing the dLGN through a pioneering surgical protocol for precise viral stereotactic injections targeted to the dLGN in P0 pups, we could study the impact of spontaneous activity from the periphery on the dendritic development of L4 V1 neurons. Though these experiments are still ongoing to strengthen our observations, preliminary results indicate that spontaneous thalamocortical activity might be instructive for dendritic development of pyramidal neurons in L4 of V1.

3.1 Early postnatal development is characterized by parallel changes in thalamocortical axon ingrowth, synchronous activity patterns, and dendritic morphology

Previous studies exploring thalamocortical axon ingrowth have been conducted in a variety of species looking at innervation patterns of the cortex in general. Furthermore, these studies did not explore whether developing axonal arbors possessed synaptic structures. A comprehensive overview of the dynamics of thalamocortical ingrowth in a specific region, such as L4 of V1, was therefore lacking. The current work closes this knowledge gap by providing information on the precise timing of thalamocortical axon ingrowth in L4 of V1 and exploring the presence of presynaptic vesicles during early postnatal development. To this end, we introduced the expression of the fluorescent protein tdTomato in dLGN neurons through targeted viral stereotactic injections following a novel surgical protocol. Our data reveals that thalamocortical axon ingrowth is not yet complete at birth. Instead, the number of axons/axonal arborizations increases in L4 of V1 until postnatal P10 after which axonal coverage (i.e., the percentage of RFP+ pixels) remains stable. Though axonal coverage remains relatively constant up until eye opening at P14, a finer mesh of axonal arborizations seems to arise based on visual evaluation of the images acquired in L4 of V1, indicating that a restructuration of the existing axonal arbors is taking place within this time period. Furthermore, though we did not quantitatively test this, the number of axonal varicosities that colocalized with the presynaptic marker

vlgut2 appears to increase in parallel with axonal ingrowth, which suggests that the number of presynaptic structures increases during early postnatal development.

Interestingly, while previous studies have indicated that the majority of thalamocortical axons have grown out of the subplate and innervated the cortical plate at birth (Auladell et al., 2000; Del Rio et al., 2000; Deng and Elberger, 2003), our results indicate that the innervation of the target layer L4 requires several days to be completed. Whether more thalamocortical axons accumulate in the subplate and extend in the cortical plate after birth, or whether some of the axons already grown into the cortical plate are slowed down on their way to the appropriate layer, remains to be investigated. Another interesting observation is that the total axonal coverage in L4 remains stable after P10, indicating that pruning of axonal arborizations on a macroscopic scale appears to be absent, an event that is reported to be essential in strengthening correct connections and eliminating aberrant ones during development (Oşan et al., 2011). Yet, the lack of reduction in net axonal coverage reported in the present study does not necessarily argue against pruning of individual axonal arbors. Indeed, the growth of new axonal branches or the extension of existing branches could counteract the loss created by pruning events. Since we only assessed thalamocortical axon ingrowth as a whole, we cannot address this question.

Despite growing interest in understanding how spontaneous wave activity generated in the periphery affect visual circuitry, little attention has gone to map the spatial-temporal characteristics of these spontaneous waves in areas downstream of the retina, such as V1. Longitudinal two-photon calcium imaging in V1 performed by our lab provide a first detailed description of the characteristics of synchronous firing events in V1 during early postnatal development. These synchronous events likely originate from spontaneous activity in the periphery, including retinal waves, and from spontaneous wave activity generated in the thalamus. Synchronous events were rare within the first postnatal week of development, with one wave occurring every five minutes. The wave frequency increased steadily from P8 until the day before eye opening at P13 to two waves per minute. Interestingly, there was a sharp peak visible in the number of neurons participating in a synchronous event at P9 to 80% followed by a quick drop to 40% at P10. The increase in wave frequency in the second postnatal week of development reported by my colleague Dr. Susanne Falkner, coincides with the transition from the cholinergic stage II retinal waves to glutamatergic stage III waves. Recordings in the retina have shown that the wave frequency of the latter is higher relative to the earlier stage II waves, which probably translates in the higher wave frequency recorded in the cortex at the end of the second postnatal week. Interestingly, a recent study by Gribizis and colleagues (2019) performing simultaneous wide-field imaging of wave activity in the thalamocortical axons and visual cortex, reported that the capacity of thalamocortical axons to drive wave events in V1 decreased during development; glutamatergic waves were less often able to elicit V1 synchronous firing events compared to cholinergic waves. However, it is unknown whether the loss of peripheral drive led to a decrease in wave frequency in their experimental paradigm, as these results were not reported. Though at first sight the two-photon data described in this thesis seem to contradict the findings reported by Gribizis and colleagues (2019), an increase in wave frequency elicited by spontaneous activity from the periphery could occur at the same time as the cortex gains independence from peripheral drive, if the retinal wave frequency substantially increases at the same time.

Alternatively, the increase in wave frequency could also be explained by the occurrence of synchronous events elicited by an alternative origin, such as the cortex, during the end of the second postnatal week. This is, however, unlikely as the evidence available to date indicates that synchronous activity in V1 before eye opening is mainly attributed to thalamocortical input (F. Siegel et al., 2012). Nevertheless, since the data presented in this thesis cannot exclude this possibility and the study of

Gribizis and colleagues (2019) did not report data on wave frequency, it remains an open question how wave activity in V1 increases before eye opening while the visual cortex simultaneously is driven less by peripheral input.

While dendritic morphology is a determinant factor for a neuron's function, much remains to be understood on how the dendritic tree is formed and reshaped during development (Richards et al., 2020). Specifically, no study to date reports on the dendritic development of L4 neurons of V1 in early postnatal development. In collaboration with Shirley Dixit, I explored the dendritic morphology of sparsely labelled L4 neurons of V1 at different ages during the first two weeks of postnatal development in the MORF3xRorb-IRES-Cre mouse. Due to the large heterogeneity in dendritic morphology, not all observed differences reached significance in the current dataset. We are currently adding more replicates to account for this effect. Nevertheless, several trends did emerge when evaluating the presented data, indicating that the basal dendritic morphology of pyramidal L4 neurons undergoes major changes during early postnatal development. The significant increase in dendrite length as well as the significant increase in Sholl radius and convex volume between P4 and P10, suggest that the so-called reach of a neuron and thus the functional connectivity capacity of a neuron increases during early postnatal development. Furthermore, the number of branch points as well as the number of secondary and tertiary dendrites increased between P4 and P10, indicating that the complexity of the dendritic structure increases. Interestingly, these dendritic parameters showed a tendency to decrease between P10 and P15, suggesting that part of the dendritic complexity previously gained is subsequently lost by the loss of secondary and tertiary dendrites. This raises the hypothesis that the loss in dendritic complexity is caused by the pruning of aberrant secondary and tertiary branches. However, since we did not perform longitudinal live imaging of the same neurons over development, it is possible that all dendritic trees visible at P15 are newly formed and that the changes observed in dendritic parameters are caused by a change in turnover rate rather than by the stabilization of existing dendritic segments and the pruning of erroneous segments. Structural two-photon imaging in the somatosensory barrel cortex, provide evidence for the latter; L4 stellate cells located at the edge of a barrel eliminate their erroneous dendritic projections extending outwards of the barrel, while strengthening and elaborating the existing dendrites located in the centre of the barrel cortex during development (Nakazawa et al., 2018).

Another interesting observation is that the number of primary dendrites did not change during early postnatal development. This coincides with findings by Richards and colleagues (2020), which reported that the number of primary arbors in pyramidal L2/3 neurons in V1 remained stable between P7 and P21. These results therefore suggest that the number of primary dendrites is defined early in development. Our findings indicate that, for L4 pyramidal neurons in V1, the number of primary dendrites might already be established before P4 and is therefore not likely to be affected by both structural and functional thalamocortical input.

3.2 Functional thalamocortical input is likely to affect dendritic development of L4 neurons in V1

The above-described developmental processes in thalamocortical axon ingrowth, dendrite arborization and maturation of activity patterns are not segregated processes that happen to occur within the same time window but rather are closely intertwined. While the relation between spontaneous activity from the periphery and dendritic morphology was studied in the barrel cortex, the question how functional thalamocortical input affects dendritic development of cortical neurons in the visual system remained previously unanswered. Our results provide some insight in this

relationship. Using the novel stereotactic protocol for viral injections in the neonate mouse, we introduced the expression of the molecular silencer Kir2.1 as well as the fluorescent protein tdTomato in MORF3-Rorb-IRES-cre pups, to both markedly reduce activity in the dLGN as well as to visualize thalamocortical axons. Animals from the control group were injected with a virus matching in serotype, promoter and viral titer, to introduce the expression of merely the fluorescent protein. Though we did not yet perform experiments to functionally verify the silencing effect upon Kir2.1 expression, there is a precedent of several studies demonstrating a successful activity reduction upon Kir2.1 expression in the neonate brain (Mizuno et al., 2007; Moreno-Juan et al., 2017).

After establishing that Kir2.1 expression in the dLGN did not grossly impact structural thalamocortical input, we explored differences in basal dendritic morphology between the experimental and control group at P13. Though the group size is too small to draw definite conclusions, interesting observations can be made based on the parametric analyses of the basal dendritic morphology. First, silencing thalamocortical activity seemed to be associated with a higher dendritic length as well as an increased number of branching points. The increase in branching is likely attributed to the addition of more tertiary dendrites, as the number of tertiary dendrites increased when thalamocortical activity was silenced by Kir2.1 expression. The number of primary dendrites was not affected by silencing thalamocortical activity, further strengthening the hypothesis that the number of primary dendrites is genetically defined early in development and that this is not affected by functional input from the periphery. Furthermore, neurons in the experimental group had a significantly higher Sholl radius and an apparent larger convex volume, parameters that indicate that the reach or the so-called connective zone of a L4 pyramidal neuron is increased upon silencing thalamocortical activity. Overall, the trend emerges that silencing thalamocortical activity leads to an increased level of dendritic complexity.

The apparent increase in dendritic length and Sholl radius observed for the Kir2.1 group could be explained by a distortion in structural thalamocortical axon ingrowth in V1. For instance, larger thalamocortical axon termination zones have been reported in the $\beta2^{-/-}$ mouse (Chandrasekaran, 2005; McLaughlin et al., 2003; Mrsic-Flogel, 2005). While we excluded gross changes in structural thalamocortical input by evaluating the net axonal coverage in L4 of V1, we cannot exclude that axonal branching is affected on an individual level. If thalamocortical axons indeed have larger termination zones, signalling molecules excreted by the axon could direct the growth of dendrites of the target neurons towards the extended axonal arborizations, resulting in an increased length and reach of the basal dendrites of L4 neurons in V1, as is observed in the present study. However, since we did not find a significant difference in net axonal coverage between experimental conditions, the extent of axonal branching for larger axonal termination zones have to be decreased. If the aberrant structural input would direct dendritic restructuration in L4 pyramidal neurons, a decrease in dendritic branching is likely to occur to match the decrease in axonal branching. Our data indicate that actually the opposite, an increase in dendritic branching, is happening. We therefore believe that the absence of mainly functional thalamocortical input, and not a change in structural input, is responsible for the changes in dendritic morphology associated with Kir2.1 expression.

Considering the role attributed to activity-dependent genetic programs in dendritic pruning, we hypothesize that the apparent increase in dendritic complexity is caused by a decrease in pruning events in absence of spontaneous thalamocortical input. An alternative explanation is that all dendritic trees in neurons in the Kir2.1 condition are newly formed, and that the observed increase in dendritic complexity is caused by an increase in turnover rate favouring the outgrowth of new dendrites. Structural two-photon imaging of L4 stellate cells in the barrel cortex suggest that the first scenario is more likely to occur, as they report a lower dendritic turnover rate in stellate cells in animals in which the infraorbital nerve was cut (Nakazawa et al., 2018). However, future longitudinal structural imaging

of sparsely labelled L4 pyramidal V1 neurons have to performed to test our hypothesis. These experiments, however, have been technically challenging to conduct. First of all, no reliable fluorescent sparse labelling strategy exists today that is suited for live imaging of a genetically specified subpopulation of neurons. Available sparse labelling strategies are largely based on leaky expression systems and often exhibit low intracellular fluorophore concentrations. Our lab recently made advances in introducing the expression of a fluorescent protein in a genetically defined subpopulation in a sparse way to allow for structural two-photon imaging. The second challenge is that the Cre/loxP expression system is already in use to sparsely label target neurons in the cortex, and thereby unavailable to allow for the expression of molecular silencers in a specific region. Furthermore, the two viral strategies available to introduce transgene expression in the neonate mouse are characterized by limited spatial control of transgene expression. Though previous studies resorted to rigorous methods to silence activity from the periphery, for instance by enucleation, these gross manipulations often challenged the interpretation of the results. The novel surgical protocol for targeted stereotactic injections in the neonate mouse described in this thesis finally provides a tool that achieves precise transgene expression in the neonate brain, thereby providing a solution to the second of these technical challenges.

3.3 The newly established surgical protocol for targeted viral injections in the neonate mouse opens up new strategies to study previously unanswered questions

We developed a reproducible and reliable surgical protocol for viral injections in P0 mice to specifically target the dLGN, while keeping transgene expression in surrounding thalamic nuclei to a minimum. A high transgene expression level of the fluorescent protein tdTomato was already visible as early as P3, making it possible to visualize thalamocortical axons in the visual cortex. For injections in the dLGN, serotype AAV9 was the most efficient in transducing dLGN neurons. Importantly, a viral titer of at least 10^{12} GC/mL yielded the best outcome.

The described protocol excels in spatial control of transgene expression, among the two existing protocols for viral injections in the neonate, namely ventricle injections and transverse sinus injections as these will lead to whole-brain viral delivery (Hamodi et al., 2020; Kim et al., 2013). By injecting a small volume of 8nl over a prolonged period (10 minutes), spatial control of expression can be achieved for small brain regions such as the dLGN at P0. Though the success of hitting a small region is dependent on a few variables that are challenging to control, such as the placement of the head in the stereotactic frame, subsequent practice resulted in a reliable success ratio of 50-70%. More importantly, the success ratio did not depend on the experimenter performing the surgeries as the protocol was also successfully executed by others after being taught. While we currently targeted the dLGN, the surgical protocol can easily be adapted to target other brain regions by adjusting stereotactic injection coordinates.

A big advantage of the newly developed surgical protocol is that spatial precision of transgene expression does not depend on the Cre/loxP expression system, leaving the option open to use this system for other applications. This makes it possible to study previously unanswered questions, one of which we addressed in the current thesis. Importantly, the injection protocol can be used to introduce the transgene expression of various proteins, including the expression of fluorescent proteins and molecular manipulators of activity. Furthermore, we have shown that the innate fluorescent protein expression is sufficient to allow for cleared brain light sheet imaging and structural two-photon imaging at an early age. By introducing a fluorescent calcium indicator in the target

neurons through the Cre/loxP expression system, simultaneous two-photon calcium imaging can also be performed. This is only one example of the endless methodological strategies now available.

3.4 Future directions

Several interesting hypotheses can be formulated when interpreting the results on structural thalamocortical axon ingrowth, dendritic development and functional activity in V1 during early development in relation to each other. One of these, the question if thalamocortical activity influences dendritic development of L4 V1 neurons was directly tested in the present thesis, but several open questions remain to be explored.

For instance, an interesting observation can be made when evaluating the description of synchronous activity patterns in V1 in parallel to the dendritic development of L4 V1 neurons. Interestingly, the peak dendritic complexity of L4 neurons observed at P10 coincides with the peak in the number of neurons that participate in a synchronous event. Given that the increase in reach and dendritic branching increases the capacity of the neuron to connect with neighbouring neurons, it is tempting to think that a transient circuitry connecting neighbouring L4 neurons around this age, is responsible for the observed increase in correlated firing of L4 neurons. These transient connections would then presumably be eliminated by subsequent pruning leading to a decrease in participation ratio. Evidence for the existence of transient L4 circuitry during development, comes from a recent study by De Léon Reyes and colleagues (2019). This study demonstrated that L4 pyramidal neurons send transient callosal projections during early development, which are eliminated in a matter of days. Interestingly, the pruning of these transient connections also seemed to depend on thalamocortical input as bilateral whisker cauterization resulted in a significant increase in the number of callosal projecting neurons in adulthood. Furthermore, previous studies exploring dendritic dynamics by longitudinal imaging revealed that the extension and elimination of dendritic processes can occur rapidly (Mizuno et al., 2007; Nakazawa et al., 2018).

It is also important to note that the studied developmental processes in the present thesis are not the only factors at play. For instance, the formation of the cortico-thalamic feedback loop, the maturation of the inhibitory circuitry in the cortex and general developmental processes such as myelination, are all taking place within the first two weeks of postnatal development and are likely to affect other developmental processes, including the ones studied in this thesis. However, since it is impossible to study the relation between all these developmental processes at once, focusing on the relation between few of these developmental processes, is the only way to shed light on how the brain is shaped during development.

3.5 Concluding remarks

Taken together, the data presented in this thesis provide a valuable description of the development of structural thalamocortical ingrowth, functional thalamocortical input and of L4 pyramidal dendritic restructuration in V1 during early postnatal development. Furthermore, many interesting hypotheses on the relation between the described developmental processes can be formulated. The extensive description of the developmental processes that are essential for the establishment of the thalamocortical circuitry and connectivity capacity of L4 V1 neurons presented in this thesis provide a good starting point to study these questions. Furthermore, the novel method for spatially localized and precise viral injections in the neonate brain will provide a valuable tool for testing these hypotheses in future experiments.

In addition, while experiments are still ongoing to corroborate our findings, the data presented in this thesis suggest that functional thalamocortical activity might be instructive for the dendritic development of pyramidal L4 neurons in V1. A major open question, however, is how spontaneous activity from the periphery and its specific spatial-temporal characteristics interact with gene expression to steer molecular developmental programs underlying the observed changes in dendritic morphology.

4. Material and Methods

4.1 Mice and animal experimentation

All animal experiments were approved by the Cantonal Veterinary Office of Basel-Stadt and executed according to Swiss laws. C57BL/6JRj pups (Janvier labs) were both used to assess thalamocortical axon ingrowth and for the pilot experiment exploring the transduction efficiency of various AAV capsid types and promoters. For these experiments, we either ordered a pregnant female directly from Janvier or bred litters inhouse.

We kindly received two males of the MORF3 mouse line from prof. William Yang (UCLA). The sperm of these animals were used for in-vitro fertilization of C57BL/6J females after which the offspring was bred for multiple generations to establish the MORF3 mouse line in a C57BL/6J background. The MORF3xRorb-IRES-Cre transgenic line was generated inhouse by crossing heterozygous MORF3 animals with heterozygous Rorb-IRES-Cre mice (Jackson Laboratory, strain #023526). The offspring was bred for at least one generation to establish the colony. Since homozygous Rorb females demonstrated decreased fertility, only animals that were heterozygous for Rorb were used for breeding. All MORF3xRorb-IRES-Cre pups used for our experiments were heterozygous for both Rorb and MORF3.

4.2 Viral and plasmid vectors

The following plasmids were acquired through Addgene: pAAV-EF1a-tdTomato-WPRE-pGHpA (#67527), pCAG-Kir2.1-T2A-tdTomato (#60598), and pGEMTEZ-TeTxLC (#32640). We received the pCAG-hM4D-2A-tdTomato as a gift from the Ghosh lab. The coding sequence of the respective molecular manipulators was fused to a T2A (2a) and tdTomato sequence and placed in an adenoviral backbone under the control of the human Synapsin 1 (syn) promoter.

The CAG-tdTomato, syn-tdTomato and CAG-eGFP plasmids from our own plasmid collection were used for respectively the thalamocortical axon ingrowth study and the pilot study testing the transduction efficiency of various promoters and capsid types. The latter plasmid, CAG-GFP was therefore packaged in the AAV1, AAV8 and AAV9 serotype. All other virus preparations were made using the AAV9 serotype. Viruses were produced inhouse and stored at -80℃. The viral titer was determined through qPCR. For stereotactic injections, all viral preparations with a titer below 10^{11} GC/mL were discarded. Viruses used for stereotactic injections were stored up to three days at 4℃ for future use.

4.3 Stereotactic injections

For the initial pilot experiment testing which AAV serotype is best suited for transduction of dLGN neurons, we injected three different capsid types carrying GFP under the control of promoter CAG: AAV serotypes 1 (viral titer $4.0*10^{11}$GC/ml), 8 ($8.0*10^{12}$GC/ml) and 9 ($3.0*10^{12}$GC/ml). For testing the dynamics of the promoters CAG, ef1α and synapsin, we injected either AAV9 CAG-tdTomato ($3.2*10^{12}$GC/ml), ef1α-tdTomato ($4.4*10^{12}$GC/ml) or syn-tdTomato ($3.6*10^{12}$GC/ml). The injection protocol followed, is largely as described below in section 4.3.1. The difference is that we used a Hamilton® Neuros syringe (0.5µL, 32G, model 7000.5) for the initial pilot experiments. With the Hamilton® syringe the lower limit of injection volume was 75nl.

For the thalamocortical axon ingrowth experiment, we injected the AAV9 CAG-tdTomato virus at a viral titer of 10^{12}GC/ml. We choose to use the fluorescent protein tdTomato over GFP, as tdTomato

has a better signal-to-noise ratio compared to GFP. For the experiments studying the effect of silencing thalamocortical activity on morphological development we injected AAV9 syn-Kir2.1-2a-tdTomato in the experimental group and syn-tdTomato in the control group. These injections were performed according to the protocol described below.

4.3.1 Surgical protocol for stereotactic viral injections targeted to the dLGN of the neonate mouse

We developed a novel surgical protocol for viral injections targeting the dLGN in the neonate pup at P0. To this end, pups were removed from their home cage the day of birth and placed on a heating pad awaiting surgery. Before removing the pups from the mother, we closely observed the mother's behaviour in response to the presence of the experimenter's hand in the cage. Mothers that displayed signs of stress were more likely to reject the pups after surgery. Furthermore, we only performed surgeries on pups which showed a clear milk belly. This, to ensure that the pups were strong enough to survive the time apart from the mother but also since we considered this as a strong sign that the mother is able to take good care of her offspring. If milk bellies weren't visible within the first 12 hrs after birth, we did not use the respective litter.

Pups received a subcutaneous analgetic injection (Carprofen, 5µg/10ql) half an hour prior to surgery. Pups were then placed in an anaesthesia induction chamber for several minutes to ensure that the pup was vastly asleep by the administration of a mixture of isoflurane (Attane™, 56'761'002) and oxygen (Isoflurane Vaporizer, 810302). Pups were then positioned in a mould shaped out of clay, which was placed on a custom build heating pad with adjustable height. The pup was subsequently head-fixed in a KOPF® stereotactic frame (model 940, with model 926 mouse adaptor) using blunt ear bars (non-rupture ear bars, KOPF®, 8219211721). As the neonate skull is still soft, we looked for a balance between having a tight placement and not pressing in the brain too much. Since there are no anaesthesia masks available for the KOPF® system that are suited for neonates, we designed our own anaesthesia mask that was build by our in-house workshop (ID 6mm) to ensure both deep anaesthesia levels as well as limited leakage.

The head was wiped with an ethanol swab (B. Braun Medical, REF19579) after which a mixture of 1% lidocaine and 0.25% bupivacaine gel was applied to numb the skin. A small incision (<2mm) on the midline above the confluence of sinuses (see Figure 11) was made using a disinfected fine scissors (Fine Science Tools, 15005-08). Since the sagittal sutures of the neonate skull are barely visible at this age, we used the main blood vessels to determine the coordinates of injection. The injection capillary was placed above the confluence of sinuses and coordinates were set to 0. At the coordinate X=1.0, we evaluated whether the offset in Y-coordinate caused by a potential tilted placement in the stereotactic frame, would warrant new positioning. If an offset was absent or minimal (<0.05) we would continue with the surgical protocol. At X=1.0 and Y=1.2 a small craniotomy was made using a sterile 30G needle by keeping it parallel to the skull's surface. While direct penetration was possible using the injection capillary, we felt that the indentation needed to penetrate the skull led to too much damage based on initial trials using this technique which revealed a more severe gliosis reaction after injection. The z-coordinate was set at 0 on the surface of the brain. Borosilicate glass capillaries (Hilgenberg, length 100mm, wall thickness 0.45mm, OD 1.0mm, ID 0.1mm) were pulled using a vertical capillary puller (Narishige, model PC100). With these injection capillaries we injected a small volume of 8nl-15nl over a period of 10 minutes using the Picospritzer III pressure injection system (Parker). Injections of 8nl displayed the smallest amount of viral spread to adjacent regions but were characterized by a lower success rate of hitting the dLGN. After injection, we waited 5-10 minutes before retracting the capillary. Animals were bilaterally injected. During the surgery, the wound was

often rinsed with sterile saline solution (NaCl 0.9%, B Braun, 21267412) while excess fluid and blood was removed with sterile absorbent swaps (Sugi® sponge points, QUESTALPHA, REF31603). The skin was closed using Histoacryl® Flexible glue (B. Braun Surgical, REF1051250). The surgery took around 50-60 minutes to complete.

Pups were placed on a heating pad after surgery and allowed to recover for one hour before being placed back in the home cage. Pups were placed in pairs outside of the nest so we could observe the mother's behaviour when retrieving the pups. Only once, were pups immediately rejected by the mother. In this case, we could place the pups with another accepting C57BL/6JRj mum that recently gave birth. In rare instances, the mother would later cannibalize the injected pups. Though we undertook multiple steps to increase the chance of the mother's acceptance, for instance by extensive habitation, glue habituation and by restricting the mother's exposure to solely the experimenter, we did not have the idea that any of these actions had an influence. Instead, we believe that the mother's acceptance of the pups is solely dependent on the character of the mother and her ability to take care of her offspring. Mothers that had accepted pups in the past would continue to do so in the future. Importantly, during the period at which we observed most of the cannibalization events, animals were more prone to stress due to noise disturbances from a nearby construction site.

4.4 Perfusion, cryostat sectioning and immunohistochemistry

In the pilot experiment, testing the efficiency of different AAV serotypes and different promoters in transducing dLGN neurons, animals were sacrificed at P5 and P4 respectively through transcardial perfusion. To study thalamocortical axon ingrowth, pups were sacrificed at ages P3 to P7, P9, P10 and P14. Animals from the MORF3-Rorb-IRES-Cre mouse line that were used to study normal dendritic development were perfused at ages P4, P10, P13 and P15 (data from P13 are not yet available and are therefore not presented in the results section). MORF3-Rorb-IRES-Cre animals that were used to study the effect of functional thalamocortical input on dendritic development were sacrificed at P13. All animals were deeply anesthetized with a ketamine/xylazine solution (100, 10 µg/g bodyweight) before transcardial perfusion with a 4% paraformaldehyde (PFA) phosphate buffered saline (PBS) solution (using a 27Gx13mm Surflo® winged infusion perfusion needle from TERUMO). Notably, we observed that perfusion with a relatively large volume, relative to the size of the animal, over a prolonged period (>15min), was essential for a good preservation of the tissue. For instance, for animals at P3, a perfusion volume of at least 40mL was infused over a period of 20 minutes. The older the animal, the larger the perfusion volume will be, but the faster the speed of perfusion. Dissected brains were then post-fixated for 24-48hrs in 4% PFA PBS solution at 4°C. To allow for cryostat sectioning, brains were subsequently placed in a 30% sucrose solution (in PBS) to protect the tissue from freezing artefacts. After a 24-48hrs incubation period, brains were placed in a cryomold filled with embedding matrix (OCT embedding matrix, Cellpath, REF KMA-0100-00A) and frozen at -80°C.

Forty-micron thick coronal sections were cut on a cryostat using an object temperature of -20°C and a cutting temperature of -18°C (ThermoScientific MicromHM560, with a MX35 Ultra microtome blade of 34°/80mm, REF3053835). In the initial pilot experiment, brain sections were collected in PBS and subsequently stained using a free-floating immunohistochemistry (IHC) protocol. Since we observed that brain sections at young ages were very susceptible for damage using the free-floating protocol, we decided to collect brain slices directly on object slides (ThermoScientific, SUPERFROST® Plus, 25x75x1.0mm, REF J1800AMNZ) to perform on-slide antibody staining for the brains used in the thalamocortical axon ingrowth experiment. After optimization of the perfusion protocol and cutting technique, we decided to use free-floating sections for the experiments exploring dendritic morphology in sparsely labelled L4 pyramidal neurons.

Though the IHC protocol for the study of thalamocortical axon ingrowth was performed on slices directly collected on the slide, the protocol did not differ much from the protocol used for staining free-floating sections for the pilot experiment. Free-floating sections were stained using custom-built insets, which allowed a quick interexchange of washing/incubation solutions. First, sections were washed 3x in PBS for 10 minutes before membrane permeabilization through incubation in 0.1% Triton-X100/PBS (Sigma Life Sciences, T9284-500ML) for 10 minutes. Sections were then washed for 10 minutes in PBS after which a blocking solution consisting of 3% BSA (Bovine Serum Albumin, SIGMA Life Sciences, 1002892520) and 5% NDS (normal donkey serum, Jakson ImmunoResearch Laboratories, inc, 017-000-127) in PBS was applied either to the well or directly on the slide. For the latter, brain slices were encircled with a hydrophobic marker (PAP-Pen Mini, Science Services) to allow for volume application. After an incubation period of one hour, the blocking solution was removed, and the antibody solution was applied. The respective primary antibodies used were diluted according to their working solution in 500µl or 600 µl 1%NDS/PBS solution for free-floating sections and sections on slide, respectively. In general, we implemented an overnight primary antibody incubation period at 4°C, as this led to the best result. For staining with the olig2 antibody, we cooked the slices in citratbuffer (10mM NaCitrat, 0.05% Tween20, pH6) to improve permeabilization. To this end, slices were cooked for 20 minutes on 95°C after which slices were washed 3x for 10 minutes with PBS before continuing with the blocking step. After incubation with the primary antibody solution, slices were briefly washed with 0.1% Tx100/PBS for 5 minutes and subsequently washed 3x with PBS for 10 minutes. Secondary antibodies were diluted in 500µl 1% NDS/PBS and applied to the wells/slides. Incubation with the secondary antibody solution took place at RT for 1.5hrs in the dark. All subsequent steps were performed in the dark as well. After incubation, sections were washed 3x in PBS for 10 minutes. Slices were then stained with DAPI (1:5000) for 10 minutes after which sections were washed again 3x in PBS. Finally, free-floating sections were mounted on microscopic slides and air-dried while being light shielded. Slides were then dehydrated by short incubation (<15s) in 70% EtOH following abs. EtOH. DAKO Fluorescence mounting medium (Dako North America, Inc, REFS3023) was applied after which a cover glass was placed. This mounting medium is able to preserve fluorescent signal for at least a month.

The free-floating staining protocol for the MORF3-Rorb-IRES-cre mice was slightly adjusted. Again, sections were rinsed with PBS, after which slides were incubated for an hour in a blocking solution consisting of 3% BSA and 3% NDS in 0.1% Triton X-100/PBS. Primary antibodies were solved in the blocking solution and sections were incubated overnight at 4°C. The following day, sections were washed 3x for 15 minutes with 0.05% Triton-X100/PBS after which slides were incubated for 2 hrs at RT in the dark. Sections were then directly stained with DAPI and subsequently washed for 10 minutes with first 0.05% Triton X-100/PBS followed by PBS. Sections were mounted on object slides and this time Prolong Diamond antifade reagent (ThermoFisher, P36965) was used as a mounting medium. This mounting medium allows mounted samples to be stored for multiple months.

4.4.1 Antibodies

For the pilot experiment, the following commercially available antibodies were used: monoclonal mouse anti-S100 (β2 subunit, SIGMA Aaldrich, 048K4863, 1:100), polyclonal rabbit anti-GFAP (Dako, REFZ0334, 1:500), polyclonal chicken anti-GFP (Aves Labs Inc., GFP-1020, 1:500), polyclonal rabbit anti-RFP (Rockland, 600-401-379, 1:200), monoclonal rabbit anti-NeuN (Abcam, ab177487, 1:1000), and rabbit anti-Olig2 (Merck, AB9610, 1:500). Brain slices that were used to study thalamocortical axon ingrowth were stained with both polyclonal rabbit anti-RFP (Rockland, 600-401-379, 1:200) and polyclonal guinea pig anti-vGluT2 (Synaptic Systems, 135404, 1:500). While the innate fluorescent expression level was high enough to detect small axonal structures in the cortex, we wanted to

increase the signal-to-noise ratio by antibody staining to ensure that we are able to detect all axonal arborizations in the cortex for our quantifications. To study the dendritic morphology in sparsely labelled neurons in the visual cortex, we used the mouse anti-V5-tag (BioRad, MCA1360, 1:1000) to visualize the sparsely labelled neurons and rabbit anti-Er81 (Colombia University, for purchase please contact sm325@cumc.columbia.edu, 1:2000) to mark layer 5 neurons in the cortex in order to distinguish $Rorb^+$ layer 5 (L5) neurons from $Rorb^+$ L4 neurons.

The following commercially available secondary antibodies were used: Alexa®488-conjugated anti-rabbit (Thermo Fisher, A-21206, 1:1000) and anti-mouse (Thermo Fisher, A-21202, 1:1000) and anti-chicken (Thermo Fisher, A-11039, 1:1000) , Alexa®568 conjugated anti-rabbit (Thermo Fisher, A-11011, 1:1000), Cy3-conjugated anti-mouse (Jackson ImmunoResearch, 715-165-150, 1:500), Cy5-conjugated anti-rabbit (Jackson ImmunoResearch, 711-175-152 1:500) and anti-guinea pig (Jackson ImmunoResearch, 706-175-148, 1:500).

4.5 Clearing protocol for the neonate brain

The cleared brain protocol used to create the figure in chapter 2.2.5 is largely based on the Cubic L clearing protocol described by Tainaka and colleagues (2018). The protocol is slightly adjusted for clearing of the neonate brain. Cubic L brain clearing is based on two processes: the step of making the brain transparent through delipidation using a CUBIC L solution, and the step in which the refractive index (RI) of the tissue is matched with the RI of the microscope's objective. Cubic L solution consisted of 10 wt% N-butyldiethanolamine and 10 wt% Triton X-100 dissolved in distilled H2O. For RI matching, a CUBIC RA solution was made with an RI of 1.5 to match the 5x objective used for imaging. The CUBIC RA solution was made by dissolving 45 wt% Antipyrine and 30 wt% N-methylnicotinamide in distilled water. Pups were transcardially perfused at P5 with first 15mL 50mM phosphate buffered saline (PBS) (pH 7.4) followed by a perfusion of 20mL 4% PFA in 50mM PBS. The brain was dissected after which the tissue was washed with 50mM PBS for at least 1-2 hrs. We immediately proceeded with delipidation by placing the tissue in a 5mL Eppendorf tube filled with prewarmed CUBIC L solution. While for adult tissue an incubation period of multiple days is required, an incubation period of 36 hours on 37°C was sufficient to clear the brain of the neonate mouse. The CUBIC L solution was replaced for fresh solution once during the incubation period. After successful delipidation of the tissue, the brain was briefly washed with a 50mM PBS solution with a pH of 9.15 (achieved by adding N-butyldiethanolamine) after which the brain was incubated overnight at 37°C in CUBIC RA solution at which propidium iodide was added at 0.2 wt%. The brain was washed afterwards with CUBIC RA solution after which we imaged the sample.

4.6 Image acquisition, analysis and quantification

Images for the pilot experiment and the mapping of thalamocortical axon ingrowth were acquired with the LSM880 inverted Zeiss point scanning confocal microscope. Confocal stacks were acquired for the pilot experiment using a 25x PLAN APO objective (0.80 NA). Snapshots were acquired at 10x magnification (0.45 NA) to provide an overview of axonal ingrowth in V1. Confocal stacks within L4 of V1 were acquired with a 63x objective (1.40 NA). For presentation purposes, the brightness and contrast level of images were adjusted. For all analyses we used the raw image.

To assess the morphology of sparsely labelled neurons, we acquired tiled stacks at 60x magnification (1.30 NA) using the fast-spinning disk confocal system, Olympus SpinSR. Individual tiles were stitched offline and converted into an Imaris file using the stitcher-program built by our inhouse Imaging Core Facility. Using another inhouse built converter program, the Imaris file was converted and compressed to a JPX2000 file, which was compatible with the Neurolucida 360® neuronal reconstruction software.

Furthermore, to assess the injection site of animals injected with viral constructs, we imaged all slices using the Zeiss Axio Scan.Z1 slide scanner at 10x magnification (0.45 NA).

The cleared brains shown in chapter 2.2.5, were imaged with the Zeiss Z1 Lightsheet microscope (5x, 0.16 NA). Data was post-processed with a maximum fusion algorithm and loaded into Arivis which made a 3D rendered object based on the data. Stills from the movie created with the Arivis Moviemaker tool are shown in Figure 13.

4.6.1 Quantification of the colocalization of transgene expression with cell type markers

To explore the transduction specificity of the tested AAV capsid types, we performed immunohistochemistry on brain slices to visualize the different cell types and assess the colocalization of these marker proteins with the fluorescent protein GFP, which was found in transduced cells (see Antibodies). First, we manually counted the number of cell nuclei (DAPI), neurons (NeuN), glia (S100 or GFAP signal) and the number of transduced cells (GFP) within a single optical section acquired in the dLGN at 25x magnification. Furthermore, we also counted the number of GFP^+ cells within each category. In addition, other brain slices were stained with an antibody against Olig2, a marker protein for oligodendrocytes, as well as with an antibody reactive to GFP. For these acquired images, we then counted the number of oligodendrocytes and defined the percentage of GFP^+ oligodendrocytes. Furthermore, we also defined to which category the GFP^+ cells belonged to, by calculating the percentage of $NeuN^+$ GFP^+ cells, $S100/GFAP^+$ GFP^+ cells and $olig2^+$ GFP^+ cells. For testing the transduction efficiency of various promoters, we counted the number of RFP^+ cells within a single optical section acquired at 25x magnification in the dLGN. The bar graphs and pie charts shown in Figure 8, 9 and 10 are made using GraphPad Prism.

4.6.2 Quantification of axonal ingrowth

To quantitively describe thalamocortical axon ingrowth during early development, we developed an algorithm together with the inhouse Imaging Core Facility to assess the axonal coverage in images acquired in L4 of V1 (63x, 1.4 NA) using ImageJ Fiji. The axonal coverage was defined as the percentage of RFP^+ pixels within a given image, which was established by using a thresholding method and a minimum size requirement of $0.07\mu m^2$ to differentiate signal from background. We tested different thresholding methods on a selection of images with varying signal quality and found that the Triangle algorithm fitted the data best. The implementation of the Triangle thresholding algorithm in ImageJ, objectively calculates a threshold for each individual image based on the distribution of pixel intensities across the entire image (Zack et al., 1977). Therefore, the algorithm is less sensitive to differences in intensity levels between images recorded across experiments. Since we are not interested to compare intensity levels of the RFP signal but just simply want to know whether an axon is present or not, this is critical for our analysis. Especially, since it could be that intensity levels are ramping up between the earliest time point evaluated, P3, and the last timepoint, P14. The optical section with the highest fluorescent intensity level within the acquired z-stack was used for axonal coverage quantification.

4.7 Dendritic tracing and parametric analyses

The high-resolution stitched images of sparsely labelled L4 neurons were used to trace neurons using the Neurolucida 360® software. Both apical as well as basal dendrites were traced semi-automatically by using the user-guided 3D image detection algorithm. After this semi-automatic tracing, tracings were checked and corrected manually when needed. Subcellular components, such as spines and other small protrusions were not traced. The apical dendrite was easy to distinguish and label even though the apical dendrite was often prematurely cut and could not be traced back all the way up to

the pial surface. Furthermore, axons, though not traced, were easy to distinguish from basal dendrites based on the absence of spiny structures. However, since spines were rare at P4, axons at this age were distinguished from basal dendrites predominantly based on their extension towards the corpus callosum. Since we did not reliably trace the thickness of dendrites, the thickness of all basal dendrites was set to 0.75 µm and the apical dendrite was set to 1.0 µm for image presentation and parametric analyses.

Commonly used parameters to describe the basal dendritic morphology were derived using the analytical software Neurolucida Explorer®. The following parameters were extracted for traced neurons: the number of nodes (i.e. branch points), the number of dendrites from different centrifugal orders (i.e. primary dendrites, secondary dendrites etc), the number of segments (i.e. branches between nodes), the total dendritic length, the length of individual dendrites and individual segments and the total length per centrifugal category, the convex volume based on individual dendrites, the total convex volume and the Sholl radius. Values for these dendritic parameters were inserted in Excel in which we calculated average values when required. Furthermore, based on the values for the total length of the dendritic tree ($L_{dendrite}$) and the number of branch points (B_{nr}) we calculated the branching index (BI) using $BI = B_{nr}/ L_{dendrite}$. Images shown in Figure 20 and Figure 23 were made using GraphPad Prism.

4.8 Statistical methods

Several exclusion criteria were defined a priori before statistically evaluating the changes in dendritic parameters. For viral injection experiments, mice which showed insufficient transgene expression in the entire span of the dLGN were excluded from further analysis based on visual evaluation. Furthermore, only sparsely labelled L4 neurons that showed minimal overlap with other labelled neurons were imaged to facilitate accurate morphological reconstruction. Imaged neurons that had multiple primary dendrites cut off by brain sectioning were also excluded from further processing.

All statistical tests were performed in GraphPad Prism (version 9.4.1). This software was also used to create the graphs describing the axonal coverage quantification and dendritic parameters. Data was tested for normality using the Shapiro-Wilk test. For the analysis of dendritic parameters during development, we performed a one-way ANOVA with multiple comparisons (Dunnett corrected) for normally distributed data. Alternatively, the non-parametric Kruskas-Wallis test was used to compare the medians between the different ages. For the thalamocortical silencing experiment, we used either an unpaired t-test or the non-parametric Mann-Whitney test to compare dendritic parameters between the syn-Kir2.1-2A-tdTomato and syn-tdTomato group. Significant results ($p<0.05$) were denoted in the graphs with an asterisk. The respective executed statistical tests, p-values and number of replicates can be found in the figure legends.

5. References

Aberle, H., 2019. Axon Guidance and Collective Cell Migration by Substrate-Derived Attractants. Front. Mol. Neurosci. 12, 148. https://doi.org/10.3389/fnmol.2019.00148

Ackman, J.B., Burbridge, T.J., Crair, M.C., 2012a. Retinal waves coordinate patterned activity throughout the developing visual system. Nature 490, 219–225. https://doi.org/10.1038/nature11529

Ackman, J.B., Burbridge, T.J., Crair, M.C., 2012b. Retinal waves coordinate patterned activity throughout the developing visual system. Nature 490, 219–225. https://doi.org/10.1038/nature11529

Ackman, J.B., Crair, M.C., 2014. Role of emergent neural activity in visual map development. Current Opinion in Neurobiology 24, 166–175. https://doi.org/10.1016/j.conb.2013.11.011

Agmon, A., Yang, L.T., O'Dowd, D.K., Jones, E.G., 1993. Organized growth of thalamocortical axons from the deep tier of terminations into layer IV of developing mouse barrel cortex. Journal of Neuroscience 13, 5365–5382.

Akin, O., Bajar, B.T., Keles, M.F., Frye, M.A., Zipursky, S.L., 2019. Cell-type-Specific Patterned Stimulus-Independent Neuronal Activity in the Drosophila Visual System during Synapse Formation. Neuron 101, 894-904.e5. https://doi.org/10.1016/j.neuron.2019.01.008

Arroyo, D.A., Feller, M.B., 2016. Spatiotemporal Features of Retinal Waves Instruct the Wiring of the Visual Circuitry. Front. Neural Circuits 10. https://doi.org/10.3389/fncir.2016.00054

Auladell, C., Pérez-Sust, P., Supèr, H., Soriano, E., 2000. The early development of thalamocortical and corticothalamic projections in the mouse. Anatomy and embryology 201, 169–179.

Azeredo da Silveira, R., Roska, B., 2011. Cell Types, Circuits, Computation. Current Opinion in Neurobiology 21, 664–671. https://doi.org/10.1016/j.conb.2011.05.007

Bagnard, D., Chounlamountri, N., Püschel, A.W., Bolz, J., 2001. Axonal Surface Molecules Act in Combination with Semaphorin 3A during the Establishment of Corticothalamic Projections. Cerebral Cortex 11, 278–285.

Bannister, A.P., 2005. Inter- and intra-laminar connections of pyramidal cells in the neocortex. Neuroscience Research 53, 95–103. https://doi.org/10.1016/j.neures.2005.06.019

Bansal, A., Singer, J.H., Hwang, B.J., Xu, W., Beaudet, A., Feller, M.B., 2000. Mice Lacking Specific Nicotinic Acetylcholine Receptor Subunits Exhibit Dramatically Altered Spontaneous Activity Patterns and Reveal a Limited Role for Retinal Waves in Forming ON and OFF Circuits in the Inner Retina. J. Neurosci. 20, 7672–7681. https://doi.org/10.1523/JNEUROSCI.20-20-07672.2000

Batista-Brito, R., Ward, C., Fishell, G., 2020. The generation of cortical interneurons, in: Patterning and Cell Type Specification in the Developing CNS and PNS. Elsevier, pp. 461–479. https://doi.org/10.1016/B978-0-12-814405-3.00020-5

Bayer, S.A., Altman, J., 1991. Neocortical development. Raven Press, New York.

Ben-Ari, Y., Cherubini, E., Corradetti, R., Gaiarsa, J.L., 1989. Giant synaptic potentials in immature rat CA3 hippocampal neurones. The Journal of Physiology 416, 303–325. https://doi.org/10.1113/jphysiol.1989.sp017762

Blankenship, A.G., Feller, M.B., 2010. Mechanisms underlying spontaneous patterned activity in developing neural circuits. Nat Rev Neurosci 11, 18–29. https://doi.org/10.1038/nrn2759

Branco, T., Häusser, M., 2011. Synaptic Integration Gradients in Single Cortical Pyramidal Cell Dendrites. Neuron 69, 885–892. https://doi.org/10.1016/j.neuron.2011.02.006

Burbridge, T.J., Xu, H.-P., Ackman, J.B., Ge, X., Zhang, Y., Ye, M.-J., Zhou, Z.J., Xu, J., Contractor, A., Crair, M.C., 2014. Visual Circuit Development Requires Patterned Activity Mediated by Retinal Acetylcholine Receptors. Neuron 84, 1049–1064. https://doi.org/10.1016/j.neuron.2014.10.051

Cadwell, C.R., Bhaduri, A., Mostajo-Radji, M.A., Keefe, M.G., Nowakowski, T.J., 2019. Development and Arealization of the Cerebral Cortex. Neuron 103, 980–1004. https://doi.org/10.1016/j.neuron.2019.07.009

Callaway, E.M., Borrell, V., 2011. Developmental Sculpting of Dendritic Morphology of Layer 4 Neurons in Visual Cortex: Influence of Retinal Input. Journal of Neuroscience 31, 7456–7470. https://doi.org/10.1523/JNEUROSCI.5222-10.2011

Cang, J., Rentería, R.C., Kaneko, M., Liu, X., Copenhagen, D.R., Stryker, M.P., 2005. Development of Precise Maps in Visual Cortex Requires Patterned Spontaneous Activity in the Retina. Neuron 48, 797–809. https://doi.org/10.1016/j.neuron.2005.09.015

Cearley, C.N., Vandenberghe, L.H., Parente, M.K., Carnish, E.R., Wilson, J.M., Wolfe, J.H., 2008. Expanded Repertoire of AAV Vector Serotypes Mediate Unique Patterns of Transduction in Mouse Brain. Molecular Therapy 16, 1710–1718. https://doi.org/10.1038/mt.2008.166

Chandrasekaran, A.R., 2005. Evidence for an Instructive Role of Retinal Activity in Retinotopic Map Refinement in the Superior Colliculus of the Mouse. Journal of Neuroscience 25, 6929–6938. https://doi.org/10.1523/JNEUROSCI.1470-05.2005

Chen, T.-W., Wardill, T.J., Sun, Y., Pulver, S.R., Renninger, S.L., Baohan, A., Schreiter, E.R., Kerr, R.A., Orger, M.B., Jayaraman, V., Looger, L.L., Svoboda, K., Kim, D.S., 2013. Ultrasensitive fluorescent proteins for imaging neuronal activity. Nature 499, 295–300. https://doi.org/10.1038/nature12354

Clancy, B., Darlington, R.B., Finlay, B.L., 2001. Translating developmental time across mammalian species. Neuroscience 105, 7–17. https://doi.org/10.1016/S0306-4522(01)00171-3

Cline, H., Haas, K., 2008. The regulation of dendritic arbor development and plasticity by glutamatergic synaptic input: a review of the synaptotrophic hypothesis: The synaptotrophic hypothesis. The Journal of Physiology 586, 1509–1517. https://doi.org/10.1113/jphysiol.2007.150029

Colonnese, M.T., Kaminska, A., Minlebaev, M., Milh, M., Bloem, B., Lescure, S., Moriette, G., Chiron, C., Ben-Ari, Y., Khazipov, R., 2010. A Conserved Switch in Sensory Processing Prepares Developing Neocortex for Vision. Neuron 67, 480–498. https://doi.org/10.1016/j.neuron.2010.07.015

Cox, C.L., Beatty, J.A., 2017. The multifaceted role of inhibitory interneurons in the dorsal lateral geniculate nucleus. Vis Neurosci 34, E017. https://doi.org/10.1017/S0952523817000141

Cruz-Martín, A., El-Danaf, R.N., Osakada, F., Sriram, B., Dhande, O.S., Nguyen, P.L., Callaway, E.M., Ghosh, A., Huberman, A.D., 2014. A dedicated circuit links direction-selective retinal ganglion cells to the primary visual cortex. Nature 507, 358–361. https://doi.org/10.1038/nature12989

De la Rossa, A., Bellone, C., Golding, B., Vitali, I., Moss, J., Toni, N., Lüscher, C., Jabaudon, D., 2013. In vivo reprogramming of circuit connectivity in postmitotic neocortical neurons. Nat Neurosci 16, 193–200. https://doi.org/10.1038/nn.3299

Deck, M., Lokmane, L., Chauvet, S., Mailhes, C., Keita, M., Niquille, M., Yoshida, M., Yoshida, Y., Lebrand, C., Mann, F., Grove, E.A., Garel, S., 2013. Pathfinding of Corticothalamic Axons Relies on a Rendezvous with Thalamic Projections. Neuron 77, 472–484. https://doi.org/10.1016/j.neuron.2012.11.031

Del Rio, J.A., Martínez, A., Auladell, C., Soriano, E., 2000. Developmental History of the Subplate and Developing White Matter in the Murine Neocortex. Neuronal Organization and Relationship with the Main Afferent Systems at Embryonic and Perinatal Stages. Cerebral Cortex 10, 784–801. https://doi.org/10.1093/cercor/10.8.784

Deng, J., Elberger, A.J., 2003. Corticothalamic and thalamocortical pathfinding in the mouse: dependence on intermediate targets and guidance axis. Anatomy and Embryology 207, 177–192. https://doi.org/10.1007/s00429-003-0338-1

Dumoulin, A., Stoeckli, E.T., 2022. Looking for Guidance – Models and Methods to Study Axonal Navigation. Neuroscience S0306452222004080. https://doi.org/10.1016/j.neuroscience.2022.08.005

Dunn, F.A., Wong, R.O.L., 2014. Wiring patterns in the mouse retina: collecting evidence across the connectome, physiology and light microscopy. J Physiol 592, 4809–4823. https://doi.org/10.1113/jphysiol.2014.277228

Dupont, E., Hanganu, I.L., Kilb, W., Hirsch, S., Luhmann, H.J., 2006. Rapid developmental switch in the mechanisms driving early cortical columnar networks. Nature 439, 79–83. https://doi.org/10.1038/nature04264

Elstrott, J., Anishchenko, A., Greschner, M., Sher, A., Chichilnisky, E.J., Feller, M.B., 2009. Direction selectivity in the retina is established independent of visual experience and early cholinergic retinal waves 16.

Evangelio, M., García-Amado, M., Clascá, F., 2018. Thalamocortical Projection Neuron and Interneuron Numbers in the Visual Thalamic Nuclei of the Adult C57BL/6 Mouse. Front. Neuroanat. 12, 27. https://doi.org/10.3389/fnana.2018.00027

Farhy-Tselnicker, I., Allen, N.J., 2018. Astrocytes, neurons, synapses: a tripartite view on cortical circuit development. Neural Dev 13, 7. https://doi.org/10.1186/s13064-018-0104-y

Faust, T.E., Gunner, G., Schafer, D.P., 2021. Mechanisms governing activity-dependent synaptic pruning in the developing mammalian CNS. Nat Rev Neurosci 22, 657–673. https://doi.org/10.1038/s41583-021-00507-y

Flanagan, J.G., 2006. Neural map specification by gradients. Current Opinion in Neurobiology 8.

Ford, K.J., Felix, A.L., Feller, M.B., 2012. Cellular Mechanisms Underlying Spatiotemporal Features of Cholinergic Retinal Waves. Journal of Neuroscience 32, 850–863. https://doi.org/10.1523/JNEUROSCI.5309-12.2012

Ford, K.J., Feller, M.B., 2012. Assembly and disassembly of a retinal cholinergic network. Visual Neuroscience 29, 61–71. https://doi.org/10.1017/S0952523811000216

Garaschuk, O., Hanse, E., Konnerth, A., 1998. Developmental profile and synaptic origin of early network oscillations in the CA1 region of rat neonatal hippocampus. Journal of Physiology 501, 219—236.

Ge, X., Zhang, K., Gribizis, A., Hamodi, A.S., Sabino, A.M., Crair, M.C., 2021. Retinal waves prime visual motion detection by simulating future optic flow. Science 373, eabd0830. https://doi.org/10.1126/science.abd0830

Gezelius, H., López-Bendito, G., 2017. Thalamic neuronal specification and early circuit formation: Thalamic Neuronal Specification and Early Circuit Formation. Devel Neurobio 77, 830–843. https://doi.org/10.1002/dneu.22460

Ghodrati, M., Khaligh-Razavi, S.-M., Lehky, S.R., 2017. Towards building a more complex view of the lateral geniculate nucleus: Recent advances in understanding its role. Progress in Neurobiology 156, 214–255. https://doi.org/10.1016/j.pneurobio.2017.06.002

Ghosh, A., Antonini, A., McConnel, S.K., Shatz, C.J., 1990. Requirement for subplate neurons in the formation of thalamocortical connections. Nature 137, 179–181.

Gonzalez-Islas, C., Wenner, P., 2006. Spontaneous Network Activity in the Embryonic Spinal Cord Regulates AMPAergic and GABAergic Synaptic Strength. Neuron 49, 563–575. https://doi.org/10.1016/j.neuron.2006.01.017

Goodman, C.S., Shatz, C.J., 1993. Developmental mechanisms that generate precise patterns of neuronal connectivity. Cell 72, 77–98. https://doi.org/10.1016/S0092-8674(05)80030-3

Greig, L.C., Woodworth, M.B., Galazo, M.J., Padmanabhan, H., Macklis, J.D., 2013. Molecular logic of neocortical projection neuron specification, development and diversity. Nature Reviews Neuroscience 14, 755–769. https://doi.org/10.1038/nrn3586

Gribizis, A., Ge, X., Daigle, T.L., Ackman, J.B., Zeng, H., Lee, D., Crair, M.C., 2019. Visual Cortex Gains Independence from Peripheral Drive before Eye Opening. Neuron S0896627319306993. https://doi.org/10.1016/j.neuron.2019.08.015

Grubb, M.S., Rossi, F.M., Changeux, J.-P., Thompson, I.D., 2003. Abnormal Functional Organization in the Dorsal Lateral Geniculate Nucleus of Mice Lacking the 2 Subunit of the Nicotinic Acetylcholine Receptor 12.

Guido, W., 2018. Development, form, and function of the mouse visual thalamus. Journal of Neurophysiology 120, 211–225. https://doi.org/10.1152/jn.00651.2017

Hamodi, A.S., Martinez Sabino, A., Fitzgerald, N.D., Moschou, D., Crair, M.C., 2020. Transverse sinus injections drive robust whole-brain expression of transgenes. eLife 9, e53639. https://doi.org/10.7554/eLife.53639

Hanashima, C., Molnár, Z., Fishell, G., 2006. Building Bridges to the Cortex. Cell 125, 24–27.

Hanganu, I.L., Ben-Ari, Y., Khazipov, R., 2006. Retinal Waves Trigger Spindle Bursts in the Neonatal Rat Visual Cortex. Journal of Neuroscience 26, 6728–6736. https://doi.org/10.1523/JNEUROSCI.0752-06.2006

Hansen, A.H., Hippenmeyer, S., 2020. Non-Cell-Autonomous Mechanisms in Radial Projection Neuron Migration in the Developing Cerebral Cortex. Front. Cell Dev. Biol. 8, 574382. https://doi.org/10.3389/fcell.2020.574382

Harris, J.A., Hirokawa, K.E., Sorensen, S.A., Gu, H., Mills, M., Ng, L.L., Bohn, P., Mortrud, M., Ouellette, B., Kidney, J., Smith, K.A., Dang, C., Sunkin, S., Bernard, A., Oh, S.W., Madisen, L., Zeng, H., 2014. Anatomical characterization of Cre driver mice for neural circuit mapping and manipulation. Frontiers in Neural Circuits 8. https://doi.org/10.3389/fncir.2014.00076

Herrmann, K., Antonini, A., Shatz, C.J., 1994. Ultrastructural Evidence for Synaptic Interactions between Thalamocortical Axons and Subplate Neurons. European Journal of Neuroscience 6, 1729–1742. https://doi.org/10.1111/j.1460-9568.1994.tb00565.x

Ho, H., Fowle, A., Coetzee, M., Greger, I.H., Watson, J.F., 2020. An inhalation anaesthesia approach for neonatal mice allowing streamlined stereotactic injection in the brain. Journal of Neuroscience Methods 342, 108824. https://doi.org/10.1016/j.jneumeth.2020.108824

Hoon, M., Okawa, H., Della Santina, L., Wong, R.O.L., 2014. Functional architecture of the retina: Development and disease. Progress in Retinal and Eye Research 42, 44–84. https://doi.org/10.1016/j.preteyeres.2014.06.003

Hübener, M., 2003. Mouse visual cortex. Current Opinion in Neurobiology 13, 413–420. https://doi.org/10.1016/S0959-4388(03)00102-8

Huberman, A.D., Feller, M.B., Chapman, B., 2008. Mechanisms Underlying Development of Visual Maps and Receptive Fields. Annual Review of Neuroscience 31, 479–509. https://doi.org/10.1146/annurev.neuro.31.060407.125533

Jacyna, S., 2009. The most important of all the organs: Darwin on the brain. Brain 132, 3481–3487. https://doi.org/10.1093/brain/awp283

Ji, X., Zingg, B., Mesik, L., Xiao, Z., Zhang, L.I., Tao, H.W., 2016. Thalamocortical Innervation Pattern in Mouse Auditory and Visual Cortex: Laminar and Cell-Type Specificity 24, 2612–2625.

Jones, E.G., Rubenstein, J.L.R., 2004. Expression of regulatory genes during differentiation of thalamic nuclei in mouse and monkey. J. Comp. Neurol. 477, 55–80. https://doi.org/10.1002/cne.20234

Kanold, P.O., 2019. The Integrative Function of Silent Synapses on Subplate Neurons in Cortical Development and Dysfunction. Frontiers in Neuroanatomy 13, 13.

Kanold, P.O., Kara, P., Reid, R.C., Shatz, C.J., 2003. Role of Subplate Neurons in Functional Maturation of Visual Cortical Columns. Science 301, 521–525. https://doi.org/10.1126/science.1084152

Kanold, P.O., Luhmann, H.J., 2010. The Subplate and Early Cortical Circuits. Annual Review of Neuroscience 33, 23–48. https://doi.org/10.1146/annurev-neuro-060909-153244

Kanold, P.O., Shatz, C.J., 2006. Subplate Neurons Regulate Maturation of Cortical Inhibition and Outcome of Ocular Dominance Plasticity. Neuron 51, 627–638. https://doi.org/10.1016/j.neuron.2006.07.008

Kerschensteiner, D., 2016. Glutamatergic Retinal Waves. Front. Neural Circuits 10. https://doi.org/10.3389/fncir.2016.00038

Kerschensteiner, D., 2014. Spontaneous Network Activity and Synaptic Development. Neuroscientist 20, 272–290. https://doi.org/10.1177/1073858413510044

Kerschensteiner, D., Guido, W., 2017. Organization of the dorsal lateral geniculate nucleus in the mouse. Vis Neurosci 34, E008. https://doi.org/10.1017/S0952523817000062

Khazipov, R., Luhmann, H.J., 2006. Early patterns of electrical activity in the developing cerebral cortex of humans and rodents. Trends in Neurosciences 29, 414–418. https://doi.org/10.1016/j.tins.2006.05.007

Khazipov, R., Sirota, A., Leinekugel, X., Holmes, G.L., Ben-Ari, Y., Buzsáki, G., 2004. Early motor activity drives spindle bursts in the developing somatosensory cortex. Nature 432, 758–761. https://doi.org/10.1038/nature03132

Kim, J.-Y., Ash, R.T., Ceballos-Diaz, C., Levites, Y., Golde, T.E., Smirnakis, S.M., Jankowsky, J.L., 2013. Viral transduction of the neonatal brain delivers controllable genetic mosaicism for visualising and manipulating neuronal circuits *in vivo*. Eur J Neurosci 37, 1203–1220. https://doi.org/10.1111/ejn.12126

Kirkby, L.A., Sack, G.S., Firl, A., Feller, M.B., 2013. A Role for Correlated Spontaneous Activity in the Assembly of Neural Circuits. Neuron 80, 1129–1144. https://doi.org/10.1016/j.neuron.2013.10.030

Kolodkin, A.L., Tessier-Lavigne, M., 2011. Mechanisms and Molecules of Neuronal Wiring: A Primer. Cold Spring Harbor Perspectives in Biology 3, a001727–a001727. https://doi.org/10.1101/cshperspect.a001727

Kriegstein, A.R., Noctor, S.C., 2004. Patterns of neuronal migration in the embryonic cortex. Trends in Neurosciences 27, 392–399. https://doi.org/10.1016/j.tins.2004.05.001

Kutsarova, E., Munz, M., Ruthazer, E.S., 2017. Rules for Shaping Neural Connections in the Developing Brain. Front. Neural Circuits 10. https://doi.org/10.3389/fncir.2016.00111

Landmesser, L.T., O'Donovan, M.J., 1984. Activation patterns of embryonic chick hind limb muscles recorded in ovo and in an isolated spinal cord preparation. Journal of Physiology 347, 189–204.

Leighton, A.H., Lohmann, C., 2016. The Wiring of Developing Sensory Circuits—From Patterned Spontaneous Activity to Synaptic Plasticity Mechanisms. Frontiers in Neural Circuits 10. https://doi.org/10.3389/fncir.2016.00071

Lodato, S., Arlotta, P., 2015. Generating Neuronal Diversity in the Mammalian Cerebral Cortex 25.

Lohmann, C., Myhr, K.L., Wong, R.O.L., 2002. Transmitter-evoked local calcium release stabilizes developing dendrites. Nature 418, 177–181. https://doi.org/10.1038/nature00850

Lokmane, L., Proville, R., Narboux-Nême, N., Györy, I., Keita, M., Mailhes, C., Léna, C., Gaspar, P., Grosschedl, R., Garel, S., 2013. Sensory Map Transfer to the Neocortex Relies on Pretarget Ordering of Thalamic Axons. Current Biology 23, 810–816. https://doi.org/10.1016/j.cub.2013.03.062

López-Bendito, G., 2018. Development of the Thalamocortical Interactions: Past, Present and Future. Neuroscience 385, 67–74. https://doi.org/10.1016/j.neuroscience.2018.06.020

López-Bendito, G., Molnár, Z., 2003. Thalamocortical projections: how are we going to get there? Nature Reviews Neuroscience 4, 276–289.

Maccione, A., Hennig, M.H., Gandolfo, M., Muthmann, O., Eglen, S.J., Berdondini, L., Sernagor, E., 2014. Following the ontogeny of retinal waves: pan-retinal recordings of population dynamics in the neonatal mouse. The Journal of Physiology 592, 1545–1563.

Magee, J.C., 2000. Dendritic integration of excitatory synaptic input. Nat Rev Neurosci 1, 181–190. https://doi.org/10.1038/35044552

Martini, F.J., Guillamón-Vivancos, T., Moreno-Juan, V., Valdeolmillos, M., López-Bendito, G., 2021. Spontaneous activity in developing thalamic and cortical sensory networks. Neuron 109, 2519–2534. https://doi.org/10.1016/j.neuron.2021.06.026

Martini, F.J., Moreno-Juan, V., Filipchuk, A., Valdeolmillos, M., López-Bendito, G., 2018. Impact of Thalamocortical Input on Barrel Cortex Development. Neuroscience 368, 246–255. https://doi.org/10.1016/j.neuroscience.2017.04.005

Masland, R.H., 2012. The Neuronal Organization of the Retina. Neuron 76, 266–280. https://doi.org/10.1016/j.neuron.2012.10.002

McAllister, A.K., 2000. Cellular and Molecular Mechanisms of Dendrite Growth. Cerebral Cortex 10, 963–973.

McLaughlin, T., O'Leary, D.D.M., 2005. MOLECULAR GRADIENTS AND DEVELOPMENT OF RETINOTOPIC MAPS 32.

McLaughlin, T., Torborg, C.L., Feller, M.B., O'Leary, D.D.M., 2003. Retinotopic Map Refinement Requires Spontaneous Retinal Waves during a Brief Critical Period of Development. Neuron 40, 1147–1160. https://doi.org/10.1016/S0896-6273(03)00790-6

Miller, B., Chou, L., Finlay, B.L., 1993. The Early Development of Thalamocortical and Corticothalamic Projections. The journal of Comparative Neurology 16–41.

Mizuno, H., Hirano, T., Tagawa, Y., 2007. Evidence for Activity-Dependent Cortical Wiring: Formation of Interhemispheric Connections in Neonatal Mouse Visual Cortex Requires Projection Neuron Activity. Journal of Neuroscience 27, 6760–6770. https://doi.org/10.1523/JNEUROSCI.1215-07.2007

Mizuno, H., Luo, W., Tarusawa, E., Saito, Y.M., Sato, T., Yoshimura, Y., Itohara, S., Iwasato, T., 2014. NMDAR-Regulated Dynamics of Layer 4 Neuronal Dendrites during Thalamocortical Reorganization in Neonates. Neuron 82, 365–379. https://doi.org/10.1016/j.neuron.2014.02.026

Molnár, Z., Adams, R., Blakemore, C., 1998. Mechanisms underlying the early establishment of thalamocortical connections in the rat. Journal of Neuroscience 18, 5723–5745.

Molnár, Z., Luhmann, H.J., Kanold, P.O., 2020. Transient cortical circuits match spontaneous and sensory-driven activity during development 11.

Monavarfeshani, A., Sabbagh, U., Fox, M.A., 2017. Not a one-trick pony: Diverse connectivity and functions of the rodent lateral geniculate complex. Vis Neurosci 34, E012. https://doi.org/10.1017/S0952523817000098

Moreno-Juan, V., Filipchuk, A., Antón-Bolaños, N., Mezzera, C., Gezelius, H., Andrés, B., Rodríguez-Malmierca, L., Susín, R., Schaad, O., Iwasato, T., Schüle, R., Rutlin, M., Nelson, S., Ducret, S., Valdeolmillos, M., Rijli, F.M., López-Bendito, G., 2017. Prenatal thalamic waves regulate cortical area size prior to sensory processing. Nat Commun 8, 14172. https://doi.org/10.1038/ncomms14172

Mrsic-Flogel, T.D., 2005. Altered Map of Visual Space in the Superior Colliculus of Mice Lacking Early Retinal Waves. Journal of Neuroscience 25, 6921–6928. https://doi.org/10.1523/JNEUROSCI.1555-05.2005

Nadarajah, B., Parnavelas, J.G., 2002. Modes of neuronal migration in the developing cerebral cortex. Nat Rev Neurosci 3, 423–432. https://doi.org/10.1038/nrn845

Nakazawa, S., Mizuno, H., Iwasato, T., 2018. Differential dynamics of cortical neuron dendritic trees revealed by long-term in vivo imaging in neonates. Nat Commun 9, 3106. https://doi.org/10.1038/s41467-018-05563-0

Neniskyte, U., Gross, C.T., 2017. Errant gardeners: glial-cell-dependent synaptic pruning and neurodevelopmental disorders. Nat Rev Neurosci 18, 658–670. https://doi.org/10.1038/nrn.2017.110

Niell, C.M., 2015. Cell Types, Circuits, and Receptive Fields in the Mouse Visual Cortex. Annual Review of Neuroscience 38, 413–431. https://doi.org/10.1146/annurev-neuro-071714-033807

Niell, C.M., Meyer, M.P., Smith, S.J., 2004. In vivo imaging of synapse formation on a growing dendritic arbor. Nat Neurosci 7, 254–260. https://doi.org/10.1038/nn1191

Oishi, K., Nakagawa, N., Tachikawa, K., Sasaki, S., Aramaki, M., Hirano, S., Yamamoto, N., Yoshimura, Y., Nakajima, K., 2016. Identity of neocortical layer 4 neurons is specified through correct positioning into the cortex. eLife 5, e10907. https://doi.org/10.7554/eLife.10907

Olivetti, P.R., Lacefield, C.O., Kellendonk, C., 2020. A device for stereotaxic viral delivery into the brains of neonatal mice. BioTechniques 69, 307–312. https://doi.org/10.2144/btn-2020-0050

Oşan, R., Su, E., Shinbrot, T., 2011. The Interplay between Branching and Pruning on Neuronal Target Search during Developmental Growth: Functional Role and Implications. PLoS ONE 6, e25135. https://doi.org/10.1371/journal.pone.0025135

Ozkan, A., MacDonald, J.L., Fame, R.M., Itoh, Y., Peter, M., Durak, O., Macklis, J.D., 2020. Specification of cortical projection neurons, in: Patterning and Cell Type Specification in the Developing CNS and PNS. Elsevier, pp. 427–459. https://doi.org/10.1016/B978-0-12-814405-3.00019-9

Parnavelas, J.G., 2000. The origin and migration of cortical neurones: new vistas. Trends in Neurosciences 23, 126–131. https://doi.org/10.1016/S0166-2236(00)01553-8

Penn, A.A., Shatz, C.J., 1999. Brain Waves and Brain Wiring: The Role of Endogenous and Sensory-Driven Neural Activity in Development. Pedriatic Research 45, 447–458.

Polleux, F., 1998. Patterning of Cortical Efferent Projections by Semaphorin-Neuropilin Interactions. Science 282, 1904–1906. https://doi.org/10.1126/science.282.5395.1904

Polleux, F., Morrow, T., Ghosh, A., 2000. Semaphorin 3A is a chemoattractant for cortical apical dendrites. Nature 404, 567–573. https://doi.org/10.1038/35007001

Portera-Cailliau, C., Weimer, R.M., De Paola, V., Caroni, P., Svoboda, K., 2005. Diverse Modes of Axon Elaboration in the Developing Neocortex. PLoS Biol 3, e272. https://doi.org/10.1371/journal.pbio.0030272

Pouchelon, G., Gambino, F., Bellone, C., Telley, L., Vitali, I., Lüscher, C., Holtmaat, A., Jabaudon, D., 2014. Modality-specific thalamocortical inputs instruct the identity of postsynaptic L4 neurons. Nature 511, 471–474. https://doi.org/10.1038/nature13390

Raper, J., Morrison, R.D., Daniels, J.S., Howell, L., Bachevalier, J., Wichmann, T., Galvan, A., 2017. Metabolism and Distribution of Clozapine-N-oxide: Implications for Nonhuman Primate Chemogenetics. ACS Chem. Neurosci. 7.

Redmond, L., Oh, S.-R., Hicks, C., Weinmaster, G., Ghosh, A., 2000. Nuclear Notch1 signaling and the regulation of dendritic development. nature neuroscience 3, 11.

Rheaume, B.A., Jereen, A., Bolisetty, M., Sajid, M.S., Yang, Y., Renna, K., Sun, L., Robson, P., Trakhtenberg, E.F., 2018. Single cell transcriptome profiling of retinal ganglion cells identifies cellular subtypes. Nat Commun 9, 2759. https://doi.org/10.1038/s41467-018-05134-3

Richards, S.E.V., Moore, A.R., Nam, A.Y., Saxena, S., Paradis, S., Van Hooser, S.D., 2020. Experience-Dependent Development of Dendritic Arbors in Mouse Visual Cortex. J. Neurosci. 40, 6536–6556. https://doi.org/10.1523/JNEUROSCI.2910-19.2020

Rochefort, N.L., Narushima, M., Grienberger, C., Marandi, N., Hill, D.N., Konnerth, A., 2011. Development of Direction Selectivity in Mouse Cortical Neurons. Neuron 71, 425–432. https://doi.org/10.1016/j.neuron.2011.06.013

Rompani, S.B., Müllner, F.E., Wanner, A., Zhang, C., Roth, C.N., Yonehara, K., Roska, B., 2017. Different Modes of Visual Integration in the Lateral Geniculate Nucleus Revealed by Single-Cell-Initiated Transsynaptic Tracing. Neuron 93, 767-776.e6. https://doi.org/10.1016/j.neuron.2017.01.028

Rossi, F.M., Pizzorusso, T., Porciatti, V., Marubio, L.M., Maffei, L., Changeux, J.-P., 2001. Requirement of the nicotinic acetylcholine receptor b2 subunit for the anatomical and functional development of the visual system 6.

Roth, B.L., 2016. DREADDs for Neuroscientists. Neuron 89, 683–694. https://doi.org/10.1016/j.neuron.2016.01.040

Rubin, C.M., van der List, D.A., Ballesteros, J.M., Goloshchapov, A.V., Chalupa, L.M., Chapman, B., 2011. Mouse Mutants for the Nicotinic Acetylcholine Receptor ß2 Subunit Display Changes in Cell Adhesion and Neurodegeneration Response Genes. PLoS ONE 6, e18626. https://doi.org/10.1371/journal.pone.0018626

Ruthazer, E.S., Akerman, C.J., Cline, H.T., 2003. Control of Axon Branch Dynamics by Correlated Activity in Vivo. Science 301, 66–70. https://doi.org/10.1126/science.1082545

Sanes, J.R., Masland, R.H., 2015. The Types of Retinal Ganglion Cells: Current Status and Implications for Neuronal Classification. Annual Review of Neuroscience 38, 221–246. https://doi.org/10.1146/annurev-neuro-071714-034120

Schoenemann, P.T., 2006. Evolution of the Size and Functional Areas of the Human Brain. Annu. Rev. Anthropol. 35, 379–406. https://doi.org/10.1146/annurev.anthro.35.081705.123210

Seabrook, T.A., Burbridge, T.J., Crair, M.C., Huberman, A.D., 2017. Architecture, Function, and Assembly of the Mouse Visual System. Annu. Rev. Neurosci. 40, 499–538. https://doi.org/10.1146/annurev-neuro-071714-033842

Siegel, F., Heimel, J.A., Peters, J., Lohmann, C., 2012. Peripheral and Central Inputs Shape Network Dynamics in the Developing Visual Cortex In Vivo. Current Biology 22, 253–258. https://doi.org/10.1016/j.cub.2011.12.026

Siegel, M., Donner, T.H., Engel, A.K., 2012. Spectral fingerprints of large-scale neuronal interactions. Nature Reviews Neuroscience. https://doi.org/10.1038/nrn3137

Sretavan, D., Shatz, C.J., 1984. Prenatal development of individual retinogeniculate axons during the period of segregation. Nature 845–848.

Stellwagen, D., Shatz, C.J., 2002. An Instructive Role for Retinal Waves in the Development of Retinogeniculate Connectivity. Neuron 33, 357–367. https://doi.org/10.1016/S0896-6273(02)00577-9

Sweeney, S.T., Broadie, K., Keane, J., Niemann, H., O'Kane, C.J., 1995. Targeted expression of tetanus toxin light chain in Drosophila specifically eliminates synaptic transmission and causes behavioral defects. Neuron 14, 341–351. https://doi.org/10.1016/0896-6273(95)90290-2

Tainaka, K., Murakami, T.C., Susaki, E.A., Shimizu, C., Saito, R., Takahashi, K., Hayashi-Takagi, A., Sekiya, H., Arima, Y., Nojima, S., Ikemura, M., Ushiku, T., Shimizu, Y., Murakami, M., Tanaka, K.F., Iino, M., Kasai, H., Sasaoka, T., Kobayashi, K., Miyazono, K., Morii, E., Isa, T., Fukayama, M., Kakita, A., Ueda, H.R., 2018. Chemical Landscape for Tissue Clearing Based on Hydrophilic Reagents. Cell Reports 24, 2196-2210.e9. https://doi.org/10.1016/j.celrep.2018.07.056

Thompson, A., Gribizis, A., Chen, C., Crair, M.C., 2017a. Activity-dependent development of visual receptive fields. Current Opinion in Neurobiology 42, 136–143. https://doi.org/10.1016/j.conb.2016.12.007

Thompson, A., Gribizis, A., Chen, C., Crair, M.C., 2017b. A transient network of intrinsically bursting starburst cells underlies the generation of retinal waves. Current Opinion in Neurobiology 42, 136–143. https://doi.org/10.1038/nn1644

Thorn, C.F., Müller, D.J., Altman, R.B., Klein, T.E., 2018. PharmGKB summary: clozapine pathway, pharmacokinetics. Pharmacogenetics and Genomics 28, 214–222. https://doi.org/10.1097/FPC.0000000000000347

Tian, N., Copenhagen, D.R., 2003. Visual Stimulation Is Required for Refinement of ON and OFF Pathways in Postnatal Retina. Neuron 39, 85–96. https://doi.org/10.1016/S0896-6273(03)00389-1

Tiriac, A., Smith, B.E., Feller, M.B., 2018. Light Prior to Eye Opening Promotes Retinal Waves and Eye-Specific Segregation. Neuron 100, 1059-1065.e4. https://doi.org/10.1016/j.neuron.2018.10.011

Tolner, E.A., Sheikh, A., Yukin, A.Y., Kaila, K., Kanold, P.O., 2012. Subplate Neurons Promote Spindle Bursts and Thalamocortical Patterning in the Neonatal Rat Somatosensory Cortex. Journal of Neuroscience 32, 692–702. https://doi.org/10.1523/JNEUROSCI.1538-11.2012

Tolonen, M., Palva, J.M., Andersson, S., Vanhatalo, S., 2007. Development of the spontaneous activity transients and ongoing cortical activity in human preterm babies. Neuroscience 145, 997–1006. https://doi.org/10.1016/j.neuroscience.2006.12.070

Tritsch, N.X., Yi, E., Gale, J.E., Glowatzki, E., Bergles, D.E., 2007. The origin of spontaneous activity in the developing auditory system. Nature 450, 50–55. https://doi.org/10.1038/nature06233

Ueda, H.R., Ertürk, A., Chung, K., Gradinaru, V., Chédotal, A., Tomancak, P., Keller, P.J., 2020. Tissue clearing and its applications in neuroscience. Nat Rev Neurosci 21, 61–79. https://doi.org/10.1038/s41583-019-0250-1

Ujfalussy, B.B., Makara, J.K., 2020. Impact of functional synapse clusters on neuronal response selectivity. Nat Commun 11, 1413. https://doi.org/10.1038/s41467-020-15147-6

van Lier, M., Saiepour, M.H., Kole, K., Cheyne, J.E., Zabouri, N., Blok, T., Qin, Y., Ruimschotel, E., Heimel, J.A., Lohmann, C., Levelt, C.N., 2020. Disruption of Critical Period Plasticity in a Mouse Model of Neurofibromatosis Type 1. J. Neurosci. 40, 5495–5509. https://doi.org/10.1523/JNEUROSCI.2235-19.2020

Veldman, M.B., Park, C.S., Eyermann, C.M., Zhang, J.Y., Zuniga-Sanchez, E., Hirano, A.A., Daigle, T.L., Foster, N.N., Zhu, M., Langfelder, P., Lopez, I.A., Brecha, N.C., Zipursky, S.L., Zeng, H., Dong, H.-W., Yang, X.W., 2020. Brainwide Genetic Sparse Cell Labeling to Illuminate the Morphology of Neurons and Glia with Cre-Dependent MORF Mice. Neuron 108, 111-127.e6. https://doi.org/10.1016/j.neuron.2020.07.019

Voufo, C., Chen, A.Q., Smith, B.E., Feller, M.B., Tiriac, A., 2022. Cellular Mechanisms Underlying Embryonic Retinal Waves (preprint). Neuroscience. https://doi.org/10.1101/2022.08.14.503889

Wang, W.Z., Hoerder-Suabedissen, A., Oeschger, F.M., Bayatti, N., Ip, B.K., Lindsay, S., Supramaniam, V., Srinivasan, L., Rutherford, M., Møllgård, K., Clowry, G.J., Molnár, Z., 2010. Subplate in the developing cortex of mouse and human: Subplate in the mouse and human. Journal of Anatomy 217, 368–380. https://doi.org/10.1111/j.1469-7580.2010.01274.x

Watt, A.J., Cuntz, H., Mori, M., Nusser, Z., Sjöström, P.J., Häusser, M., 2009. Traveling waves in developing cerebellar cortex mediated by asymmetrical Purkinje cell connectivity. Nat Neurosci 12, 463–473. https://doi.org/10.1038/nn.2285

White, M.D., Milne, R.V.J., Nolan, M.F., 2011. A Molecular Toolbox for Rapid Generation of Viral Vectors to Up- or Down-Regulate Neuronal Gene Expression in vivo. Frontiers in Molecular Neuroscience 4. https://doi.org/10.3389/fnmol.2011.00008

Winnubst, J., Cheyne, J.E., Niculescu, D., Lohmann, C., 2015. Spontaneous Activity Drives Local Synaptic Plasticity In Vivo. Neuron 87, 399–410. https://doi.org/10.1016/j.neuron.2015.06.029

Wong, R.O.L., Ghosh, A., 2002. Activity-dependent regulation of dendritic growth and patterning. Nat Rev Neurosci 3, 803–812. https://doi.org/10.1038/nrn941

Woodworth, M.B., Greig, L.C., Kriegstein, A.R., Macklis, J.D., 2012. SnapShot: cortical development. Cell 151, 918–918.

Wu, Z., Yang, H., Colosi, P., 2010. Effect of Genome Size on AAV Vector Packaging. Molecular Therapy 18, 80–86. https://doi.org/10.1038/mt.2009.255

Xu, H., Furman, M., Mineur, Y.S., Chen, H., King, S.L., Zenisek, D., Zhou, Z.J., Butts, D.A., Tian, N., Picciotto, M.R., Crair, M.C., 2011. An Instructive Role for Patterned Spontaneous Retinal Activity in Mouse Visual Map Development. Neuron 70, 1115–1127. https://doi.org/10.1016/j.neuron.2011.04.028

Xu, H.-P., Burbridge, T.J., Ye, M., Chen, M., Ge, X., Zhou, Z.J., Crair, M.C., 2016. Retinal Wave Patterns Are Governed by Mutual Excitation among Starburst Amacrine Cells and Drive the Refinement and Maintenance of Visual Circuits. J. Neurosci. 36, 3871–3886. https://doi.org/10.1523/JNEUROSCI.3549-15.2016

Yu, C.R., Power, J., Barnea, G., O'Donnell, S., Brown, H.E.V., Osborne, J., Axel, R., Gogos, J.A., 2004. Spontaneous Neural Activity Is Required for the Establishment and Maintenance of the Olfactory Sensory Map 14.

Zack, G.W., Rogers, W.E., Latt, S.A., 1977. Automatic measurement of sister chromatid exchange frequency. J Histochem Cytochem. 25, 741–753. https://doi.org/10.1177/25.7.70454

Zhang, C., Kolodkin, A.L., Wong, R.O., James, R.E., 2017. Establishing Wiring Specificity in Visual System Circuits: From the Retina to the Brain. Annu. Rev. Neurosci. 395–424.

Zhao, C., Kao, J.P.Y., Kanold, P.O., 2009. Functional Excitatory Microcircuits in Neonatal Cortex Connect Thalamus and Layer 4. Journal of Neuroscience 29, 15479–15488. https://doi.org/10.1523/JNEUROSCI.4471-09.2009

Zheng, J., Lee, S., Zhou, Z.J., 2004. A Developmental Switch in the Excitability and Function of the Starburst Network in the Mammalian Retina. Neuron 44, 851–864. https://doi.org/10.1016/j.neuron.2004.11.015

6. Acknowledgements

First I would like to thank Peter, for taking a chance on me when hiring me and not giving up on me when I was personally struggling. I probably have given you many headaches over the last years! I especially want to thank you for your support the last year, when I realized that my future lies someplace other than academia. You were very supportive and helped me reformulate my project so that I could still finish my PhD on a positive note. You are a wonderful teacher, and I learned a lot from our scientific discussions and feedback on my writing and presentations. The skills I learned from you will be valuable throughout my working live, wherever I might end up.

A special thanks is also directed to Susanne, for being a wonderful mentor throughout the first years of my PhD. I am still astonished by your patience in teaching me your skills in the surgery room as well as in the lab. The work in this thesis would never have been completed if I didn't had you as a teacher to show me the ropes. I also value the many personal conversations we had over the past years, and your advice.

I also want to especially thank Shirley for joining forces in this project and your endless effort. I applaud you for your endless enthusiasm for science and cheerful mood, you truly make our lab a happier place. You are not only a wonderful person, but also an extremely good scientist. I hope that some day you will realize this as well.

I also want to thank my fellow colleagues from the Scheiffele lab for creating such a wonderful environment to work in. I especially want to thank Zeynep, for helping me through some of my darkest days within my PhD, and Raul for always providing a listening ear. I also want to thank my dear neighbours of "Bay 4: Raul and the chickies", Julia, Raul and Sabrina, for all the random laughs we have shared in the new Biozentrum. A big thank you also goes to the people that form the cornerstone of our lab, Dietmar, Caroline, Sabrina and Anja. I am extremely grateful for your presence and your willingness to help out. My dear colleagues, including old colleagues, thank you for all the good times we have shared!

Furthermore, I want to thank Elisabeth Lambert who was always available for a coffee when I needed to be cheered up or just vent. You have been a dear friend to me ever since we met as room mates during the Fellowship for Excellence interview week and I hope our friendship will continue for many years!

I also have family and friends to thank in the Netherlands, who I will address in Dutch.

Mijn lieve papa en mama, ik kan niet uitdrukken in woorden hoe dankbaar ik ben voor jullie oneindige steun en geloof in mij. Op momenten waarop ik er niet meer in geloofde, herinnerde jullie mij eraan dat alles goed komt. Ik ben ontzettend dankbaar dat jullie altijd voor ons klaar staan en voor jullie bezoekjes in Zwitserland waarin jullie ons verwende met jullie kookkunsten en hulp in huis! Daarnaast wil ik ook mijn broer Pieter, Sandra en de kleine Mara bedanken, voor het sturen van de leukste filmpjes en foto's die zo lekker de dag breken. Mijn dank gaat ook uit naar Pieter en Helen, ik heb maar geboft met zulke lieve schoonouders!

Ik ben ook ongelooflijk dankbaar voor de vele vrienden die ons zijn blijven op zoeken in Zwitserland. Wanneer je naar het buitenland emigreert verwacht je dat je contacten verwateren, maar ik geloof dat mijn vriendschappen alleen maar meer diepgang hebben gekregen. Mijn beste vriendinnetje Milou, ook al vonden we het beide moeilijk dat we elkaar minder konden zien, bedankt dat je altijd voor me klaar staat! Lieve Marjolein, bedankt voor je opbeurende appjes (met jouw signature

hoeveelheid hoofdletters en smileys) op momenten waarop ik wel wat vrolijkheid kon gebruiken. Ik vond het enorm fijn om met jouw de struggles van het PhD leven te kunnen delen en alles te relativeren. Daarnaast wil ik ook Joost en Eran bedanken voor jullie oneindige hoeveelheid bezoekjes aan Zwitserland en de leuke tijden die we beleefd hebben. Er zullen vast nog vele volgen!

Uiteraard gaat mijn grootste dank uit naar mijn man, Pieter-Paul. Ik ben ontzettend blij dat ik jou mijn man mag noemen en ben ontzettend dankbaar voor de steun die je de afgelopen jaren hebt gegeven. Dankzij jou kon ik alle perikelen in de academische wereld relativeren en kwam ik er pas echt achter wat ik belangrijk vind in het leven. Mijn lief, ik kan me geen leven zonder jou voorstellen, maar gelukkig voor mij hoeft dat ook niet!

Ten slotte wil ik graag ook het kleintje bedanken wat in mijn buik groeit. Dankzij jou bleef ik de laatste weken met beide benen op de grond staan. Wij zijn ontzettend blij met jou en we kunnen niet wachten om je te ontmoeten!

7. Appendix

7.1 List of abbreviations

L1/L2/L3/L4/L5/L6 = cortical layer 1, 2 3, 4 ,5 and 6

V1 = primary visual cortex

P1/P2 etc = postnatal day 1/2 etc.

E14/15 etc = embryonic age 14/15 etc.

SC = superior colliculus

dLGN = dorsal Lateral Geniculate Nucelus

RGC = retinal ganglion cells

On-RGCS/OFF-RGCS/ON-OFF-RGCS = retinal ganglion cells that either respond to light increments (ON), light decrements (OFF) or a combination of both (ON-OFF)

dsRGCs = direction-selective retinal ganglion cells

TC = thalamocortical

TCs = thalamocortical nerons

VZ = ventricular zone

SVZ = subventricular zone

IP = intermediate progenitor cell

VPM = ventral posteromedial nucleus

Sema3A = semaphoring 3A

nAChRs = nicotinic acetylcholinergic receptors

Ach = acetylcholine

SACs = starburst amacrine cells

GABA = γ-Aminobutyric acid

β2-/- = β2 knockout mouse model

SOM = somatostation

VB = ventrobasalis nucleus

S2 = secondary somatosensory cortex

Rorb = RAR Related Orphan Receptor B

NMDAR = N-methyl-Daspartate (NMDA)-type ionotropic glutamate receptor (NMDAR)

ION = infraorbital nerve

GFP = green fluorescent protein

tdTomato = tandem Tomato, a red fluorescent protein

PBS = phosphate buffered saline

CAG = CMV early enhancer/chicken β actin (CAG) promoter

ef1α = human elongation factor-1 alpha

syn = synapsin promoter

AAV = adeno-associated virus

PFA = paraformaldehyde

NeuN = neuronal nuclear protein

Olig2 = oligodendrocyte transcription factor 2

nl = nanoliter

mL = milliliter

GC/mL = genome copies per mL

PO = posterior nucleus

LP = lateral posterior nucleus (LP)

vLGN = ventral Lateral Geniculate Nucleus

iGL = intergeniculate leaflet

µm = micron

HPC = hippocampus

NA = nomenclature aperture

syn tdT = synapsin-tdTomato virus

syn Kir2.1 tdT = synapsin-Kir2.1-2A-tdTomato virus

TeNT = tetanus neurotoxin

DREADD = Designer Receptors Exclusively activated by Designer Drugs

hM4Di =

CNO = clozapine N-oxide

7.2 List of Figures